(2)

NAVAL POSTGRADUATE SCHOOL
Monterey, California

THESIS

Water Tunnel Flow Visualization Studies of a
Canard-Configured X-31A-Like Fighter Aircraft Model

by

Kwon, Hui Man

September, 1990

Thesis Advisor: S.K. Hebbar
Co-Advisor/Second Reader: M.F. Platzer

DISCLAIMER NOTICE

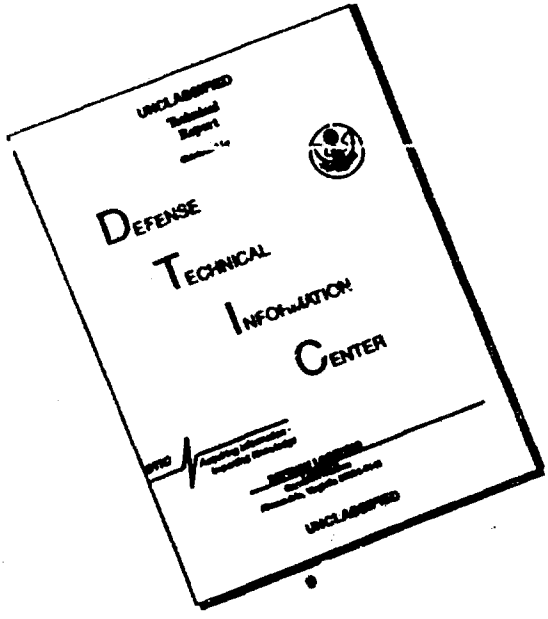

THIS DOCUMENT IS BEST QUALITY AVAILABLE. THE COPY FURNISHED TO DTIC CONTAINED A SIGNIFICANT NUMBER OF PAGES WHICH DO NOT REPRODUCE LEGIBLY.

SECURITY CLASSIFICATION OF THIS PAGE

REPORT DOCUMENTATION PAGE

1a. REPORT SECURITY CLASSIFICATION: Unclassified	1b RESTRICTIVE MARKINGS
2a. SECURITY CLASSIFICATION AUTHORITY	3. DISTRIBUTION/AVAILABILITY OF REPORT: Approved for public release; distribution is unlimited.
2b. DECLASSIFICATION/DOWNGRADING SCHEDULE	
4. PERFORMING ORGANIZATION REPORT NUMBER(S)	5. MONITORING ORGANIZATION REPORT NUMBER(S)
6a. NAME OF PERFORMING ORGANIZATION: Naval Postgraduate School; 6b. OFFICE SYMBOL (If applicable): AA	7a. NAME OF MONITORING ORGANIZATION: Naval Postgraduate School
6c. ADDRESS (City, State, and ZIP Code): Monterey, CA 93943-5000	7b. ADDRESS (City, State, and ZIP Code): Monterey, CA 93943-5000
8a. NAME OF FUNDING/SPONSORING ORGANIZATION; 8b. OFFICE SYMBOL (If applicable)	9. PROCUREMENT INSTRUMENT IDENTIFICATION NUMBER
8c. ADDRESS (City, State, and ZIP Code)	10 SOURCE OF FUNDING NUMBERS: PROGRAM ELEMENT NO; PROJECT NO.; TASK NO; WORK UNIT ACCESSION NO

11. TITLE (Include Security Classification)
Watwe tunnel flow visualization studies of a Canard-configured X-31A-like fighter aircraft model

12. PERSONAL AUTHOR(S)
Kwon,Hui Man

13a. TYPE OF REPORT	13b TIME COVERED	14. DATE OF REPORT (Year, Month, Day)	15 PAGE COUNT
Master's Thesis	FROM _____ TO _____	September 1990	118

16 SUPPLEMENTARY NOTATION The views expressed in this thesis are those of the author and do notreflect the official policy or positionof the Department of Defense or the U.S.Governmnt.

17. COSATI CODES			18 SUBJECT TERMS (Continue on reverse if necessary and identify by block number)
FIELD	GROUP	SUB-GROUP	Effect of canard location,pitch and pitch rate,vortex develop-ment and bursting,flow visualization by dye injection,water tunnel studies, X-31-like fighter aircraft model.

19 ABSTRACT (Continue on reverse if necessary and identify by block number)

A water tunnel flow visualization investigation was performed to study the vortex bursting phenomena on a 2.3% scale model of a X-31A-like fighter aircraft. The main focus of this study was two-fold:

(i) to determine the optimum canard location that produces favorable aerodynamic interference on the main wing and

(ii) to determine the effect of pitch rate on the optimum-configured model during simple pitch-up and simple pitch-down maneuvers.

It was found that a close-coupled canard configuration resulted in a more favora'-ble interference between the vortex systems of the canard and the wing. The dynamic tests indicated that the location of the wing root vortex burst point relative to the static case moved downstream with increasing pitch rate.

20 DISTRIBUTION/AVAILABILITY OF ABSTRACT	21. ABSTRACT SECURITY CLASSIFICATION
☒ UNCLASSIFIED/UNLIMITED ☐ SAME AS RPT ☐ DTIC USERS	Unclassified
22a NAME OF RESPONSIBLE INDIVIDUAL: S.K. Hebbar	22b TELEPHONE (Include Area Code): 408-646-2997; 22c OFFICE SYMBOL: AA/Hb

DD FORM 1473, 84 MAR 83 APR edition may be used until exhausted
All other editions are obsolete

SECURITY CLASSIFICATION OF THIS PAGE

☆ U.S. Government Printing Office: 1986—606 24.

Unclassified

Water Tunnel Flow Visualization Studies of a
Canard-Configured X-31A-Like Fighter Aircraft Model

by

Hui Man Kwon
Major, Republic of Korea, Air Force
B.S., Air Force Academy, Seoul,1981

Submitted in partial fulfillment
of the requirements for the degree of

MASTER OF SCIENCE IN AERONAUTICAL ENGINEERING

from the

NAVAL POSTGRADUATE SCHOOL
September 1990

Author: _____
Hui Man Kwon

Approved by: _____
S.K. Hebbar, Thesis Advisor

_____
M.F. Platzer, Co-Advisor and Second Reader

_____
E. Roberts Wood, Chairman,
Department of Aeronautics and Astronautics

ABSTRACT

A water tunnel flow visualization investigation was performed to study the vortex development and bursting phenomena on a 2.3% scale model of a X-31A-like fighter aircraft. The main focus of this study was two-fold: (i) to determine the optimum canard location that produces favorable aerodynamic interference on the main wing and (ii) to determine the effect of pitch rate on the optimum-configured model during simple pitch-up and simple pitch-down maneuvers. It was found that a close-coupled canard configuration resulted in a more favorable interference between the vortex systems of the canard and the wing. The dynamic tests indicated that the location of the wing root vortex burst point relative to the static case moved downstream with increasing pitch rate.

TABLE OF CONTENTS

ACKNOWLEDGEMENT

This thesis was sponsored by the Naval Air System Command and the Naval Postgraduate School in support of ongoing investigation of canard-configured fighter aircraft model.

My gratitude goes to my thesis advisor, Professor S.K. Hebbar, and co-advisor Professor M.F. Platzer, for their guidance, encouragement and patience throughout the course of this project.

I would like to thank to ROKAF for the opportunity to study at NPS.

I would also like to thank the many people at the Naval Postgraduate School who provided the services and expertise necessary for this research. In particular:

Mr. Al McGuire, Aeronautics Lab

Mr. Mitch Nichols, Photo Lab

Mr. John Molten, Aeronautics Metal Shop

Mr. Tony Cricelli, Aeronautics Computer Lab

Mr. Jack King, Aeronautics Lab

Finally I would like to take this opportunity to express my deepest gratitude to my wife Jeong-Sil and two sons, Daniel and Solomon for their self sacrifice and encouragement in support of my efforts.

I. INTRODUCTION

As is well known, the Wright brothers and many of the earlier aircraft designers used canard-wing configurations [Ref.1]. During world wars I and II, however, rear-tailed-type fighter aircraft became the standard configuration. Only about thirty years ago, H.Behrbohm [Ref.2] recognized and demonstrated the favorable interference effects between the vortex systems of the canard and the wing if the canard is mounted close to and above the main wing (close-coupled canard configuration). Such a design was first incorporated in the SAAB Viggen and again adopted in the SAAB Gripen. The Israeli Lavi and the new European Fighter Aircraft EFA also use the close-coupled canard configuration. A recent review of canard-related research work can be found in [Ref.3]. The authors of this review also carried out comprehensive wind tunnel investigations on a close-coupled delta-canard-wing configuration at low speed for various longitudinal and vertical canard locations and different setting angles. Earlier experimental work is documented in [Refs.4 to 9], whereas recent progress to compute such flows can be found in [Refs.10,11].

In the United States, there is increased interest in the potential of canard-wing designs for highly maneuverable fighter aircraft. Rockwell International Corporation and Messerschmitt-Boelkow-Blohm (MBB) designed and built the X-31A aircraft which uses movable canards. Its purpose is to demonstrate enhanced fighter maneuverability for the U.S. Navy (Fig.1). Test flights are expected to begin in 1990, first at Rockwell's facilities and later at the Naval Air Test Center.

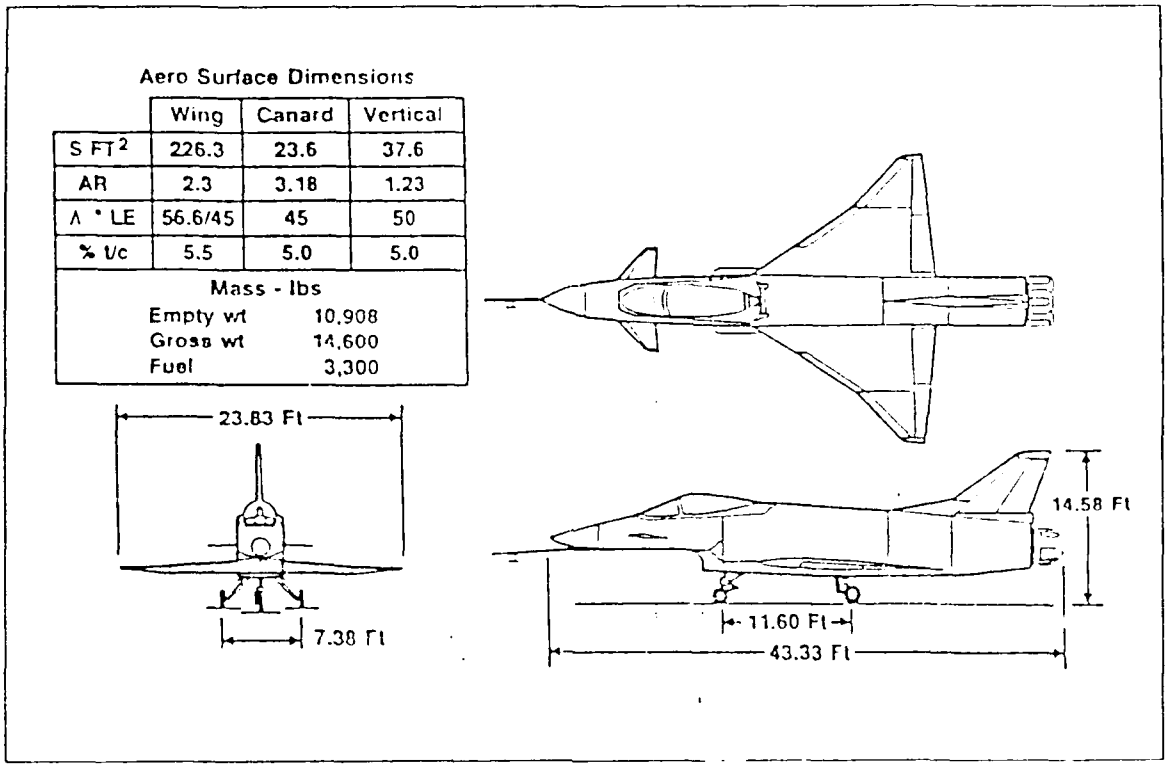

Figure 1. X-31A Configuration

As pointed out in [Ref.3], the flow physics of the canard-wing configuration is still insufficiently understood and documented. The high angle of attack flight is limited by the vortex breakdown phenomenon and by the onset of vortex asymmetry. The forebody and the strakes or canards have a strong influence on the vortex development and on the lateral and directional stability. Of special importance is the understanding of the vortex development under rapid maneuvering conditions as envisioned for the X-31A aircraft. Therefore, as part of the Naval Postgraduate School's enhanced fighter maneuverability research program, this investigation was undertaken to characterize the flow field around a maneuvering canard-configured fighter aircraft model comparable to the X-31A.

The goals of this thesis were two-fold:

a) To carry out extensive flow visualization studies in the NPS water tunnel to arrive at an optimum canard location.

b) To perform some dynamic flow visualization studies of the optimum configuration to determine the effects of pitch rate on the vortex development.

II. EXPERIMENTAL APPARATUS

A. WATER TUNNEL

The flow visualization water tunnel facility at the Naval Postgraduate School was designed by Eidetics International, Inc., Torrance, California, and installed in late 1988. Figure 2 shows the layout of the water tunnel. It is described below and more details may be found in [Ref.12-13].

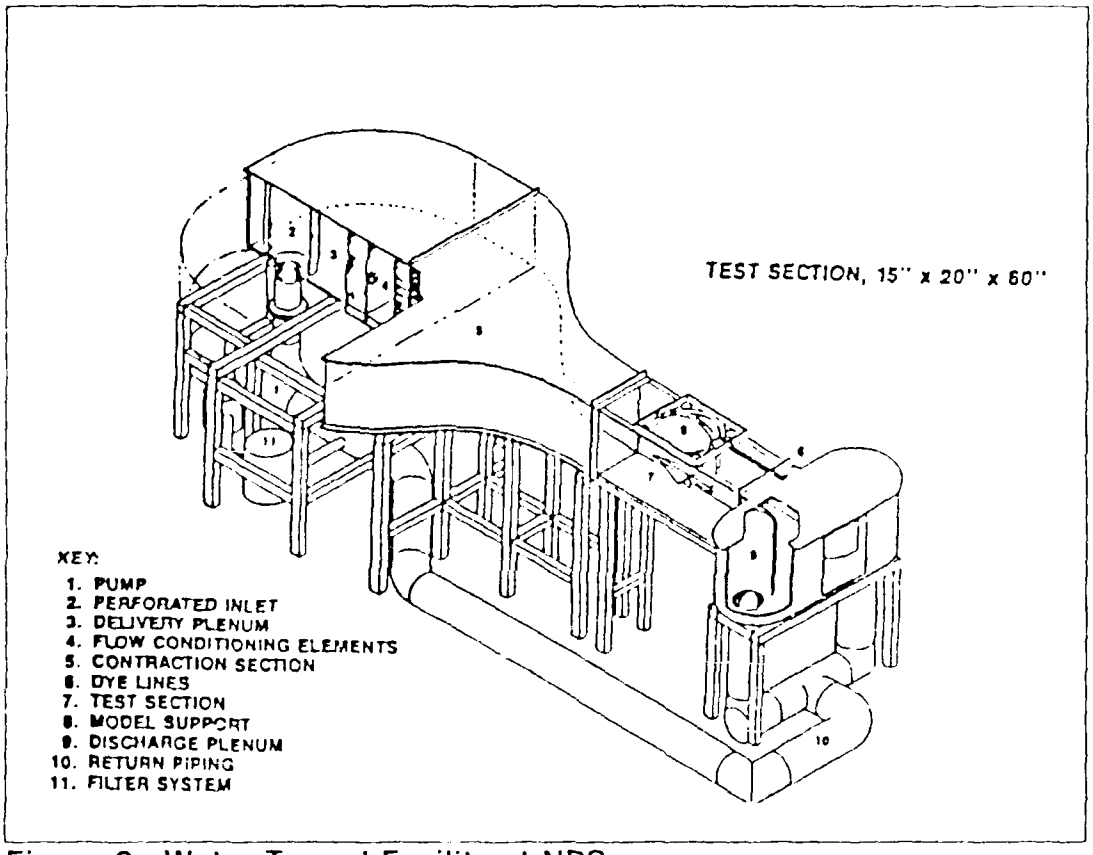

Figure 2. Water Tunnel Facility at NPS

The NPS water tunnel is a closed circuit facility for studying a wide range of aerodynamic and fluid dynamic phenomena. Its key design features are high flow quality, horizontal orientation and continuous operation. The test section is 15 inches wide, 20 inches high, and 60 inches long. The test section and discharge plenum are configured to allow simultaneous viewing of a model from the bottom, both sides and from the rear. The model is usually mounted upside down in the test section. Water velocities of up to 1 ft/sec can be obtained in the test section. The turbulence intensity level is less than 1 % RMS.

Six pressurized canisters containing water soluble food coloring dye were used for flow visualization. Each canister was connected to the model dye port through an individually routed plastic tubing. Each dye canister was pressurized by a small compressor(0-50 psi) and a pressure regulator was used to control the pressure level. To minimize the momentum of the dye itself a minimum pressure of 5 psi was used. The pitch angle of the model was controlled by a C-strut arrangement in the model support system and the yaw angle was controlled by a turntable. The model attitude was adjusted with two servo motors. Each motor had a high/low rate switch and could be controlled by a remote control. The high pitch rate and low pitch rate corresponded to 4.76 deg/sec and 1.86 deg/sec, respectively.

B. X-31A-LIKE MODEL

A somewhat simplified 2.3% scale model of the X-31A fighter aircraft was used in this investigation (Fig.3). The model has a slightly different configuration than the actual X-31A aircraft; in particular it does not have a vertical tail and a canopy. Like the X-31A aircraft the model has a double delta wing and a delta canard. The modular construction of the fuselage

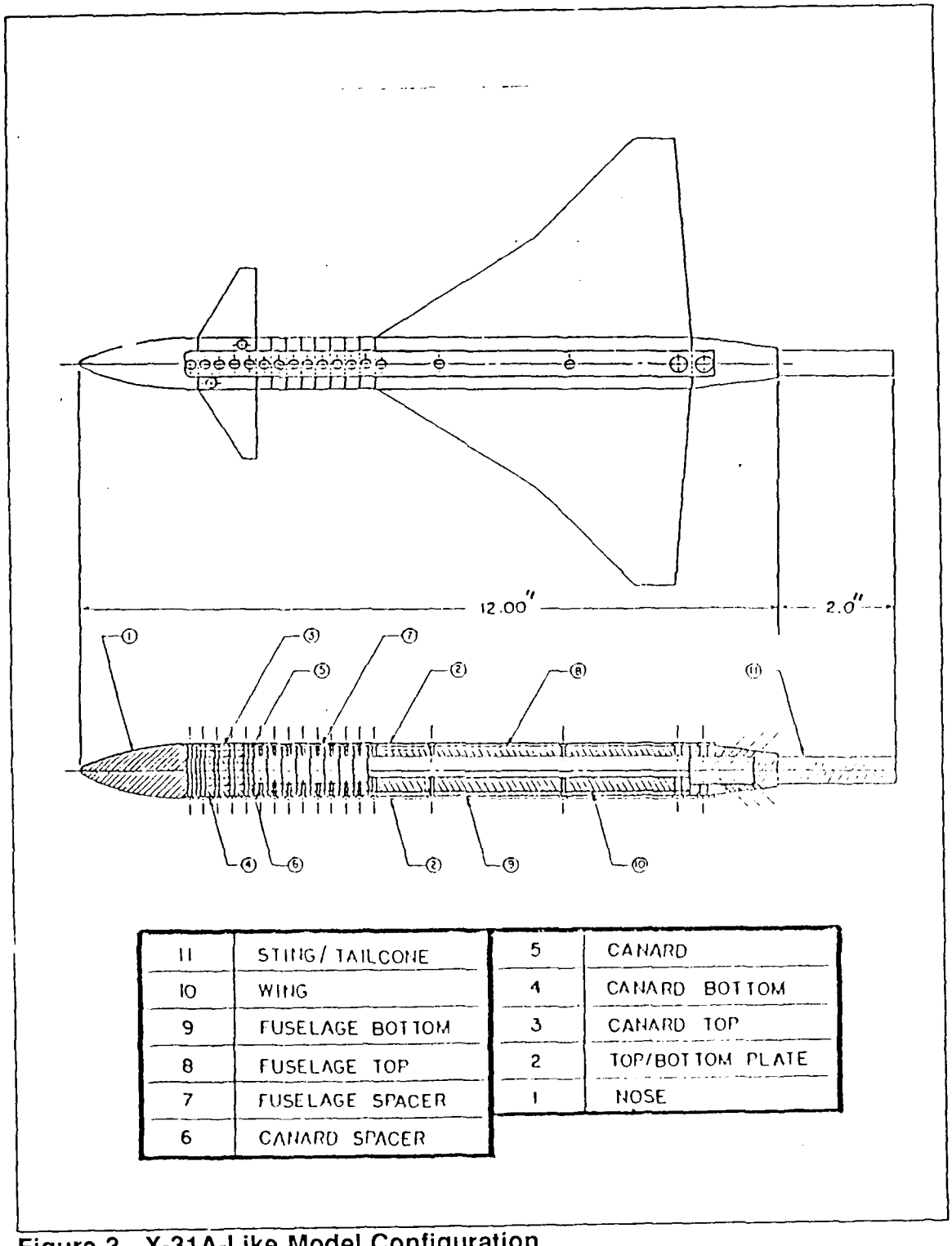

11	STING / TAILCONE	5	CANARD
10	WING	4	CANARD BOTTOM
9	FUSELAGE BOTTOM	3	CANARD TOP
8	FUSELAGE TOP	2	TOP/BOTTOM PLATE
7	FUSELAGE SPACER	1	NOSE
6	CANARD SPACER		

Figure 3. X-31A-Like Model Configuration

allowed for easy variations in the horizontal and vertical locations of the canard with respect to the main wing. Key dimensions of the model are listed below:

1. Total length= 12.0 in.
2. Span (wing, canard)= 8.0 in., 2.0 in.
3. Sweep angle (wing, canard)= 58°/ 46°, 30°
4. Wing chord= 5.5 in.(root), 2.64 in.(mid), 0.75 in.(tip)
5. Wing mean aerodynamic chord = 3.369 in.
6. Wing area= 19.866 $in.^2$
7. Canard chord= 1.0 in.(root), 0.5 in.(tip)
8. Canard Area= 1.563 $in.^2$
9. Area ratio (canard/wing)= 7.87 %
10. Canard setting angle = 2°

The geometric coordinates of canard and wing are included in Table I (Appendix C).

There were four dye injection ports on the canard and six dye injection ports on the wing (Fig.4). Dyes were delivered from the pressurized dye supply system and injected through the dye ports of the model with dye colors arranged symmetrically on either side of the fuselage.

In this investigation, the focus was on the development and bursting of vortices shed from the root of the wing. Therefore, only canard tip and wing root dye ports were used.

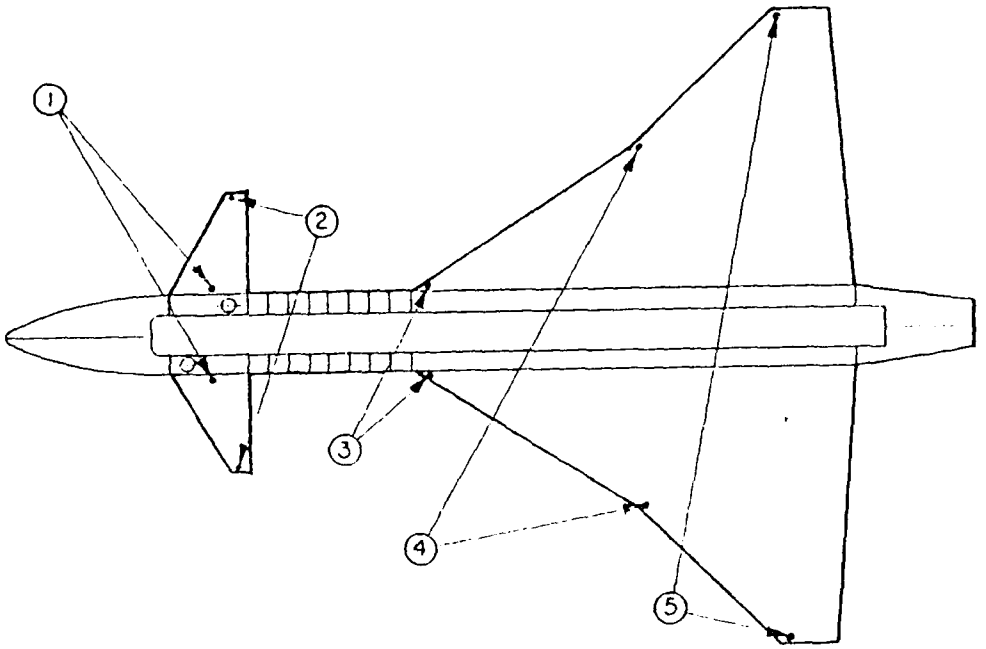

No.	LOCATION	COLOR
1	Canard Root	Pink
2	Canard Tip	Green
3	Wing Root	Red
4	Wing Mid	Blue
5	Wing Tip	Yellow

Figure 4. Dye Port Locations on X-31A-Like Aircraft Model

C. MODEL MOUNTING

It was very important to insure that the model was mounted horizontally in the water tunnel with zero pitch, zero yaw, and zero roll angle. The model mounting in the test section was achieved in the following way. First, the canard was located in the desired position with respect to the wing. The model with an extension bar was then attached to the sting holder on

the model support base by using a small hexagonal head screw. The model was introduced into the water surface by lowering the model support base to its horizontal position and the model horizontality was checked visually by the timing and the degree of wetting on both wing surfaces. To assure zero pitch angle, the centerline of the model (fuselage) was aligned with the freestream (tunnel centerline) by using spacers as needed between the model support base and the top of the test section frame. The pitch angle was calibrated by choosing a reference line on the model (say fuselage centerline). To assure zero roll angle the left and right wing tips were located at the same height from the bottom of the test section. Finally, zero yaw angle was checked by setting the model nose equidistant from either side wall of the test section and observing symmetric dye lines from both wing surfaces at zero pitch angle. The axis of rotation for the pitch motion was located 8.45 inches aft of the nose.

III. EXPERIMENTAL PROCEDURE

A. EXPERIMENTS

As previously stated, the goal of this investigation was to find the optimum canard location and to study the effects of pitch rate on the development and bursting of vortices shed from the wing root of the optimum configured model. The modular construction of the model permits 45 different canard locations in all, each location being denoted by a letter symbol followed by a number (Fig.5).

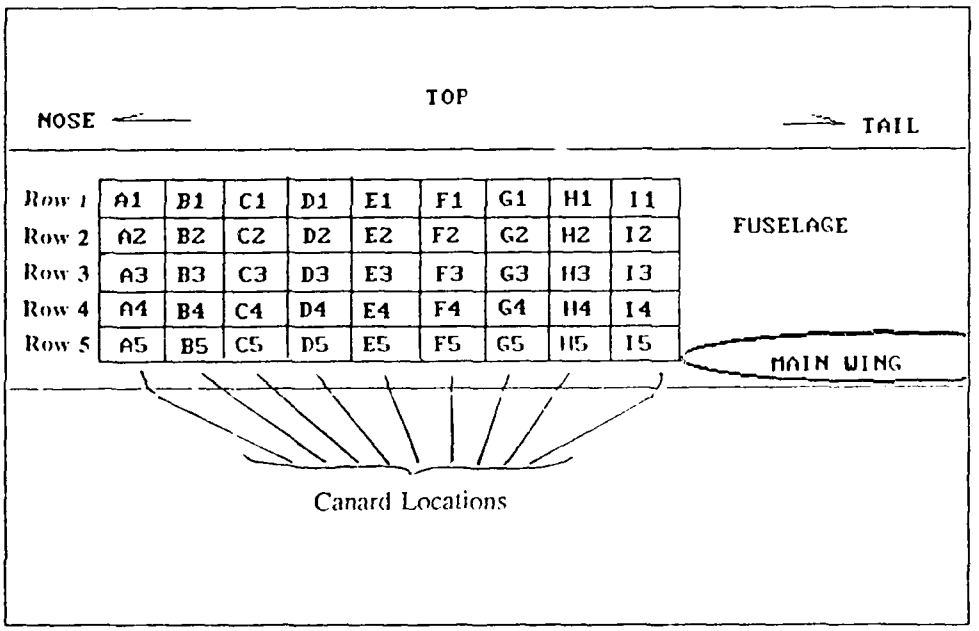

Figure 5. Identification of canard locations

The letter symbol indicates canard's horizontal distance from the wing and the number indicates its vertical distance from the wing. Practical considerations precluded use of several of these locations during the investigation. The 23 locations used for studies related to optimum canard location and their non-dimensionalized distances are listed in Table I.

Table I. NON-DIMENSIONALIZED CANARD LOCATIONS

STATION	Xwrc(%)	Zwrc(%)	STATION	Xwrc(%)	Zwrc(%)
A2	75.00	10.23	D2	61.36	10.23
A3		7.95	D3		7.95
A4		5.68	D4		5.68
A5		4.41	D5		4.41
B2	70.45	10.23	E2	56.82	10.23
B3		7.95	E3		7.95
B4		5.68	E4		5.68
B5		4.41	E5		4.41
C2	65.91	10.23	F2	52.27	10.23
C3		7.95	F3		7.95
C4		5.68	F4		5.68
C5		4.41			

The distances are measured from the quarter point of canard root chord to the quarter point of wing root chord, and wing root chord used for non-dimensionalization (Fig.6).

Before embarking on the main focus of this investigation, it was necessary to carry out a series of preliminary experiments to select proper dye ports and an appropriate range of angle of attack for flow visualization studies. The three dye ports, namely the root port, the mid port and the tip port, located along the wing leading edge were initially

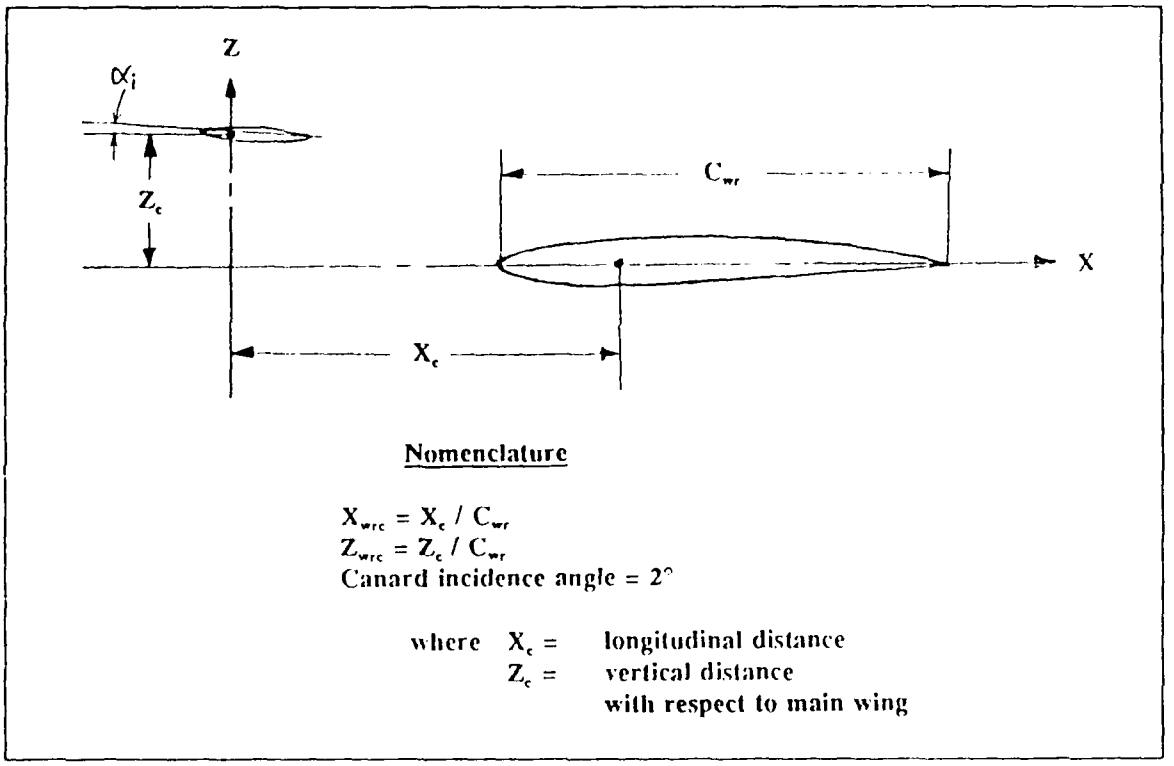

Figure 6. Description of canard location

selected for dye injection with and without the canard. The tip flow appeared smooth up to 6° angle of attack after which it reversed its direction; the mid flow appeared smooth up to 10° angle of attack after which it reversed its direction. On the other hand, the root flow appeared to exist up to about 34° angle of attack, with a fairly well defined vortex shape in the 13.5° - 29° angle of attack range. Based on these observations, it was decided to use dye injection from the root port on the wing as the primary visual tool to investigate the effects of the canard on the flow field over the wing. To determine the appropriate range of angle of attack , canard location F4 was selected arbitrarily and the dye flow from the root port visualized in the angle of attack range 0° - 30° at intervals of 2.5° (Figs.8 - 23 in Appendix A). Clear vortex flow development was observed to start at about 13.5° angle of attack, vortex burst appearing downstream of the

wing trailing edge and proceeding upstream with further increase in the angle of attack. At about 30° angle of attack range the burst location moved close to the leading edge. Based on these observations, it was decided to study the wing flow field at 0°, 15°, 20° and 25° angles of attack for each canard location.

To meet the goal of this investigation, the experimental program was carried out in two phases. The first phase involved flow visualization studies related to optimum canard location on the X-31A-like model. The experiments were carried out for static conditions at 0°, 15°, 20° and 25° angle of attack with zero yaw and covered 23 canard locations (identified in Table I). Based on the vortex burst location data gathered from these experiments canard location F3 was found to be optimum. The second phase involved the dynamic wing vortex flow visualization of the optimum configured X-31A-like model for zero yaw and two pitch rates, with angle of attack varying from 0° to 50° (simple pitch-up motion) and 50° to 0° (simple pitch-down motion).

Both still-picture photography and videotape recordings were used for documentation of the flow field of the model. The flow velocity in the water tunnel was kept nearly constant at 0.25 ft/sec which corresponds to a nominal Reynolds number of 10,200 (based on wing root chord of the model). Although the flow Reynolds number in the water tunnel is very low, studies by other researchers [Refs. 13,14,15] have indicated that water tunnel data of burst locations of vortices shed off sharp leading edges compare very favorably with the data from flight and ground tests.

B. REDUCED PITCH RATE SIMULATION

Aircraft encounter unsteadiness under all operating conditions whether due to pilot inputs (i.e., pitch-up, pitch-down, etc.), or of a natural origin (i.e., wind shear, gusts, etc.). To understand the stability of an aircraft operating in these environments, a knowledge of its response to flow unsteadiness is essential. The guiding non-dimensional parameter during pitching motions is the reduced pitch rate, k, defined by the following formula:

$$k = \frac{\omega c}{2U_{\infty}}$$

where,

k : reduced pitch rate, non-dimensional

w : pitch rate, rad/sec

c : characteristic length of the body, ft

U_{∞} : free stream velocity, ft/sec

In the case of a wing pitching about its mid-chord location, the reduced pitch rate may be interpreted as the ratio of the vertical motion of the leading edge to its longitudinal motion.

Using the above formula the reduced pitch rate for the full scale X-31A aircraft was calculated and compared with the values for the water tunnel model. For the X-31A aircraft, assumed G-loading was 5 g at 150 Knots. The reduced pitch rates for the full scale X-31A aircraft and the water tunnel model at low pitch rate motion were equal. Table II lists the reduced pitch rates and indicates that the water tunnel facility is capable of simulating the full scale values of the reduced pitch rate for the X-31A aircraft.

Table II. REDUCED PITCH RATE

PITCH RATE*	w(rad/s)	Length(ft)	U_∞(ft/sec)	k
Low pitch rate	0.03	1	0.25	0.06
High pitch rate	0.08	1	0.25	0.17
Full scale X-31A Aircraft	0.70	43.33	253.35	0.06

* The model pitch-axis was located 8.45 inches aft of the nose.

C. DATA ACQUISITION

A good deal of visual analysis of the flow field preceded the actual data collection phase. The data collection consisted of photographs taken with two 35mm automatic cameras providing a simultaneous side and planform view of the vortical flow field originating off the wing root port of the X-31A-like model. A professional video camera was also used to record the flow phenomena for static and dynamic conditions. Section E describes the lighting and camera settings utilized for this investigation.

D. DATA REDUCTION

Data reduction consisted of measuring the bursting distance of the vortex shed off the wing root port and plotting it against the angle of attack. The vortex bursting locations for the static case were determined visually through the camera viewfinder and the linear scale drawn on the starboard side of the fuselage. For the dynamic case the vortex bursting location was first measured visually by naked eye, then checked during the playback of the videotape and finally determined from the photographs. During this investigation all measurements were made on the starboard side of the aircraft model using the leading edge of the wing root chord as the reference point. The measurements of vortex bursting location were done with the utmost care and consistency, and scaled for non-dimensionalization using the wing root chord.

Some degree of imprecision may be present in the reduced data due to the difficulty in locating the vortex bursting location, particularly at lower angles of attack and at high pitch rates (see discussion in Chapter IV, also [Ref.13]). During the measurement of vortex bursting location for the static case, fluctuation in bursting location was found to vary up to ± 0.25 inches. As the vortex core was found to enlarge and reduce with some frequency, a certain amount of time was required to measure both maximum distance and minimum distance. These distances were then averaged to determine the mean bursting location (Table III). The photographs corresponding to the static conditions were timed to correspond roughly to the mean location of the vortex burst.

Table III. MEAN VORTEX CORE LENGTH BEFORE BURSTING AND FLUCTUATION LIMITS (INCHES)

Canard Location	15° AOA		20° AOA		25° AOA	
	Mean	+/-	Mean	+/-	Mean	+/-
Off	4.788	0.063	3.875	0.175	2.1	0.05
A2	4.738	0.163	4.225	0.075	2.325	0.175
A3	4.7	0.1	4.238	0.113	2.325	0.175
A4	4.675	0.125	4.325	0.1	2.325	0.125
A5	0	0	4.075	0.175	2.4	0.1
B2	4.7	0.2	3.975	0.175	2.35	0.1
B3	4.725	0.125	4.267	0.133	3.35	0.113
B4	4.675	0.142	4.117	0.117	2.358	0.142
B5	4.55	0.15	3.9	0.2	2.5	0.2
C2	4.6	0.133	4.2	0.1	2.418	0.148
C3	4.65	0.15	4.15	0.15	2.442	0.142
C4	4.538	0.188	4	0.2	2.35	0.125
C5	4.625	0.125	3.85	0.15	2.45	0.15
D2	4.5	0.2	4.2	0.1	2.55	0.15
D3	3.75	0.2	4.15	0.15	2.488	0.188
D4	4.575	0.175	3.95	0.25	2.45	0.15
D5	4.4	0.2	3.7	0.2	2.55	0.15
E2	4.7	0.1	4.3	0.1	2.35	0.15
E3	4.65	0.15	4.25	0.15	2.375	0.225
E4	4.498	0.203	3.75	0.15	2.4	0.2
E5	4.475	0.175	3.85	0.15	2.5	0.2
F2	4.65	0.15	4.258	0.175	2.6	0.217
F3	4.65	0.1	4.275	0.1	2.6	0.15
F4	4.525	0.175	3.833	0.15	2.463	0.15

E. METHOD OF PHOTOGRAPHY

The equipment used for the photographic session consisted of two 35mm cameras, five Smith-Victor 600 watt photographic lights, and a floodlight installed below the test section. For the side view photographs two of the lights were placed at a distance of three feet and at a 45° angle from the test section. Other three photographic lights were placed below the test section; one at 45°, near the front of the model and two at 45°, near the rear of the model. This in conjunction with the fixed floodlight provided enough lighting for the planform photographs. Figure 7 shows the lighting setup for both the side view and planform photographs. Essentially the same lighting arrangement with minor adjustments to suit video camera location was used during video taping of the vortical flow field on the model.

A Nikon 2000 camera which has an automatic shutter speed and manual focusing with manual aperture control and manual ASA setting was used for taking side view pictures. A Minolta 7000 camera which has all automatic functions of focusing, shutter speed control, aperture control and even automatic ASA setting function was used for taking plan view pictures. The automatic focus function was used very effectively for plan view pictures, particularly during the dynamic case, because the focusing was automatically adjusted as the angle of attack was changed. The type of film used for all the photographs was 35 mm black and white ASA 400 film. During the exposure of the film, the side view camera settings were as follows : ASA 400, aperture 11, auto shutter speed, focused on the scale drawn on the starboard side of the fuselage. The plan view camera settings were as follows : auto ASA setting (it read ASA 400 automatically), auto aperture, auto shutter speed, auto focus.

The side view camera was set on the point where the center of the camera focus was aligned with the model's pitch rotation axis, and the camera body was rotated a little bit to the left to have the model always at the center of the picture regardless of changing angle of attack. The angle of attack scale fixed to the rear side wall of the tunnel shows up in all side view photographs and helps in reading of the instantaneous angle of attack. To know the pitch angle in the planform view photographs it was necessary to take both the side view and planform view photographs simultaneously. This was accomplished by the two cameras for simultaneous exposure by using two remote shutter release cables.

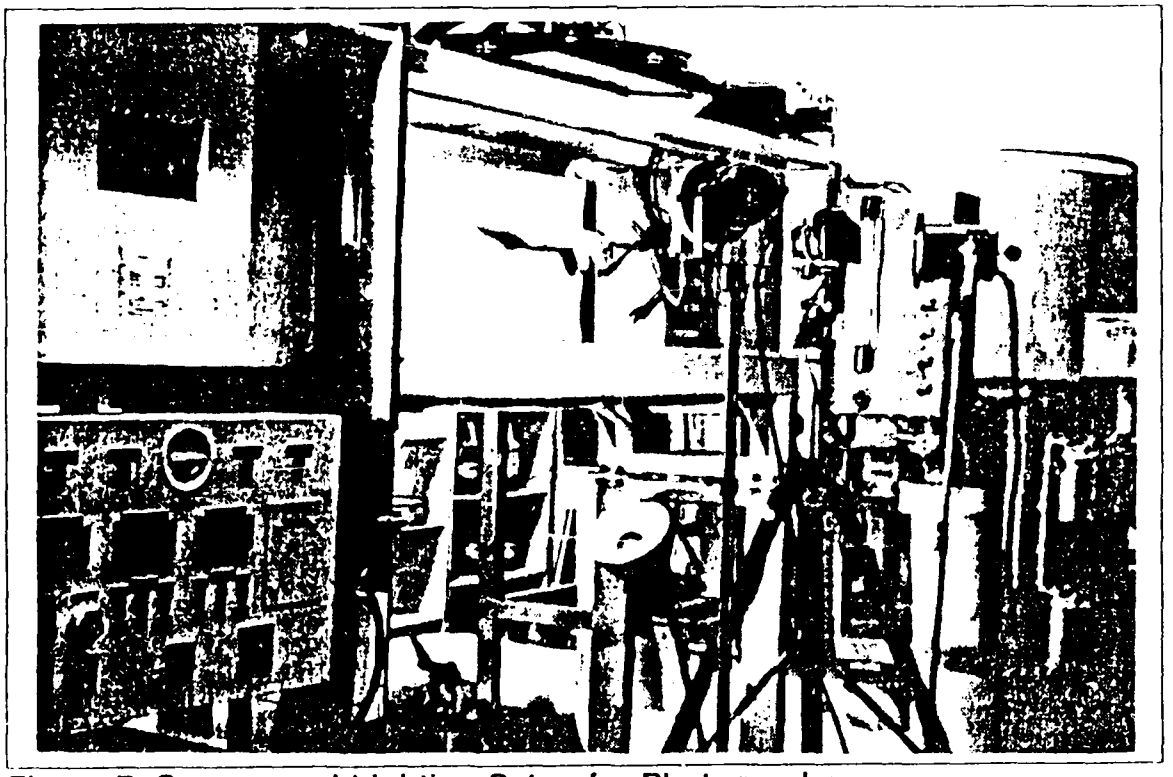

Figure 7. Camera and Lighting Setup for Photographs

IV. RESULTS AND DISCUSSION

The results of this investigation will be presented and discussed in a series of 3 photographic sequences and bursting location plots. Several rolls of 35 mm black and white film were exposed and several hours of videotape recorded during the investigation. The results of the 35 mm photography are presented in Figures 8 through 75 (see Appendix A). Figures 24-75 show two views of the flow field, one in the side view and the other in the planform view (taken from the bottom of the tunnel). The bursting location plots derived from these photographs are included in Figures 76 through 91 (see Appendix B). The raw data on vortex bursting location derived from experiments is shown in Table II (see Appendix C). First, some general comments will be made on the wing flow field visualized during the series of preliminary experiments. Then the flow visualization photographs will be examined in detail to highlight the flow field characteristics for different model orientations and different canard locations including canard off condition. Finally, with the aid of burst location plots, the effects of pitch rate on the development/bursting of wing root vortices will be discussed.

A. DESCRIPTION OF WING FLOW FIELD OF X-31A-LIKE MODEL

Sequence number 1, Figures 8 through 23. These figures show the wing flow field with canard installed at location F4. In the AOA range of 0° to 1° the flow over the wing remains particularly smooth and stable (Fig.8). At 2.5° angle of attack (Fig.9), the flow at the inner trailing edge of the wing has dispersed a little bit outward.

As the angle of attack is increased further, the flow from the inside of the wing root surface progressively disperses outward to the tip (Fig.10 through Fig.14). Finally at about 13.5° angle of attack (Fig.15) the flow fluctuates very much and begins to coil up into a vortex core shape with a maximum vortex core length on the wing surface. This vortex core is tightly wound and extends aft until undergoing vortex core breakdown. The vortex core breakdown is unquestionably signified by the stagnation of the core and abrupt expansion in its diameter. As the AOA is increased further the vortex core breakdown point moves upstream over the wing surface (Fig.16 through Fig.22), and finally the bursting occurs very close to the leading edge at about 30° angle of attack (Fig.23). In short, the vortex burst location over the wing surface moves from the trailing edge to the leading edge in the angle of attack range 14°-30°.

With the canard off and with increase in the angle of attack, it was observed during the experiments that the wing tip stalled at 5° angle of attack and reversed its direction clearly at 6° angle of attack. At the mid section of the wing the flow stalled at 10° then reversed its direction at 15° angle of attack. With canard installed at location B5, the flow from the wing tip stalled at 7° and reversed its direction at 9° angle of attack, and the flow from the mid section stalled at 11° and reversed at 18° angle of attack. These observations simply reconfirm the canard advantage, namely that a canard can be used to delay the stall phenomenon and thus enhance flight performance.

B. EFFECTS OF CANARD LOCATION ON ROOT VORTEX CORE BREAKDOWN

Sequence number 2, Figures 24 through 63. In these figures the wing flow characteristics for different canard locations are compared with those for the canard-off case. As previously mentioned in Section III, only 23 canard locations were used in this investigation. The raw data on vortex burst for these canard locations are shown in Table II (see Appendix C). Figures 24 through 63 present both side view and plan view photographs of the flow field for the canard-off case and 9 different canard locations.

1. Longitudinal location of canard

The effects can be easily visualized in the photographs for any given angle of attack by holding the vertical distance of the canard from the wing constant. For example, figures 33 and 57 can be compared for the case of 15° angle of attack and figures 35 and 59 for 25° angle of attack. A detailed observation of these photographs reveals two characteristic features of the flow field as the canard is moved closer to the wing, i.e. from front location to the rear location. At 15° angle of attack, the vortex core length appears to decrease somewhat as the canard is moved closer to the wing whereas at 20° and 25° angles of attack, the vortex core length tends to increase. These features are clearly visualized graphically in Figures 76-79. These observations simply reinforce the benefit of close-coupling of canard, namely that of improved flow field on the top wing surface resulting in enhanced lift/flight performance.

2. Vertical location of canard

As before, a close observation of the photographs for any given angle of attack reveals the fact that, as the vertical distance of the canard from the wing is increased at the same longitudinal location, the vortex core length tends to increase initially (Compare Figs. 57 and 61). This tendency is also seen in Figures 80-85.

To summarize, a close-coupled, high-location canard yields beneficial results. Location F3 was judged optimum in the present investigation.

C. EFFECTS OF ANGLE OF ATTACK ON WING ROOT VORTEX CORE BREAKDOWN

Portion of sequence number 2, Figures 56 through 59, and sequence number 3, Figures 64 to 75. These effects are discussed below in some detail for the optimum canard location F3. Figures 56 through 59 present flow visualization photographs for the static case and Figures 64 through 75 for the dynamic case at two pitch rates and zero yaw (ß=0°).

1. Static Conditions

Figure 56 shows that at zero degree angle of attack, the flow is smooth and stable. Figures 57 through 59 show the development of vortical flow field over the wing surface at higher angles of attack. The vortex bursting point moves upstream with angle of attack, thus reducing the extent of vortical flow field. Bursting points in Figs.57 through 59 are located at 84.5%, 77.7% and 47.3% of wing root chord, respectively.

2. Dynamic Conditions

Figures 63 through 74 present photographs taken at 5° AOA interval during simple pitch-up and pitch-down motions at two reduced pitch rates with the model at zero yaw. Precise measurements of vortex bursting point in the dynamic case were very difficult, if not impossible, to obtain from these photographs. Therefore, video recordings were used for this purpose. The results of the vortex bursting point measurements are shown in Table IV.

Table IV. VORTEX CORE LENGTH FOR DYNAMIC CASE (INCHES)

Pitch Rate / Direction	Angle of Attack (°)								
	10°	15°	20°	25°	30°	35°	40°	45°	50°
Static Case	-	4.65	4.275	2.6	-	-	-	-	-
Low/Up	-	-	3.75	3.5	2.5	1.5	0.6	-	-
Low/Down	-	3.7	2.5	1.7	0.3	-	-	-	-
Hi/Up	-	-	-	-	3.0	2.5	2.0	1.0	-
Hi/Down	4.0	3.3	2.75	-	-	-	-	-	-

Figures 64 through 69 show the wing flow field during simple pitch-up and pitch -down motions at low pitch rate (0° to 50° AOA). It was observed during the pitch-up experiment, that at $\alpha = 15°$ (Figure 64) the flow was flickering and the vortex was not established yet. From the video recordings it was ascertained that the flow started to coil up at 13° angle of attack and a symmetric pair of wing root vortices were developed at 17° angle of attack. As the angle of attack was increased the vortex bursting point moved upstream and finally moved to the leading edge at 41° AOA (also see Figs. 65 and 66). During the pitch-down motion, as the angle of

attack was decreased from 50° to 0°, the full vortex core was observed on the wing surface at 31° AOA, the flow finally becoming smooth at 12° AOA. With decreasing AOA the vortex core appeared to be growing and moving outboard (Figs.67 through 69).

Figures 70-75 show the wing flow field during simple pitch-up and pitch-down motions at high pitch rate (0° to 50° AOA). At α=15° (Figure 70) no vortical flow was observed. Video recordings showed that the flow started to coil up at 22° AOA and vortices developed at 25° AOA. With further increase in angle of attack the wing root vortex burst point moved upstream and finally moved to the leading edge at 50° AOA. During a simple pitch-down motion at high pitch rate the full vortex core was observed on the wing surface at 21° AOA, the flow finally becoming smooth at 12° AOA (Figs.73-75).

D. BURSTING LOCATION PLOTS

Quantitative documentation of vortex burst response discussed in earlier sections is presented graphically in Figures 76-92. The plots in Figures 76-91 are obtained from the data of Table II (Appendix C) and those in Fig.92 from Table IV. These plots help to visualize graphically the effects of various parameters on the wing root vortex core breakdown.

Figures 76-79 present plots showing the effects of canard horizontal location on wing root vortex core breakdown at three angles of attack (15°, 20°, 25°). The canard vertical distance held constant in these figures is identified by a row number (Fig.5). In each case the comparison is made with canard-off configuration. The numbers 0, 1, 2, 3, 4, 5, and 6 on the horizontal axis denote canard-off case, canard locations A, B, C, D, E and F, respectively (see Fig.5 and Table I). It is clear from these figures that at 20° AOA and above the vortex core length generally

increases as the canard moves closer to the wing (i.e., from location A to location F). A slight reduction in the vortex core length is seen at 15° AOA.

Figures 80-85 present plots showing the effects of canard vertical location on wing root vortex core breakdown at three angles of attack (15°, 20°, 25°). The canard horizontal distance held constant in these figures is identified by a canard location. In each case the comparison is made with canard-off configuration. The numbers 0, 1, 2, 3, 4 on the horizontal axis denote canard-off case, canard rows 2, 3, 4 and 5, respectively. A general trend is seen in the three graphs suggesting an initial increase in the vortex core length as the canard approaches the wing upper surface from its high location.

Figures 86-91 present plots showing the effects of angle of attack on the wing root vortex core breakdown for different canard horizontal distance held constant in these Figures is identified by a canard location. These plots clearly show that the vortex burst location moves upstream as the angle of attack increases.

Figure 92 shows burst location plots as a function of angle of attack for the optimum-canard location F3 during dynamic motion of the model at two pitch rates with zero yaw. Also shown for comparison is the corresponding bursting location plot for the static case. The dynamic effects of pitch rate are clearly seen in these plots. During the pitch-down motion in the AOA range considered, the bursting location always occurred earlier relative to the static case, whereas during the pitch-up motion the bursting location occurred later relative to the static case. Thus the burst location curve consistently undershoots the corresponding static curve during pitch-down motion and overshoots during pitch-up motion, this undershoot/overshoot increasing with the pitch rate. The vortex bursting response observed here for pitch-up and

pitch-down motions is similar to the one observed by Cavazos [Ref.13] in his experimental investigation of LEX vortices shed off a F/A-18 fighter aircraft model.

V. CONCLUSIONS AND RECOMMENDATIONS

A low speed flow visualization investigation was initiated to study the vortex development and bursting phenomena on a 2.3 % scale model of a X-31A-like fighter aircraft using dye injection in the NPS water tunnel. Two sets of experiments were carried out. In the first set the focus was on the optimum canard location that produces favorable aerodynamic interference on the main wing; in the second set the focus was on the effects of pitch rate on the optimum-configured model during simple pitch-up and simple pitch-down maneuvers. The water tunnel visualization data reported here is believed to be the first of its kind for a canard-configured X-31A-like aircraft model. The following conclusions are drawn from the results of the experimental investigation :

1. A close-coupled canard configuration results in a more favorable aerodynamic interference between the vortex systems of the canard and the wing.

2. A high-canard location (unlike a low-canard / coplanar-canard location relative to the wing) influences wing flow field favorably.

3. The dynamic tests indicate that vortex burst lag increases with pitch rate. That is, the location of the wing root vortex bursting point relative to the static case moves rearward with increasing pitch-up motion and forward with increasing pitch-down motion.

The following recommendations are made based on this investigation :

1. Automatic focus camera is necessary to take instantaneous pictures during dynamic motion.

2. Remote indicators of angle of attack and angle of yaw installed outside the test section frame will be useful during studies of dynamic motion. The readouts should appear in pictures.

LIST OF REFERENCES

1. Andy Lenon, with a foreword by Burt Rutan, *CANARD - A Revolution in Flight,* Aviation Publishers, September 1984.

2. H.Behrbohm, *Basic Low Speed Aerodynamics of the Short-Coupled Canard Configuration of Small Aspect Ratio*, SAAB TN 60 (1965).

3. D.Hummel and H.-Chr.Oelker, *Effects of Canard Position on the Aerodynamic Characteristics of a Close-Coupled Canard Configuration at Low Speed*, Agard Conference Proceedings No.465.

4. B.B.Gloss, L.W.Mckinney, *Canard-Wing Lift Interference related to Maneuvering Aircraft at Subsonic Speeds*, NASA TM X-2897 (1973).

5. B.B.Gloss, *Effect of Canard Location and Size on Canard-Wing Interference and Aerodynamic-Center Shift related to Maneuvering Aircraft at Transonic Speeds*, NASA TN D-7505 (1974).

6. W.P.Henderson, *The Effect of Canard and Vertical Tails on The Aerodynamic Characteristics of a Model with a 59° Sweptback Wing at a Mach Number of 0.30*, NASA TM X-3088 (1974).

7. J.Er-El, A.Seginer, *Vortex Trajectories and Breakdown on Wing-Canard Configurations*, J.Aircraft 22 (1985), 641-648.

8. H.-Chr. Oelker, D.Hummel, *Investigations on the vorticity sheets of a close-coupled delta-canard configuration*, ICAS-Proceedings 1988, Vol.1,649-662, See also: J.Aircraft 26 (1989), 657-666.

9. B.B.Gloss and E.J.Ray,K.E.Washburn, *Effect of Canard Vertical Location, Size, and Deflection on Canard-Wing Interference at Subsonic Speeds*, NASA-TM-X-78790, Dec 78.

10. Rachel Gordon, *Numerical Simulation of Vortical Flows over a Strake-Delta Wing and a Close Coupled Delta-Canard Configuration*, AIAA-90-3002-CP, August 20-22, 1990 / Portland, Oregon.

11. J.M.A. Longo and A. Das, *Numerical Simulation of Vortical Flows over Close-Coupled Canard-Wing Configuration*, AIAA-90-3003-CP, August 20-22, 1990 / Portland, Oregon.

12. User's Manual, *Flow Visualization Water Tunnel Operations Manual for Model 1520*, Eidetics International, Inc., Torrance, California,1988 (prepared for Naval Postgraduate School, Monterey, California).

13. Lon Cavazos, *A Flow Visualization Study of LEX Generated Vortices on a Scale Model of a F/A-18 Fighter Aircraft at High Angles of Attack*, NPS Thesis Jun 1990 / Monterey, California.

14. John H.Del Frate and Fanny A.Zuniga, *In-Flight Flow Field Analysis on the NASA F-18 High Alpha Research Vehicle with Comparisons to Ground Facility Data*, AIAA-90-0231, 28th Aerodynamic Sciences Meeting, Jan 8-11,1990/Reno,Nevada.

15. David Manor, Leonard Miller, William H.Wentz, Jr., *Static and Dynamic Water Tunnel Tests of Slender Wings and Wing-Body Configuration At Extreme Angle of Attack*, AIAA-90-3027-CP, August 20-22,1990/Portland, Oregon.

APPENDIX A. EXPERIMENTAL RESULTS (PHOTOGRAPHS)
FIGURES 8 THROUGH 75

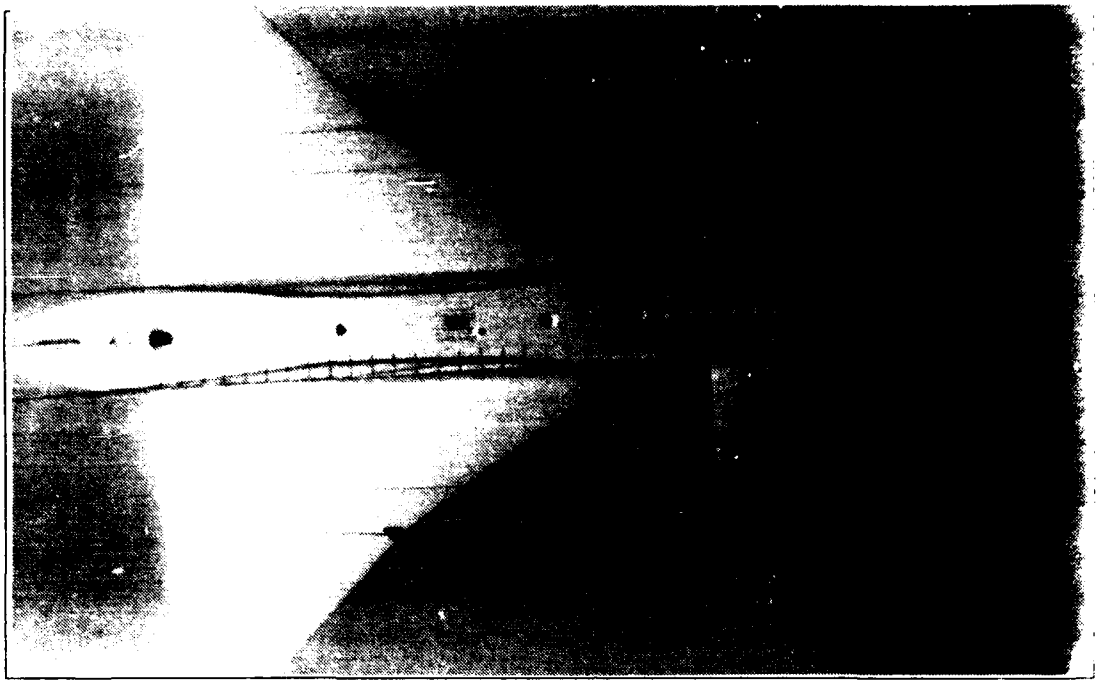

Figure 8. 0° AOA

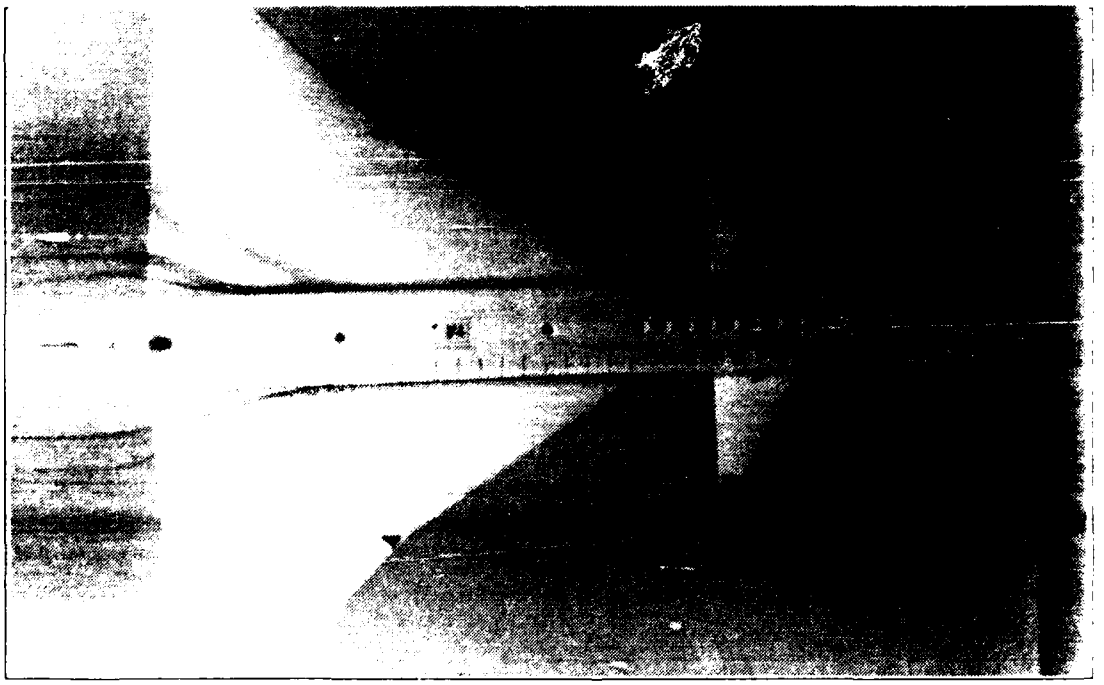

Figure 9. 2.5° AOA

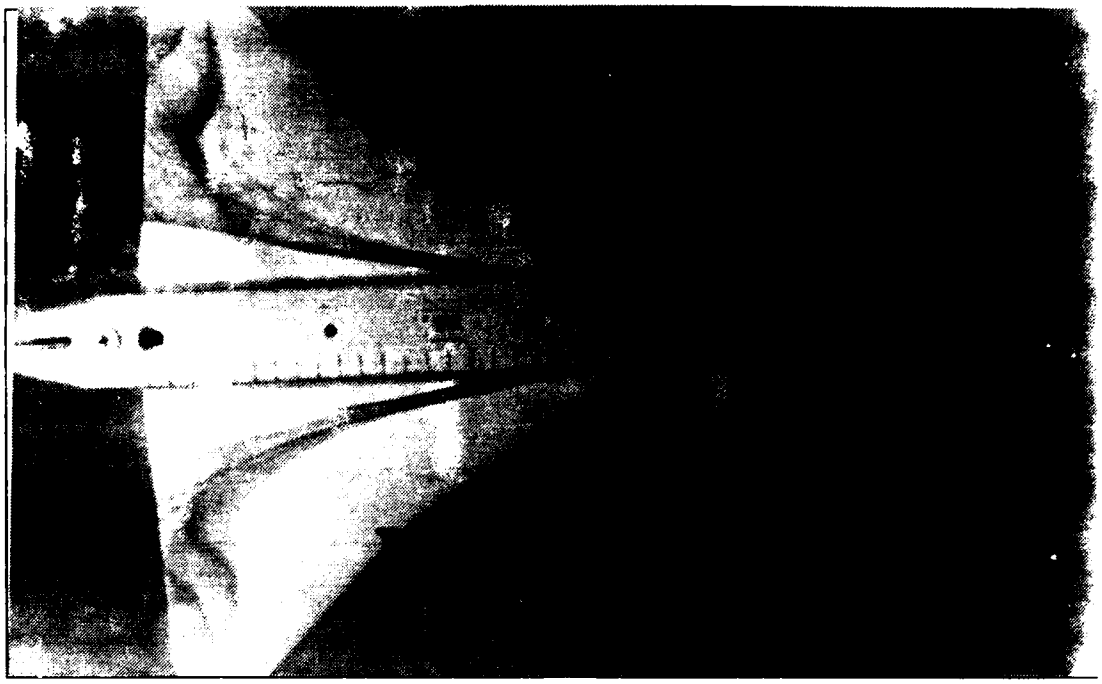

Figure 10. 5° AOA

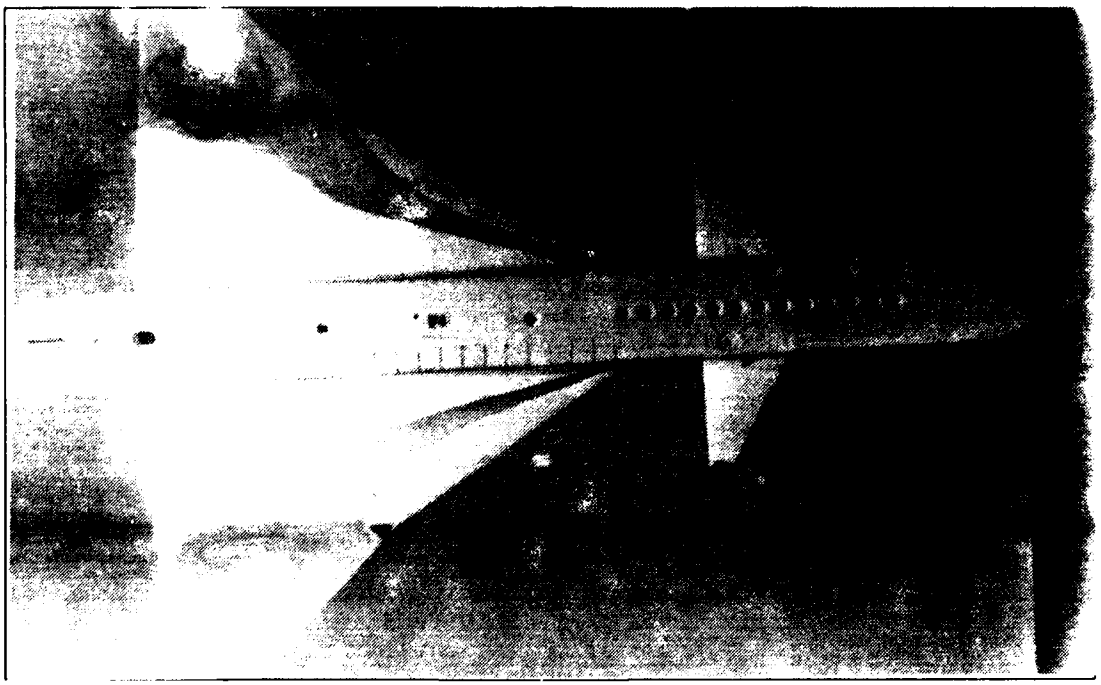

Figure 11. 7.5° AOA

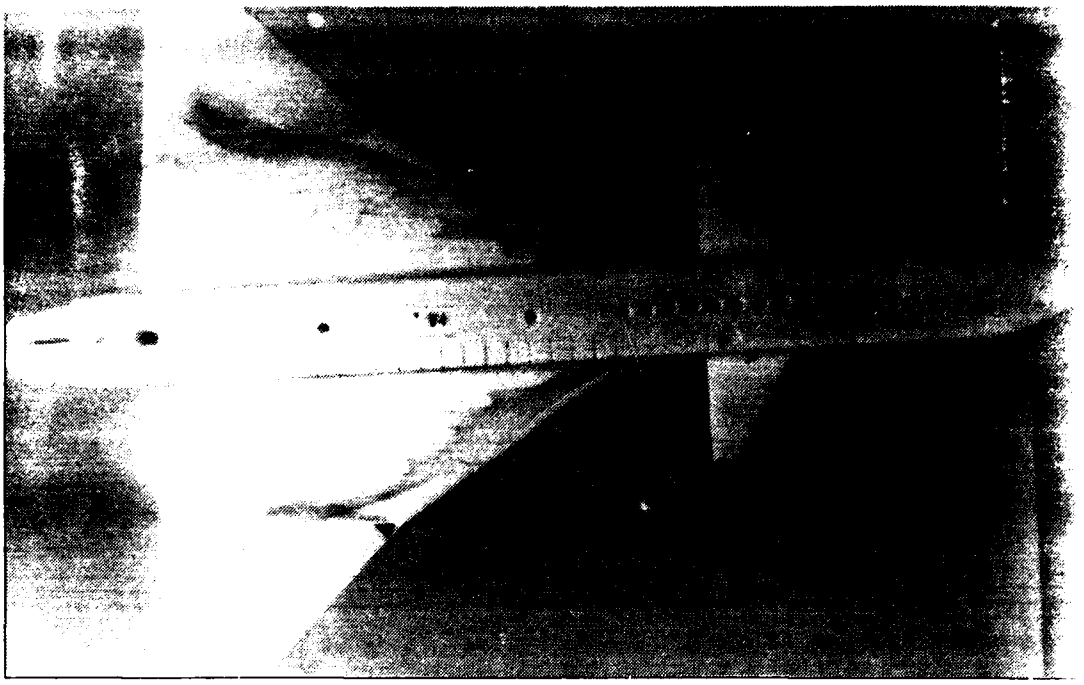

Figure 12. 10° AOA

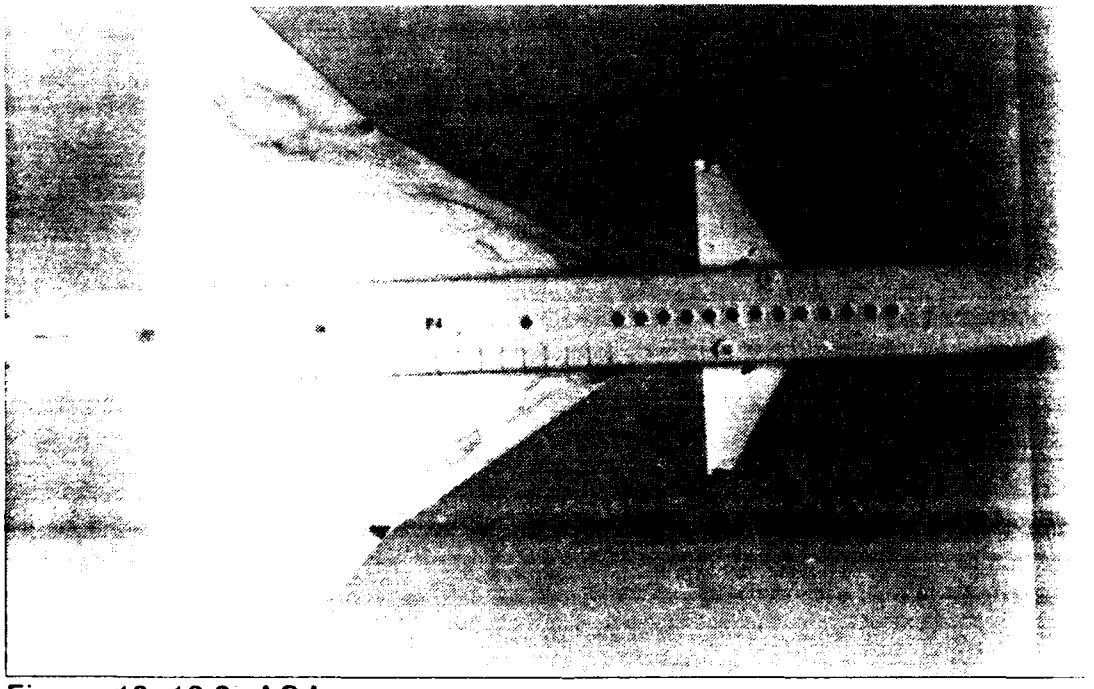

Figure 13. 12.2° AOA

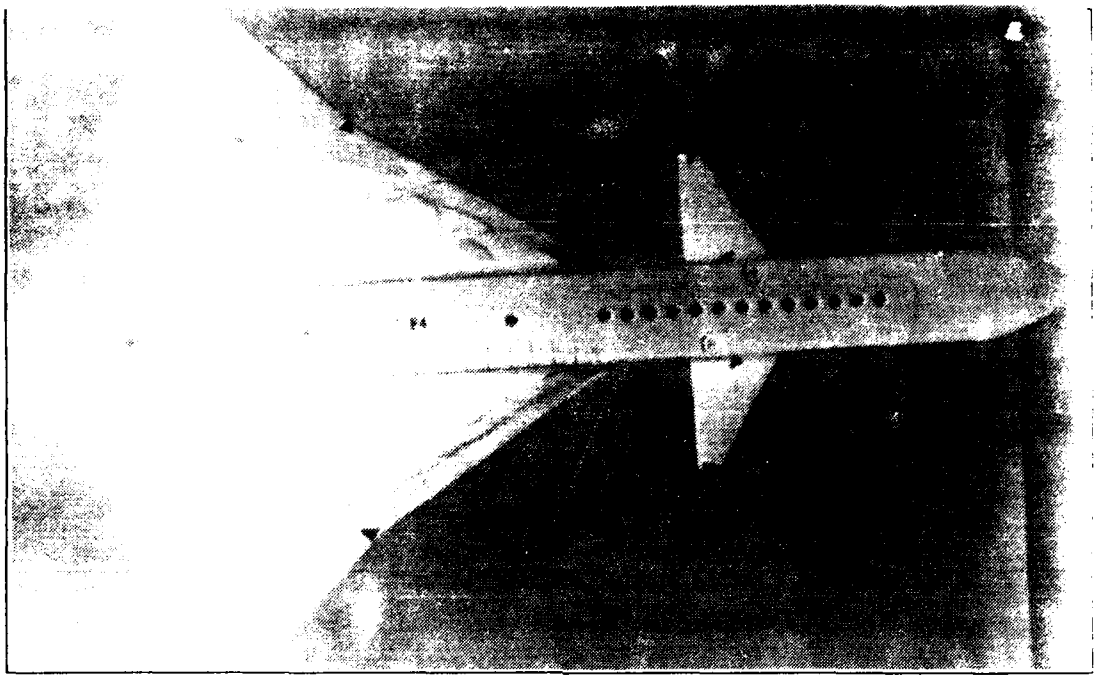

Figure 14. 12.5° AOA

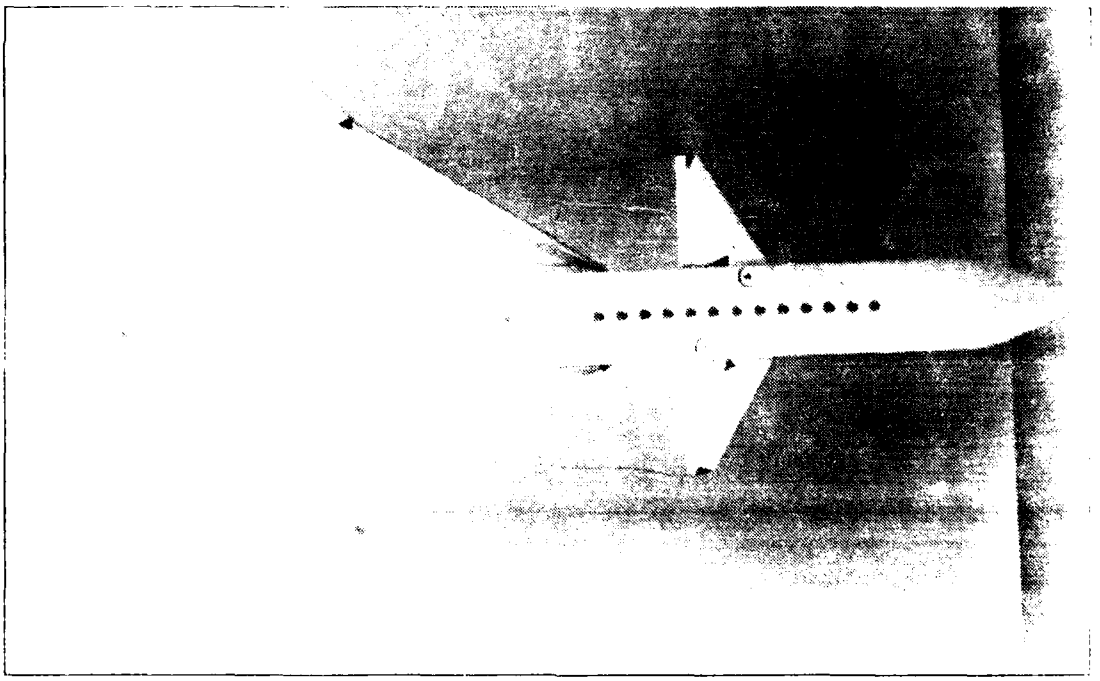

Figure 15. 13.5° AOA

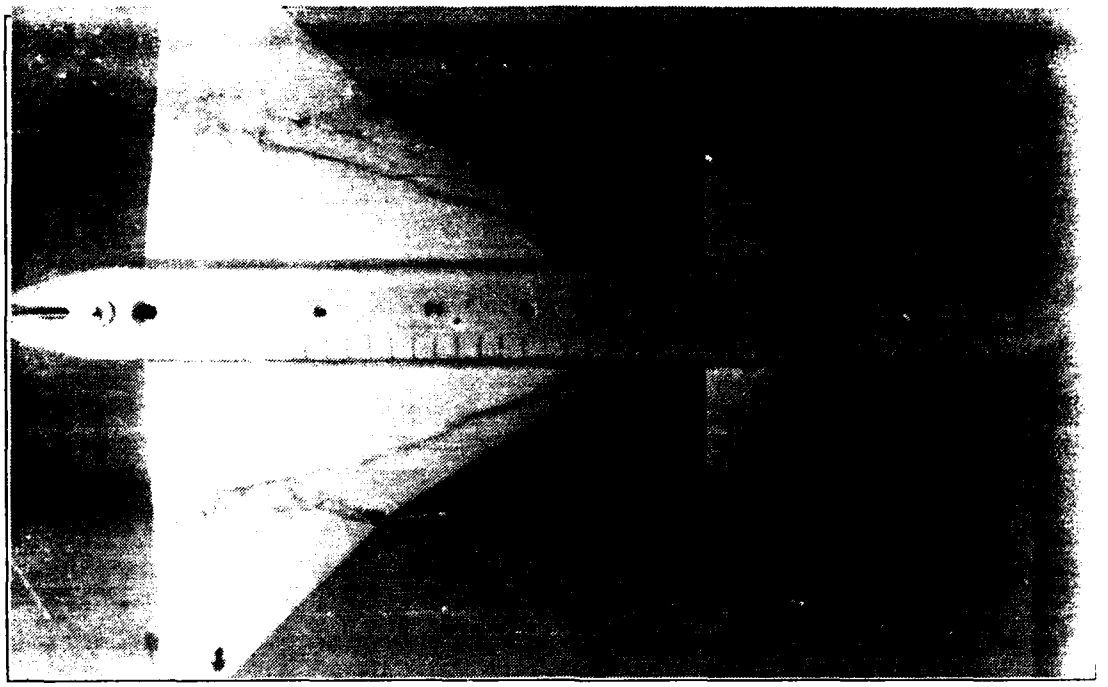

Figure 16. 14.0° AOA

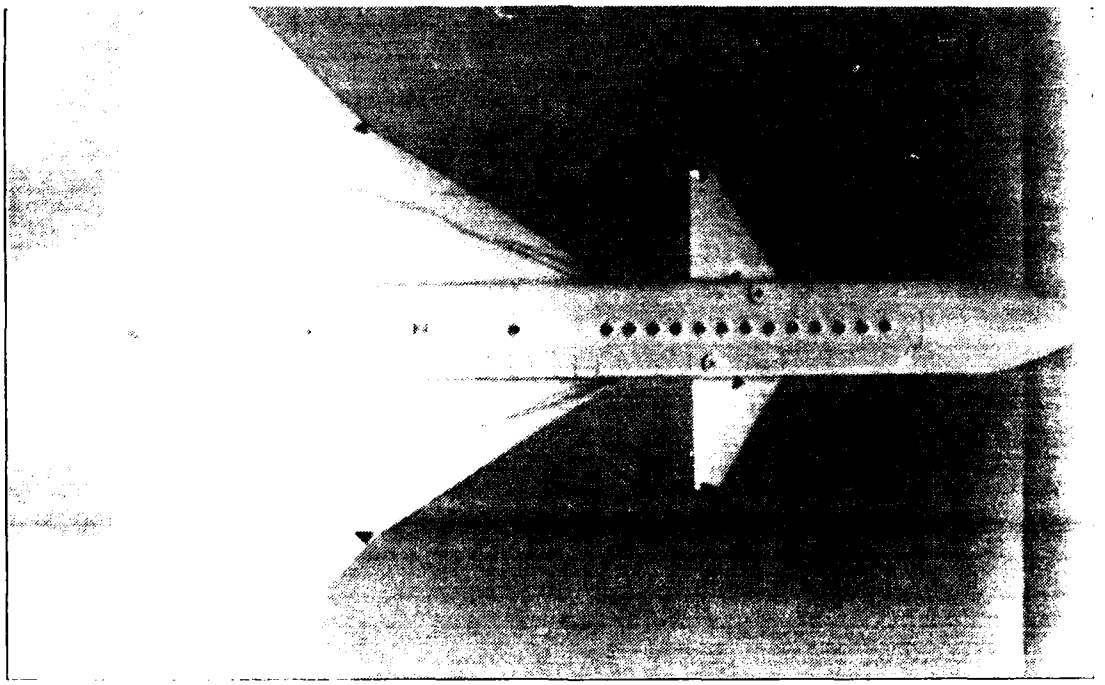

Figure 17. 15° AOA

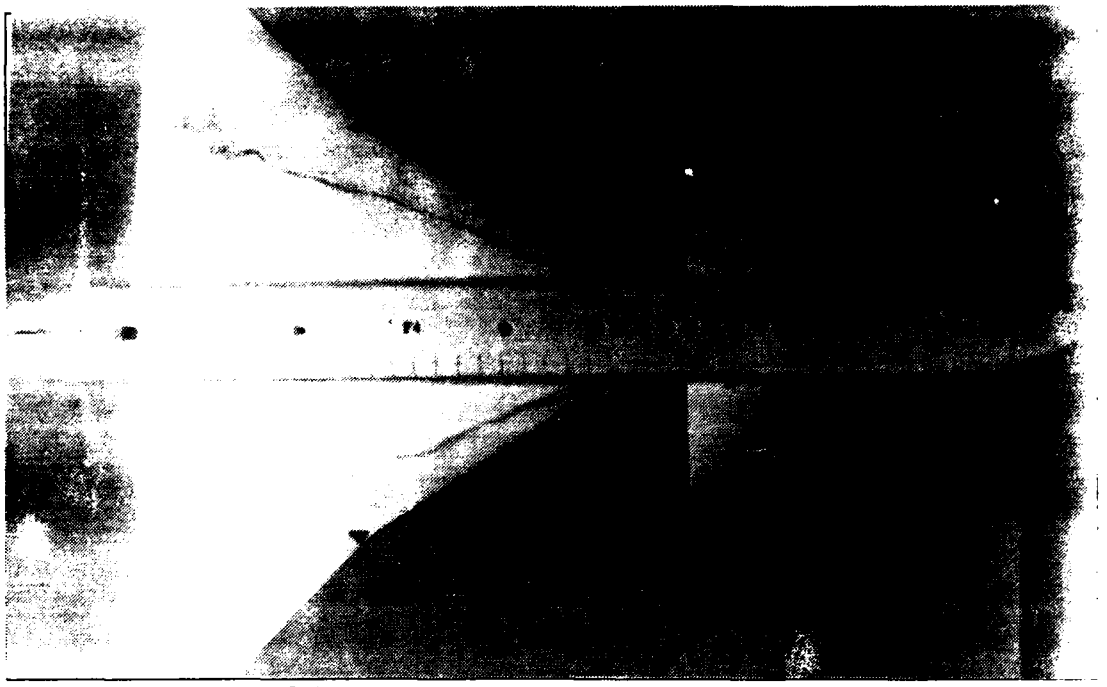

Figure 18. 17.5° AOA

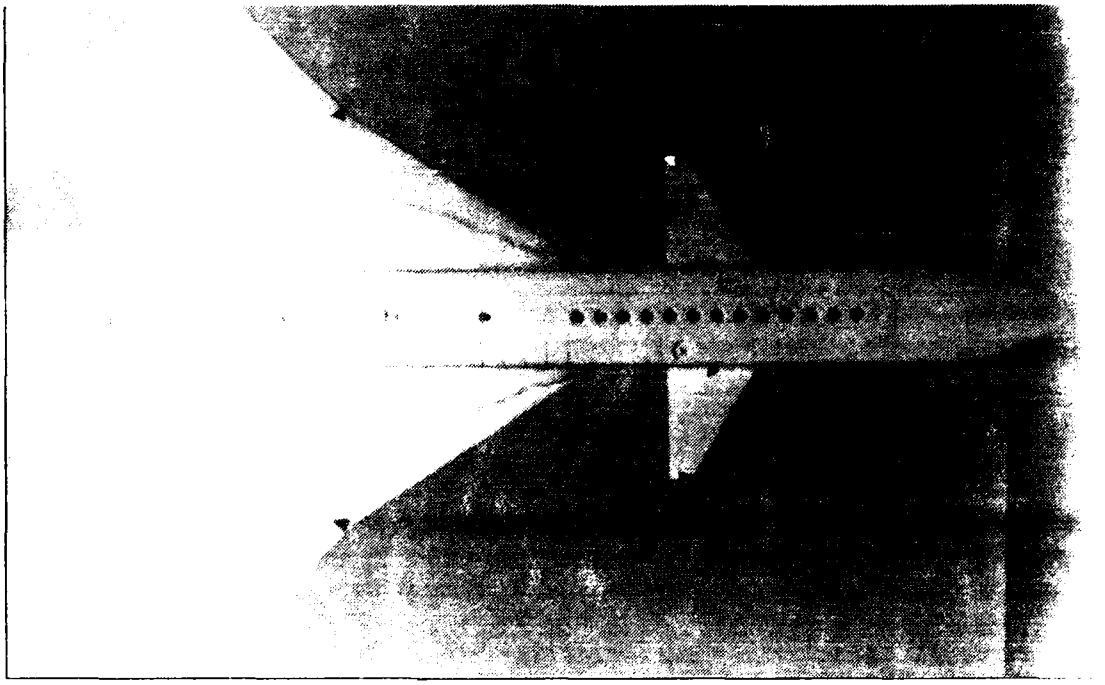

Figure 19. 20° AOA

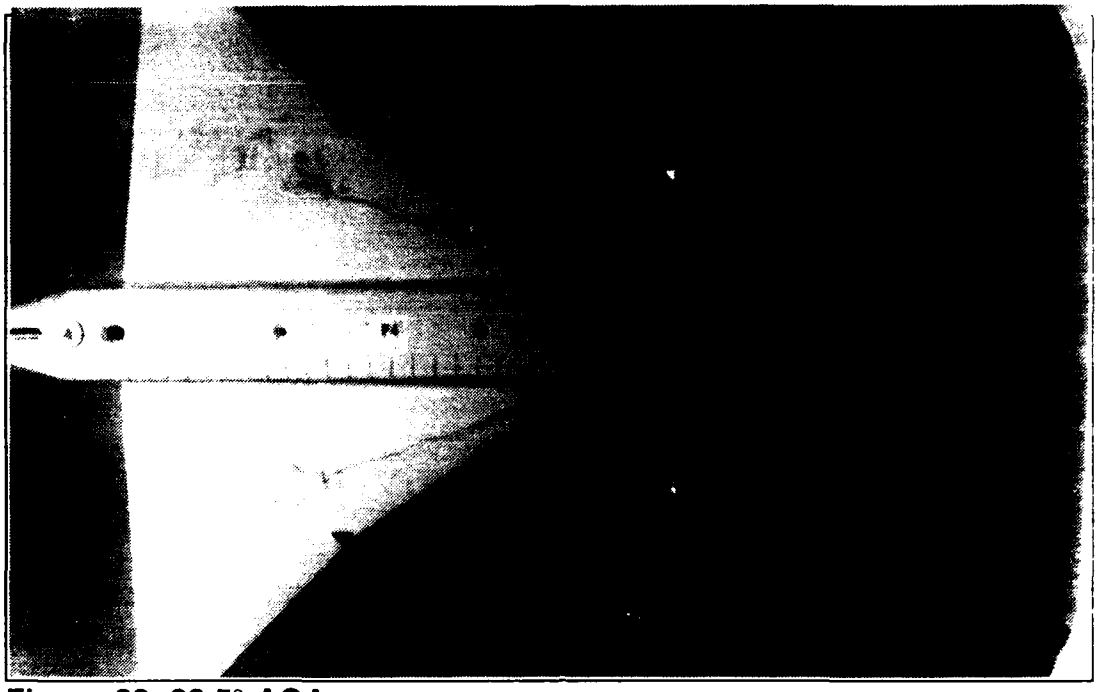

Figure 20. 22.5° AOA

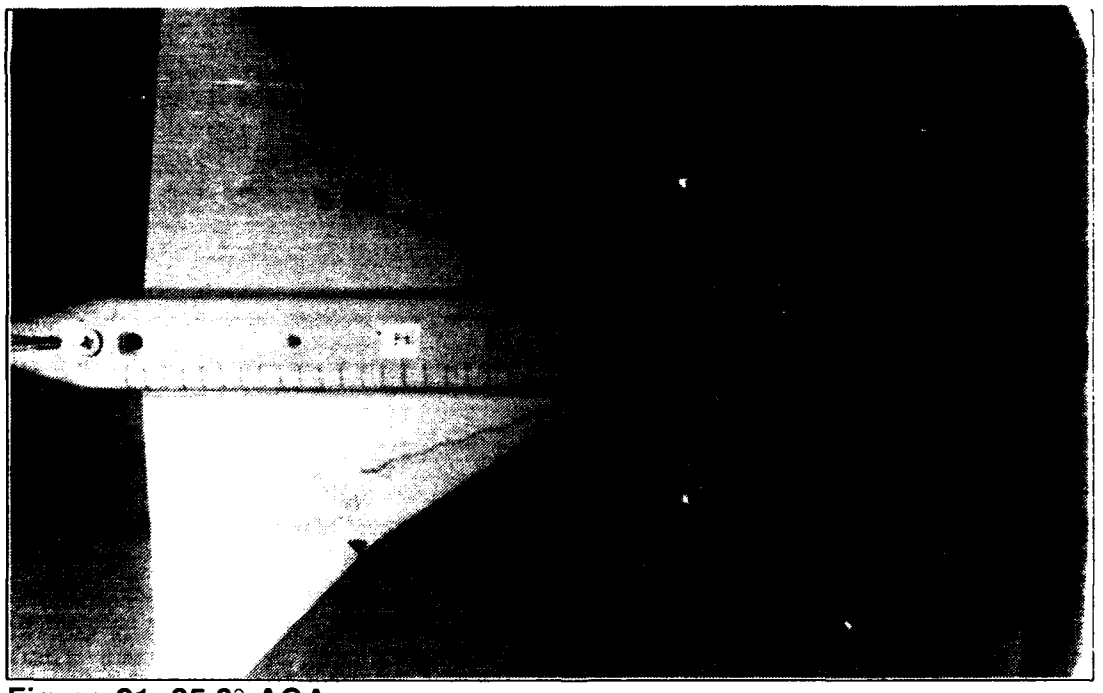

Figure 21. 25.0° AOA

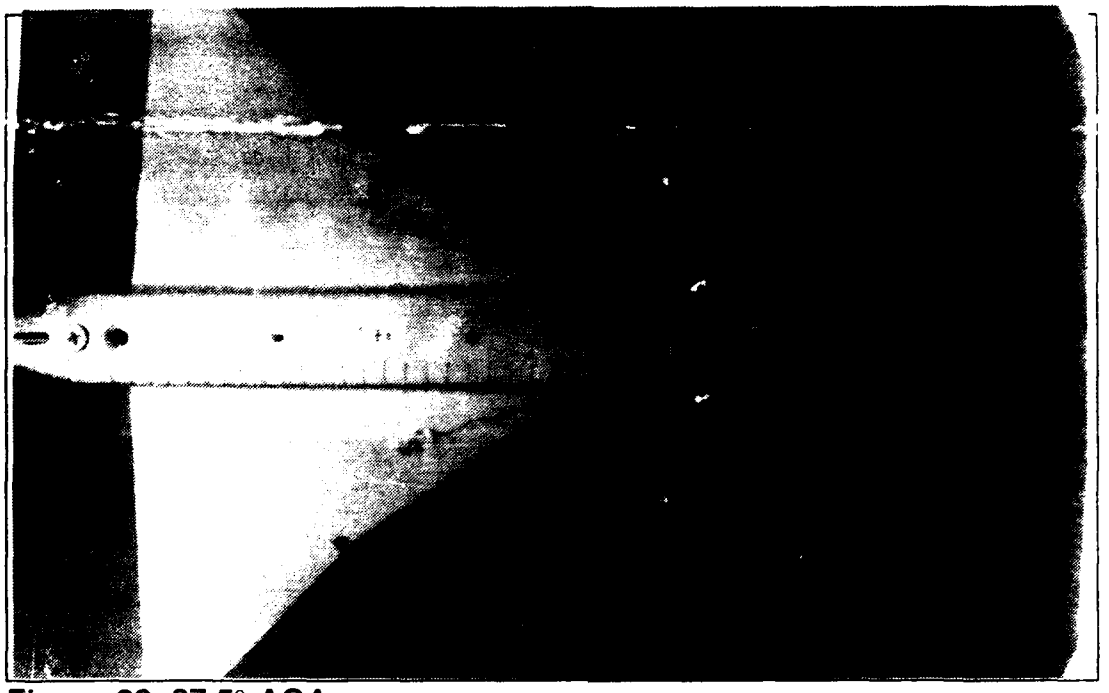

Figure 22. 27.5° AOA

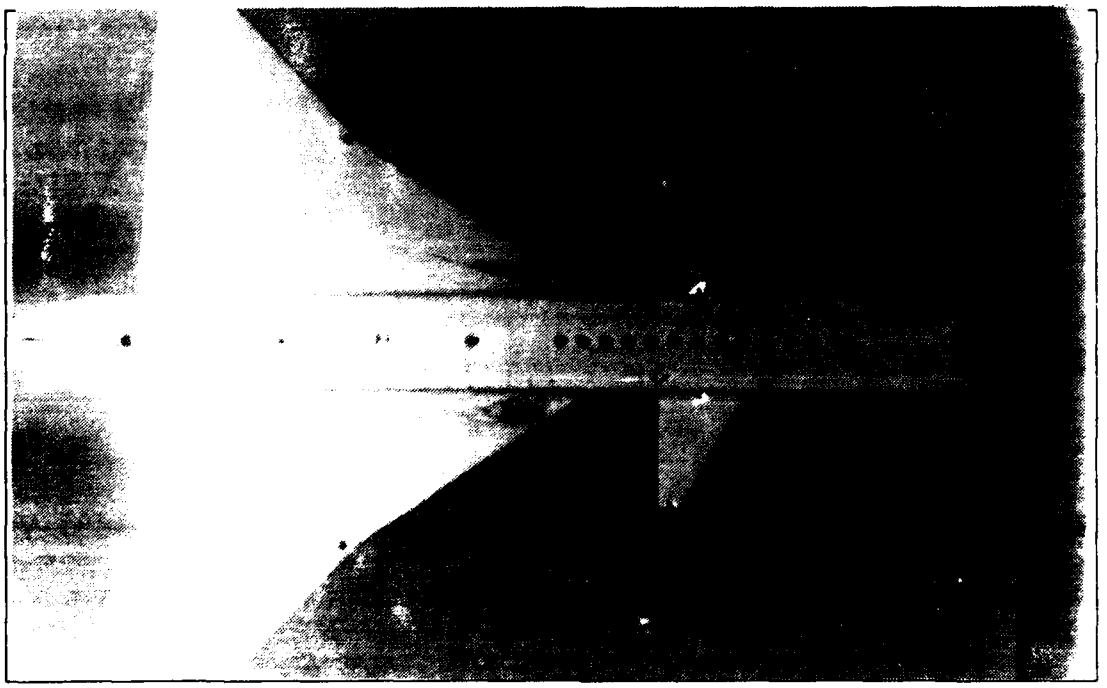

Figure 23. 30.0° AOA

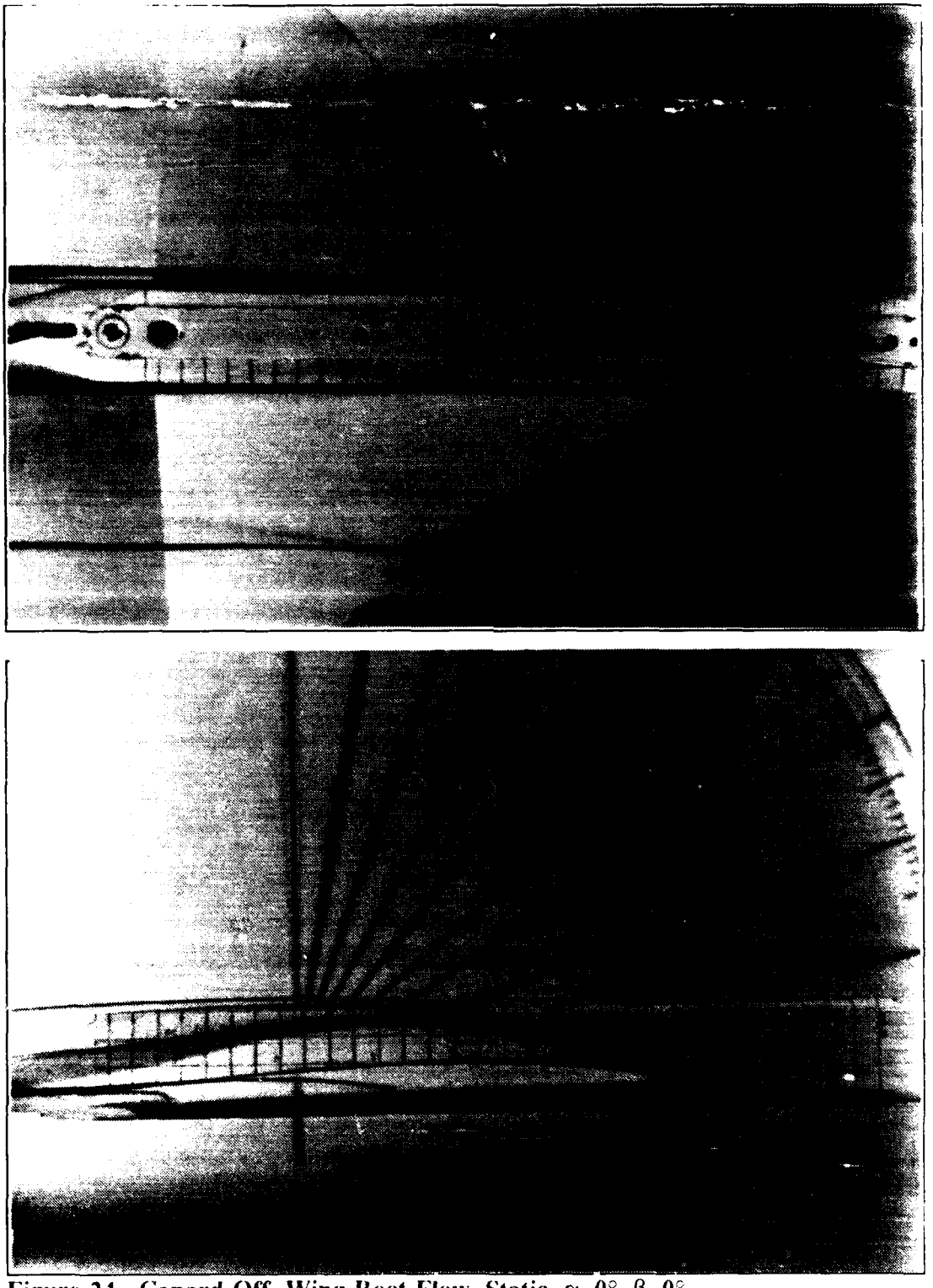

Figure 24. Canard Off, Wing Root Flow, Static, $\alpha=0^\circ$, $\beta=0^\circ$

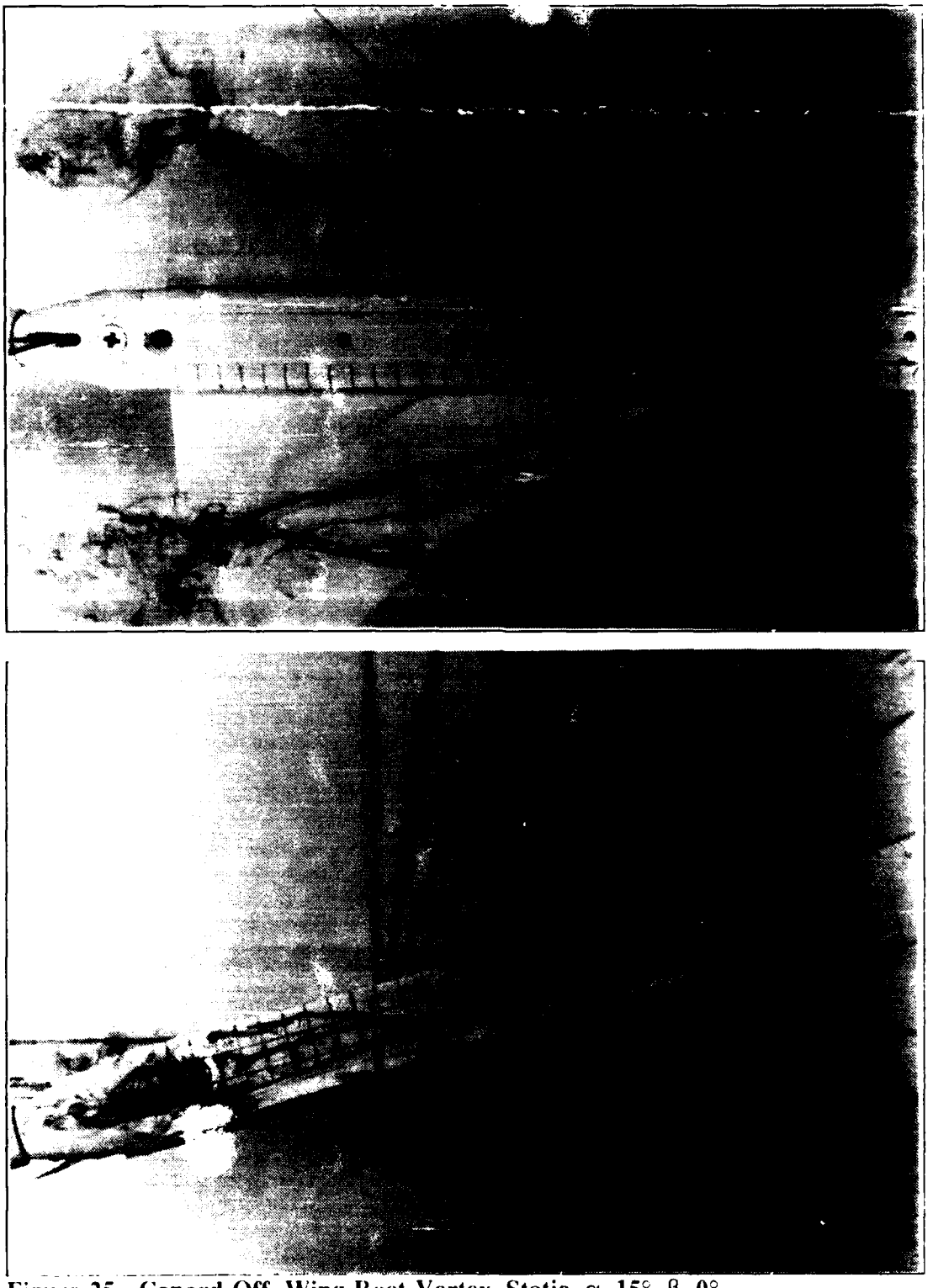

Figure 25. Canard Off, Wing Root Vortex, Static, α=15°, β=0°

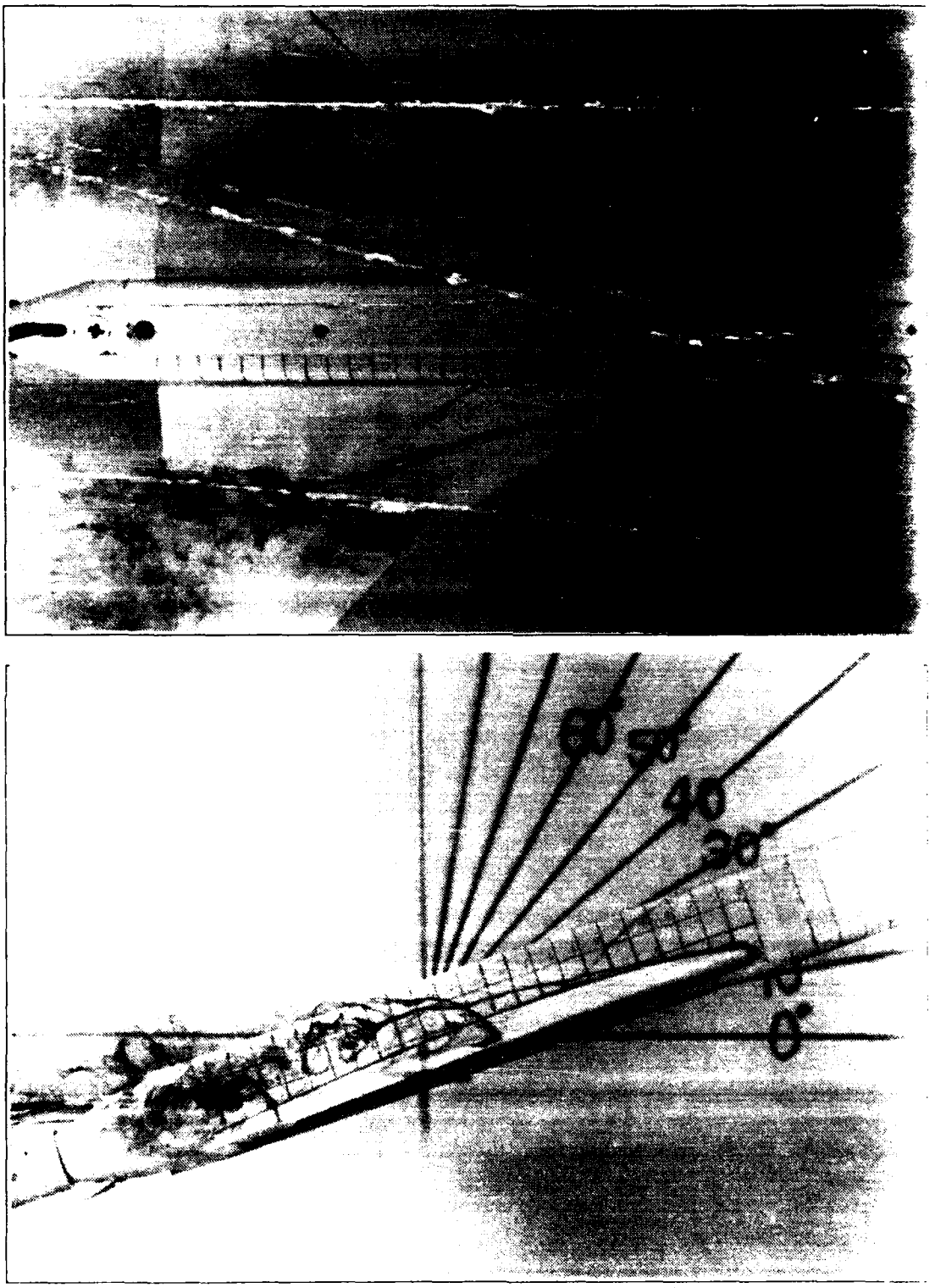

Figure 26. Canard Off, Wing Root Vortex, Static, α=20°, β=0°

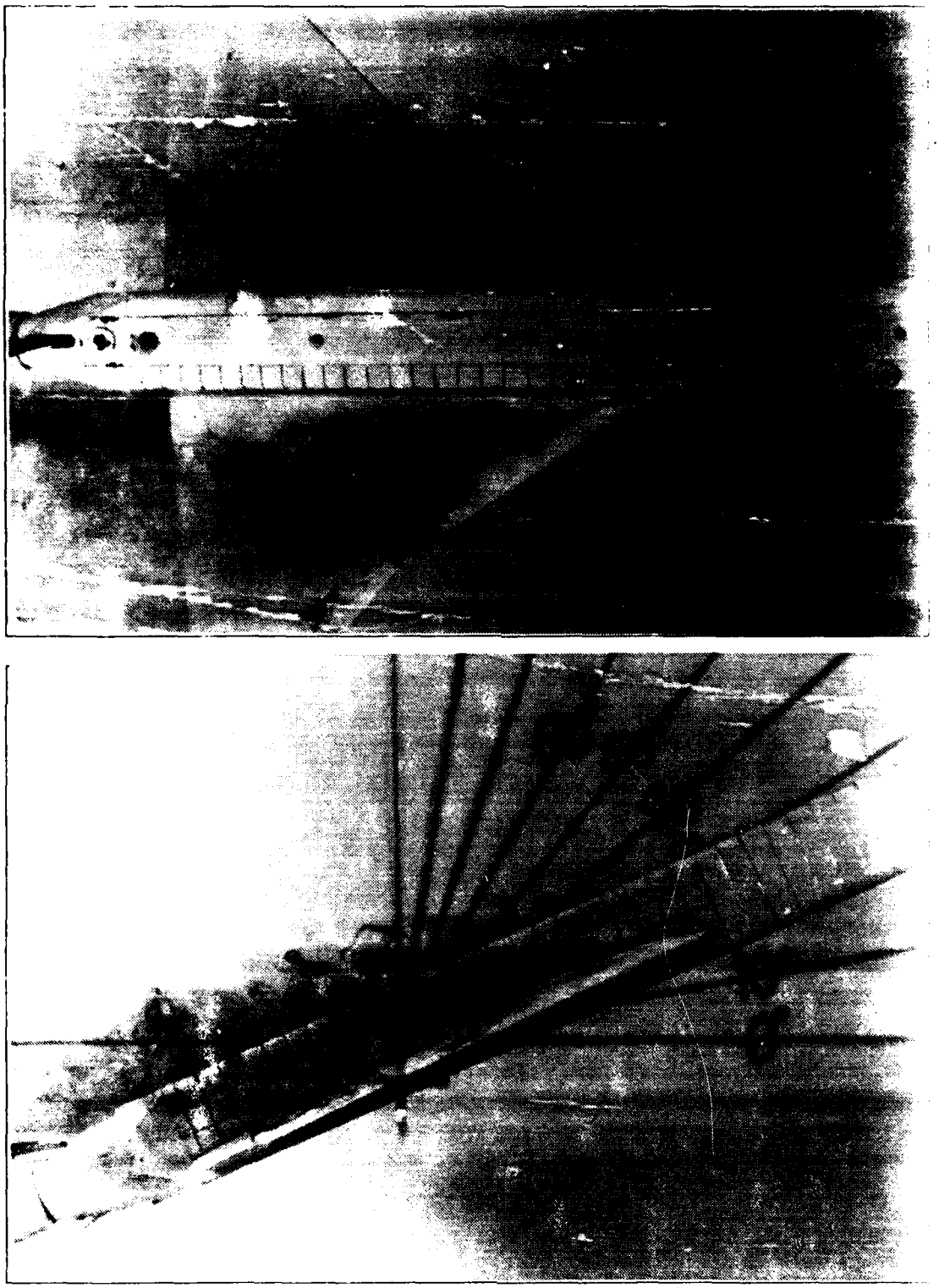

Figure 27. Canard Off, Wing Root Vortex, Static, α=25°, β=0

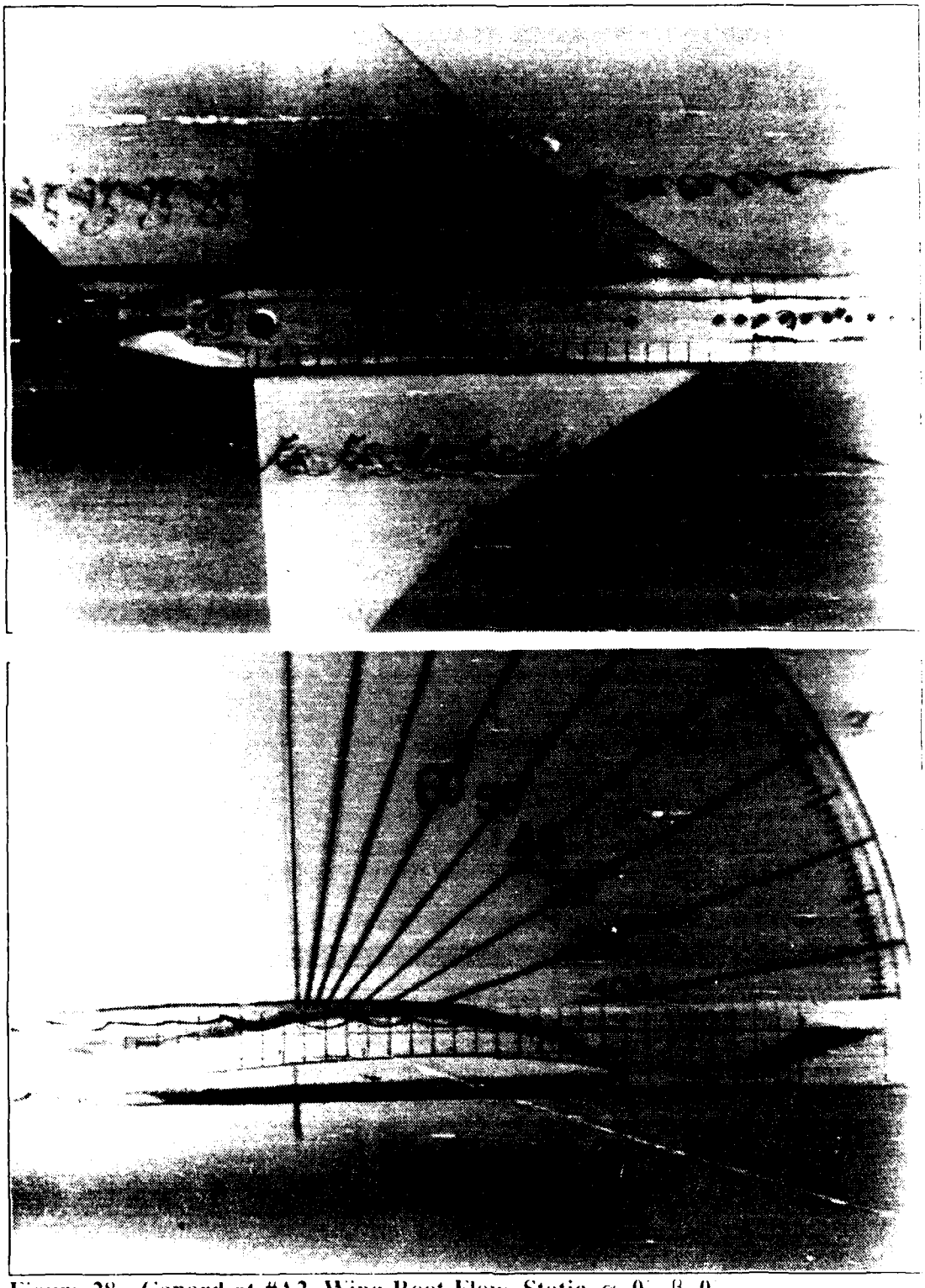

Figure 28. Canard at #A2, Wing Root Flow, Static, $\alpha=0^{\circ}$, $\beta=0^{\circ}$

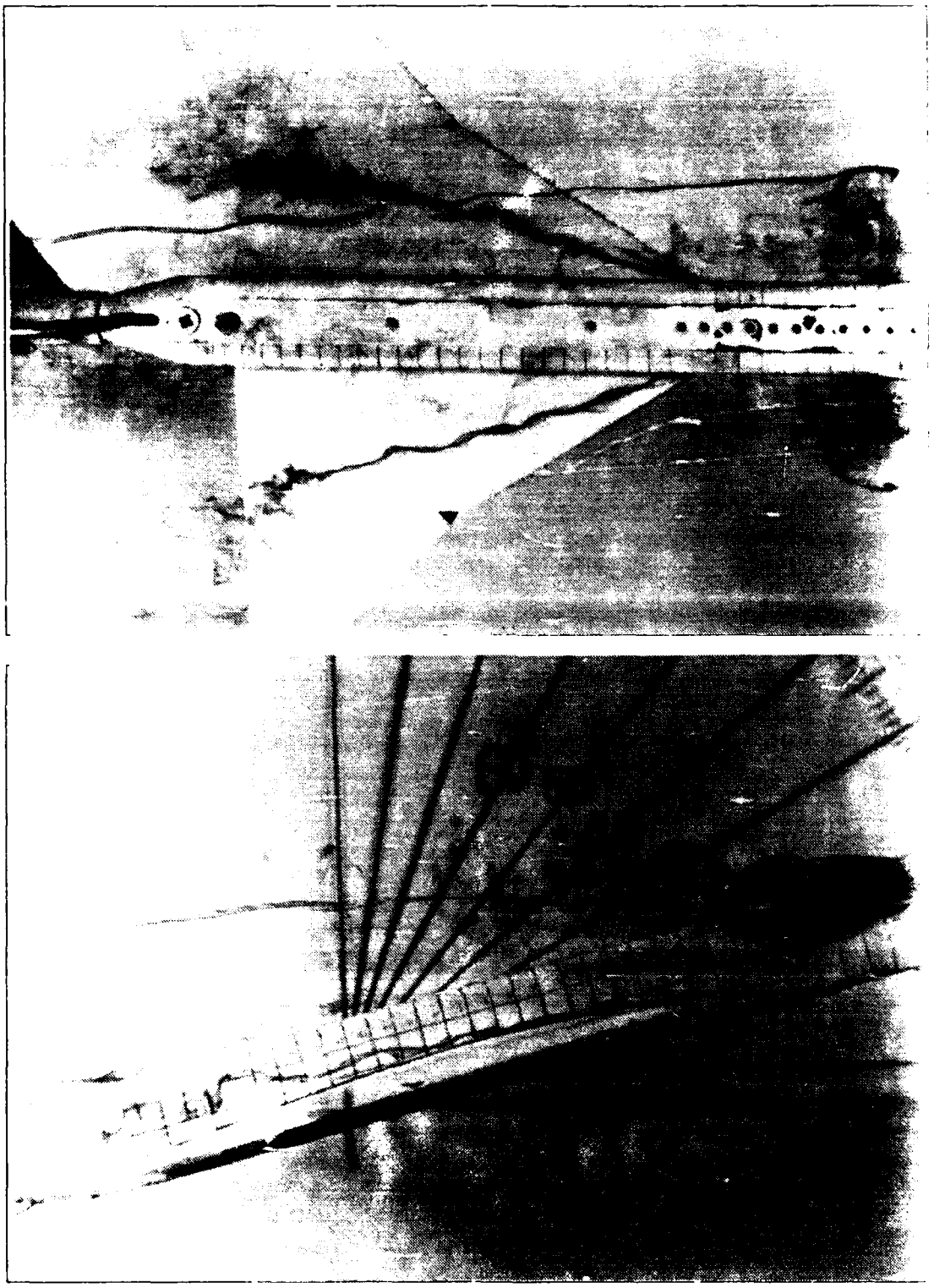

Figure 29. Canard at #A2, Wing Root Vortex, Static, α=15°, β=0

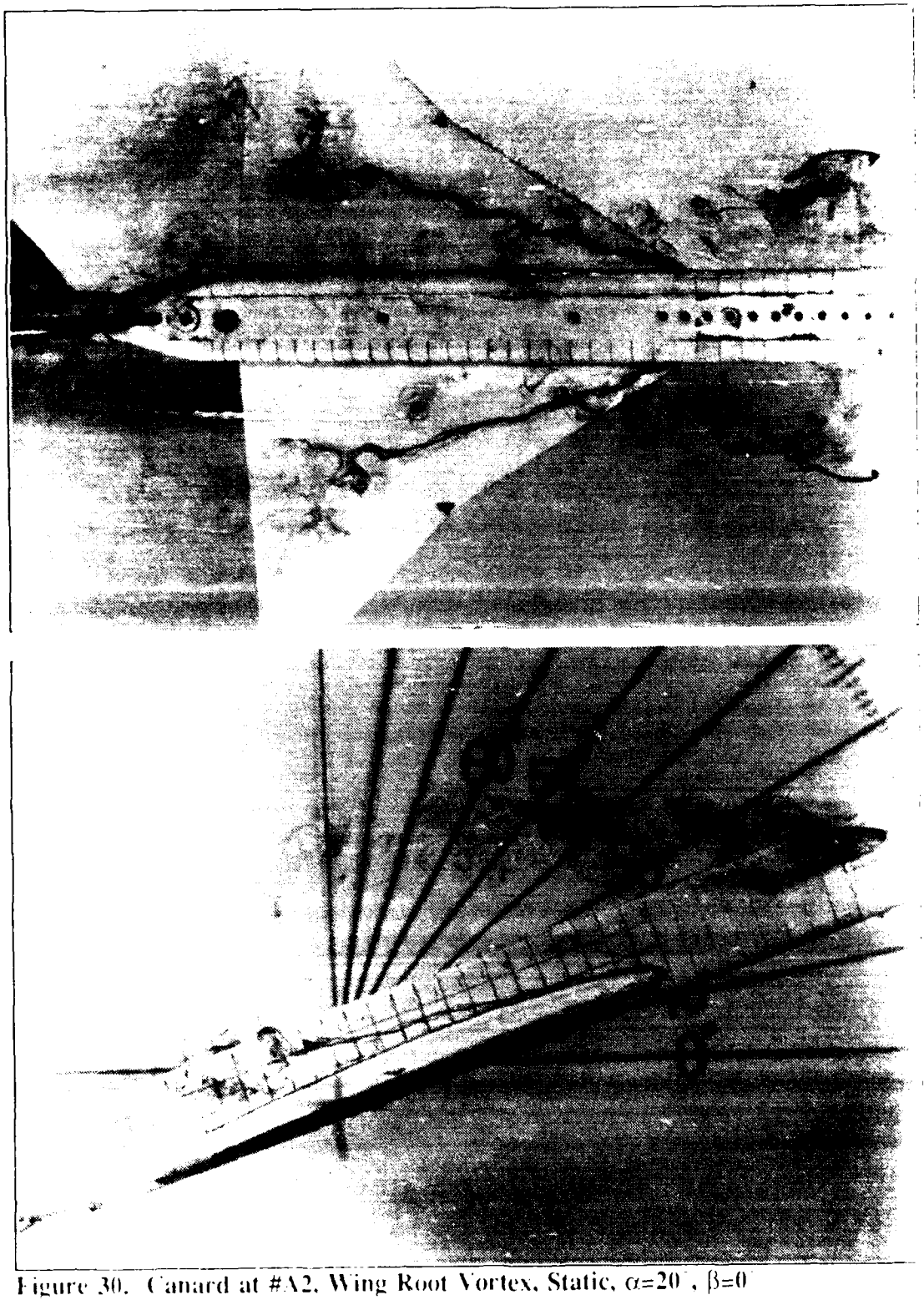

Figure 30. Canard at #A2, Wing Root Vortex, Static, α=20°, β=0°

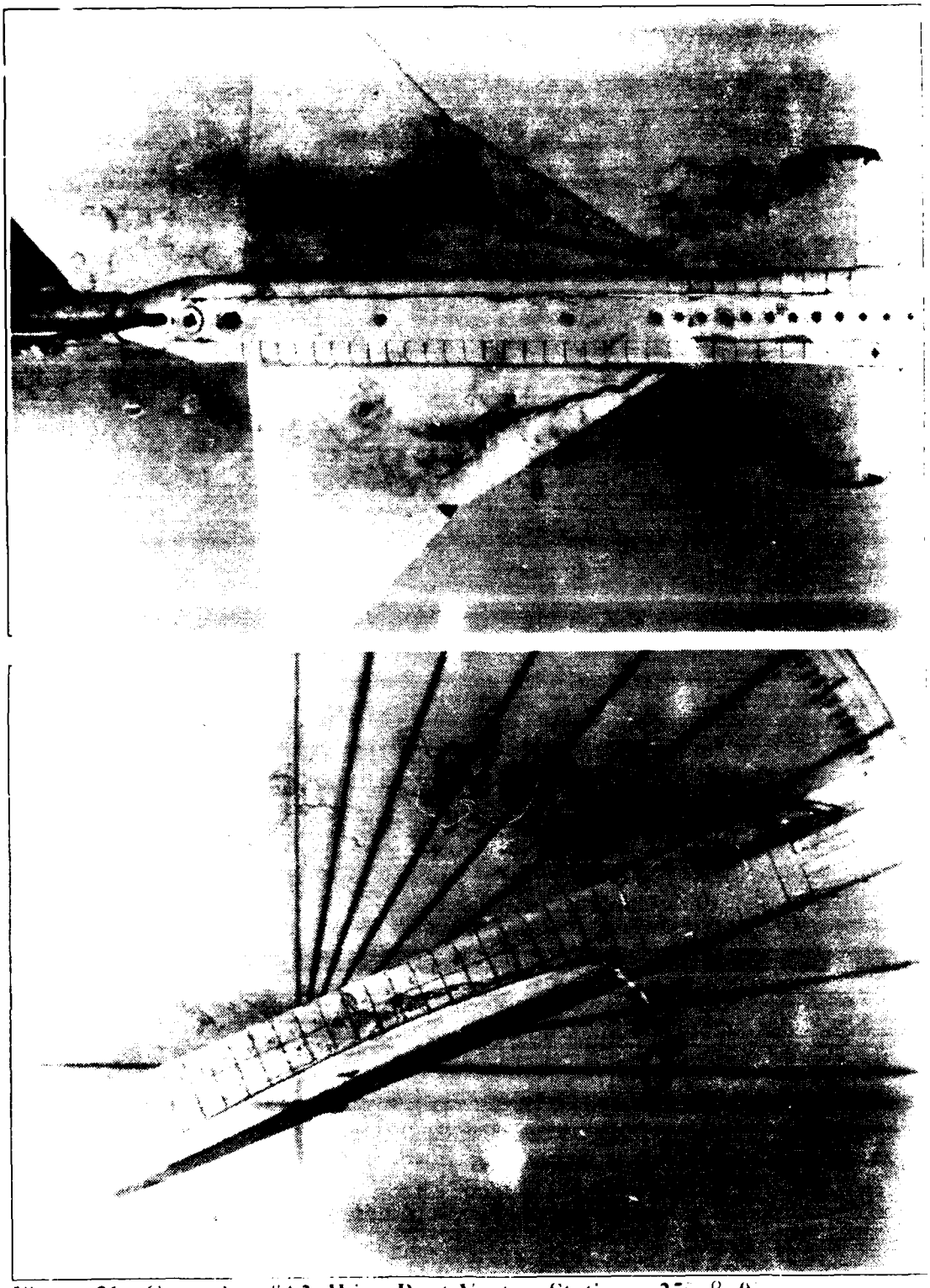

Figure 31. Canard #A2, Wing Root Vortex, Static, α=25°, β=0

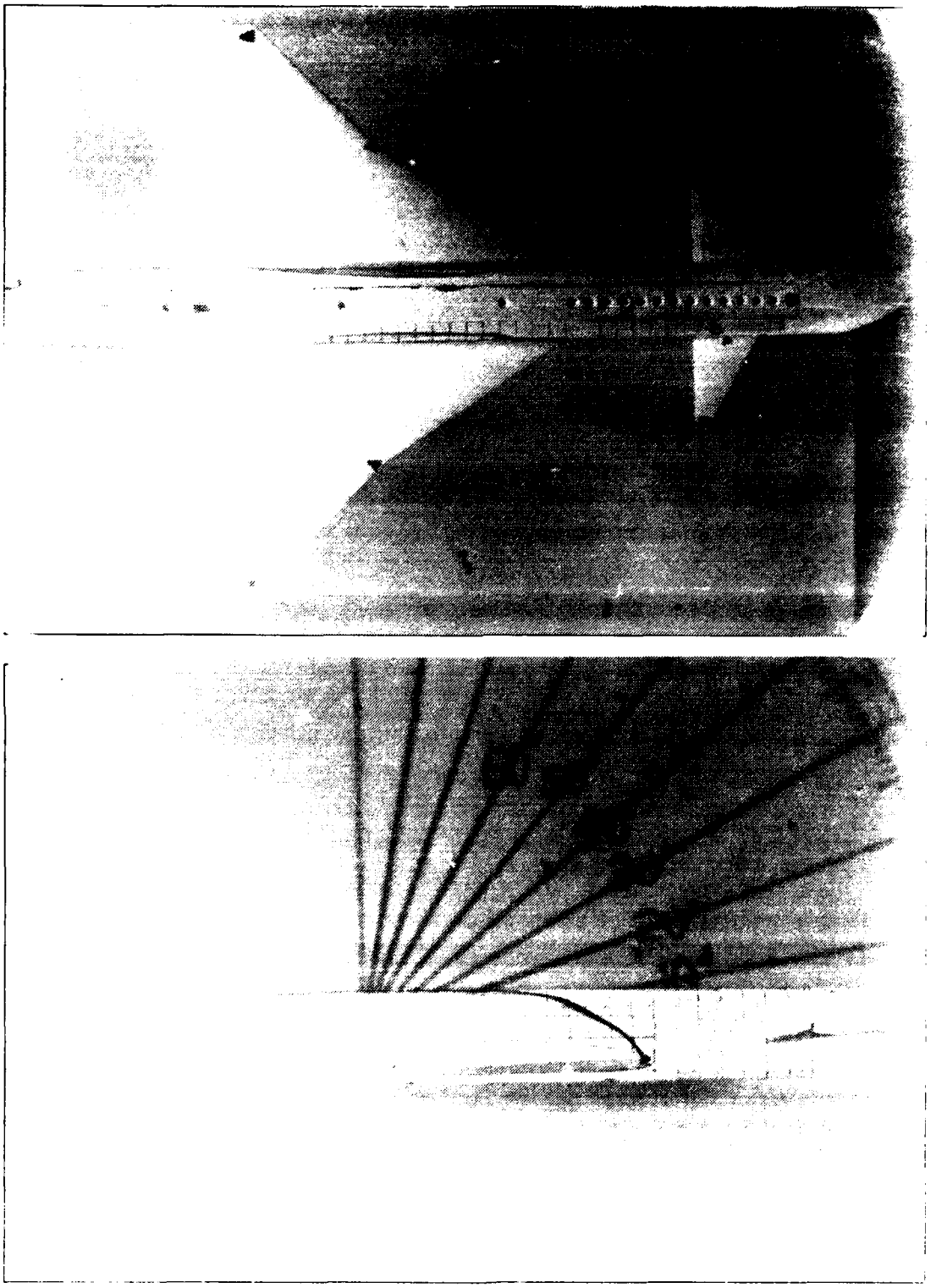

Figure 32. Canard at #B3, Wing Root Flow, Static, α=0°, β=0

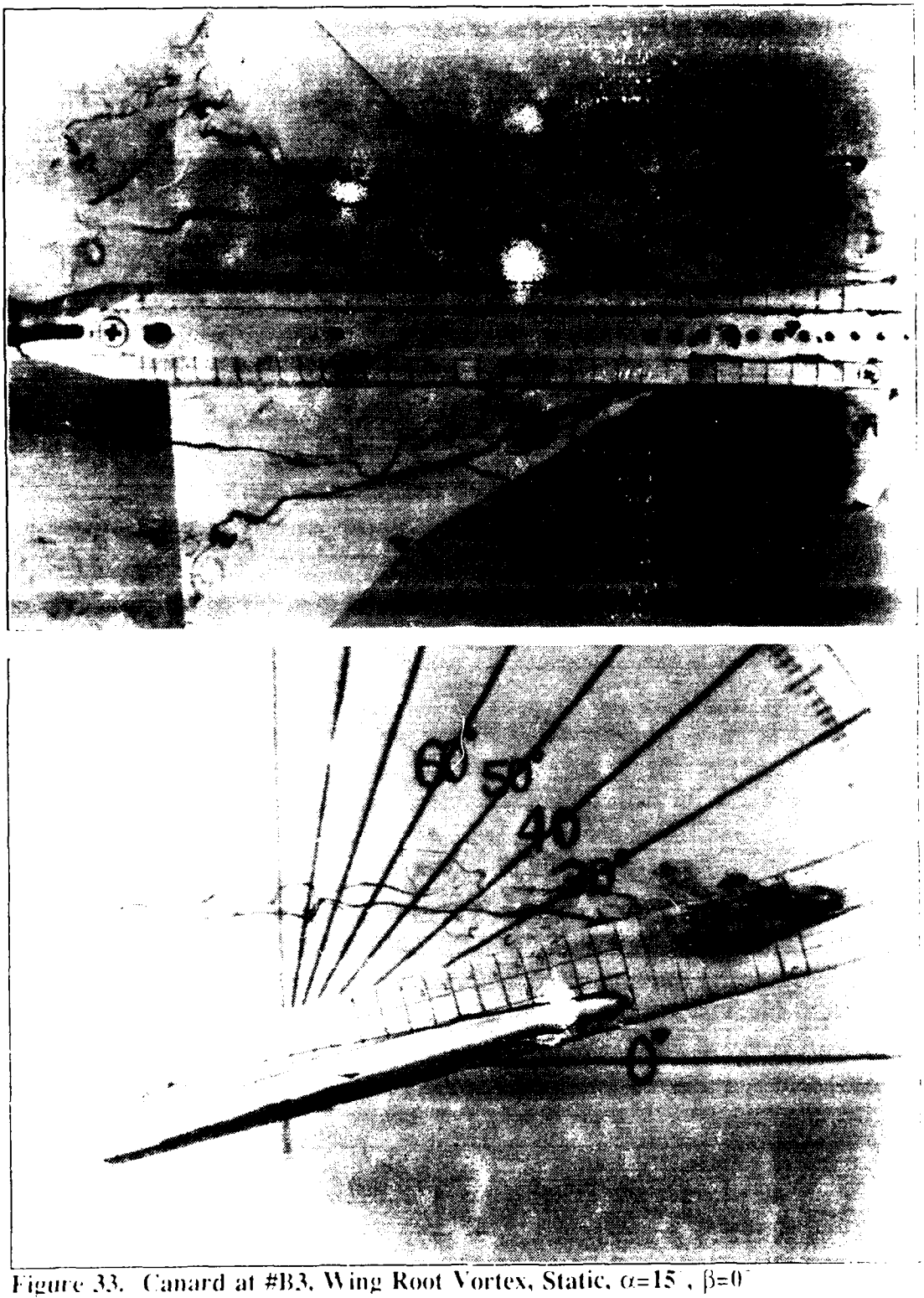

Figure 33. Canard at #B3, Wing Root Vortex, Static, α=15 , β=0

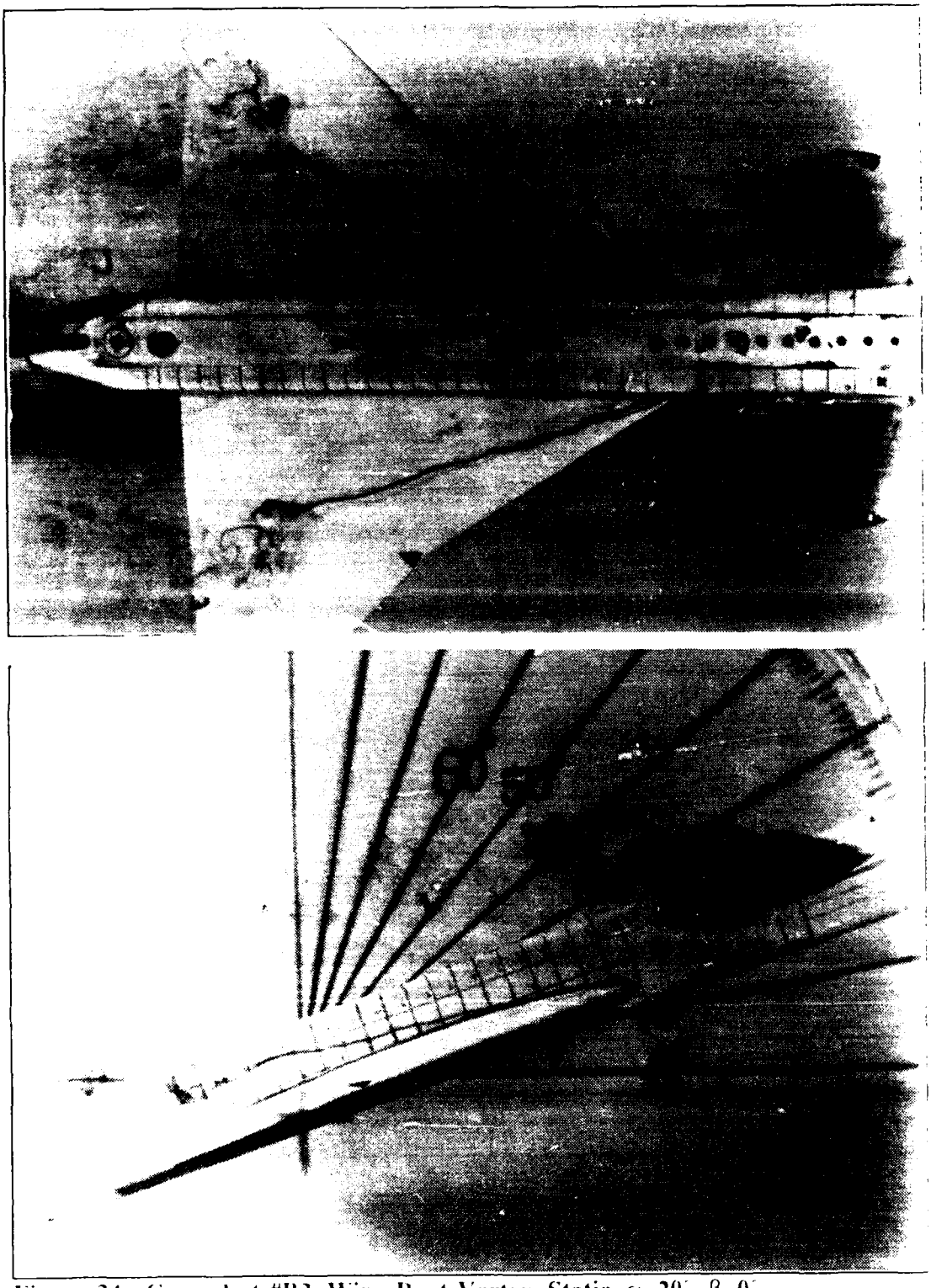

Figure 34. Canard at #B3, Wing Root Vortex, Static, α=20°, β=0°

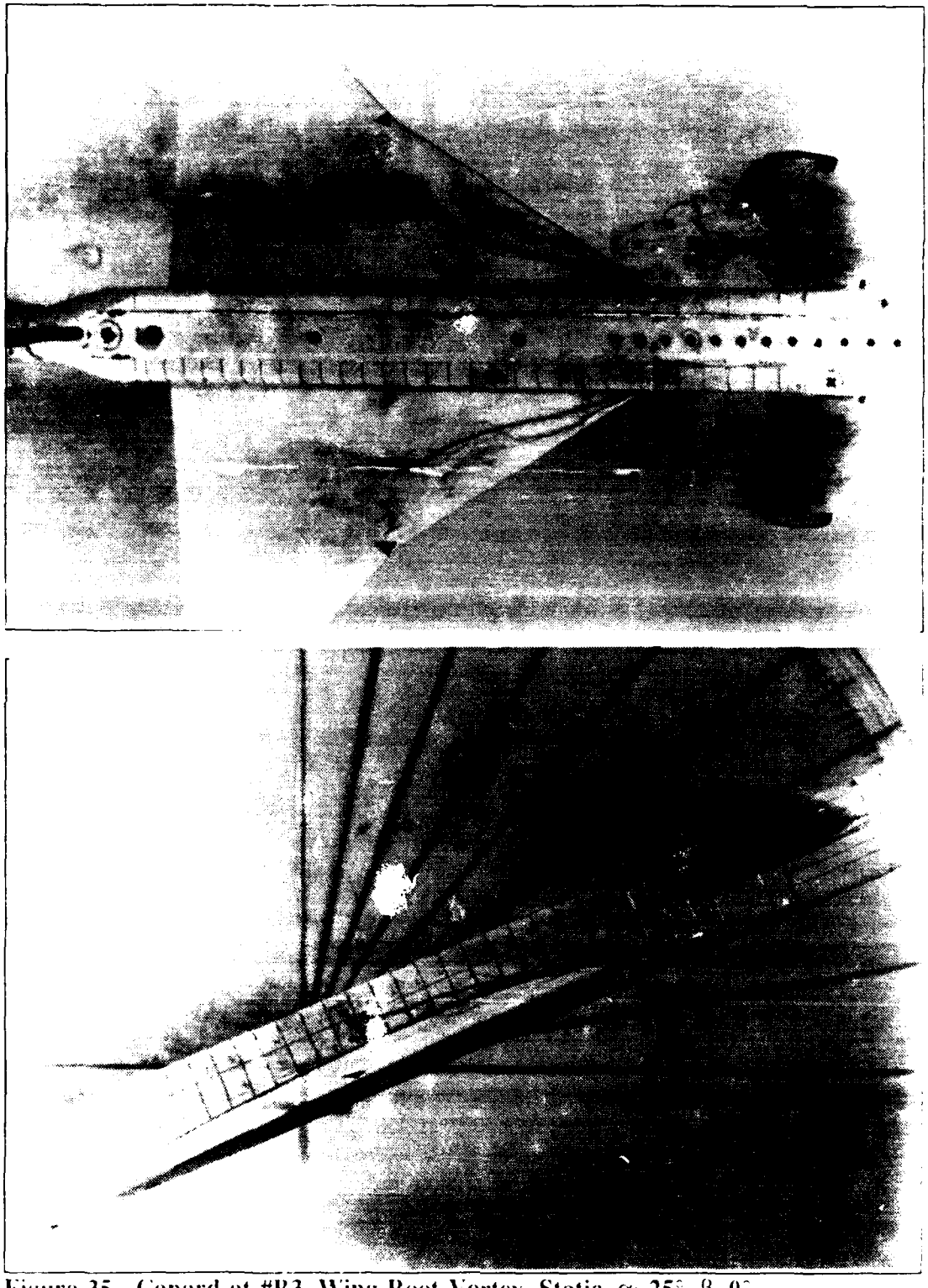

Figure 35. Canard at #B3, Wing Root Vortex, Static, α=25°, β=0°

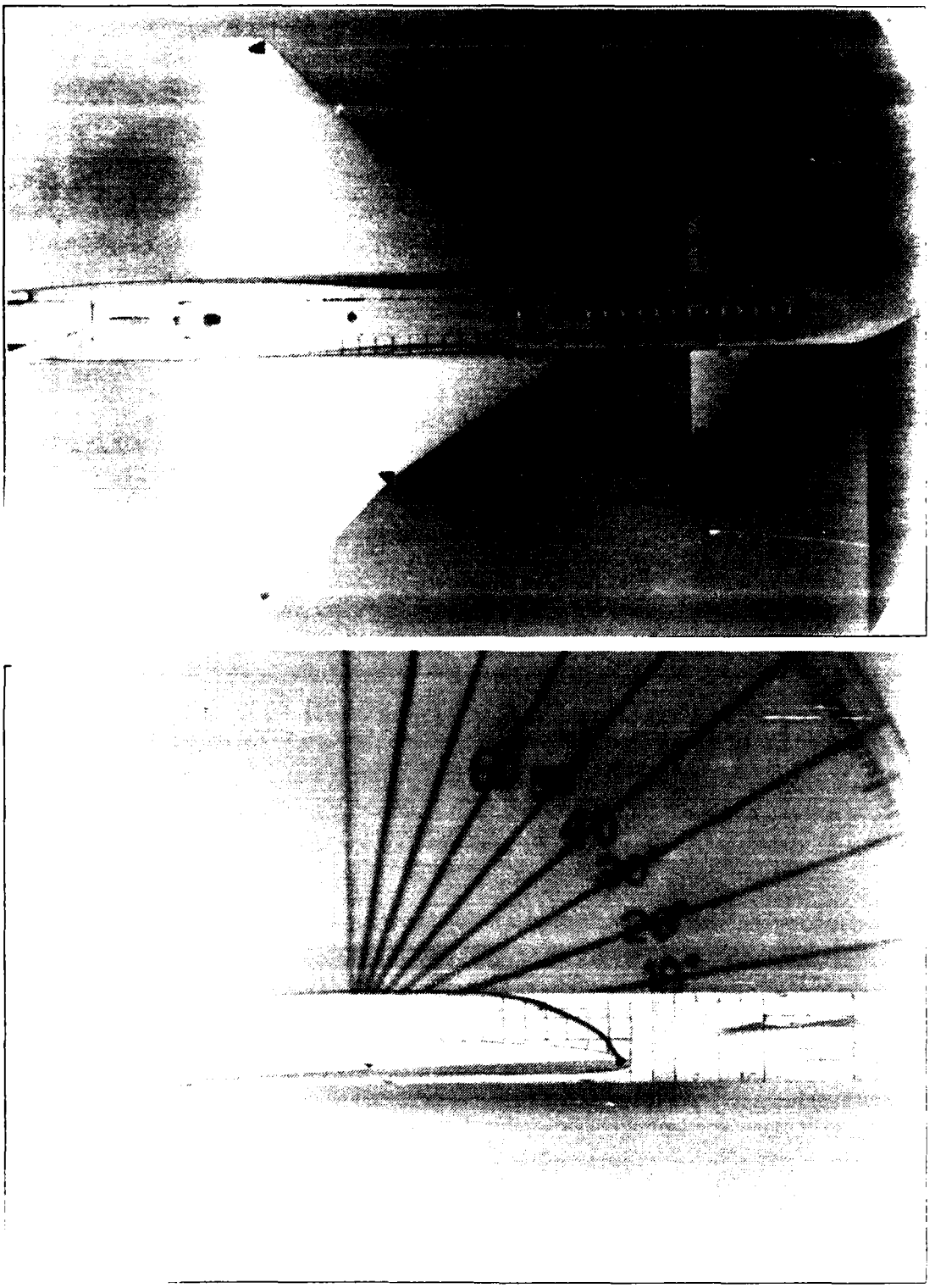

Figure 36. Canard at #C2, Wing Root Flow, Static, α=0°, β=0

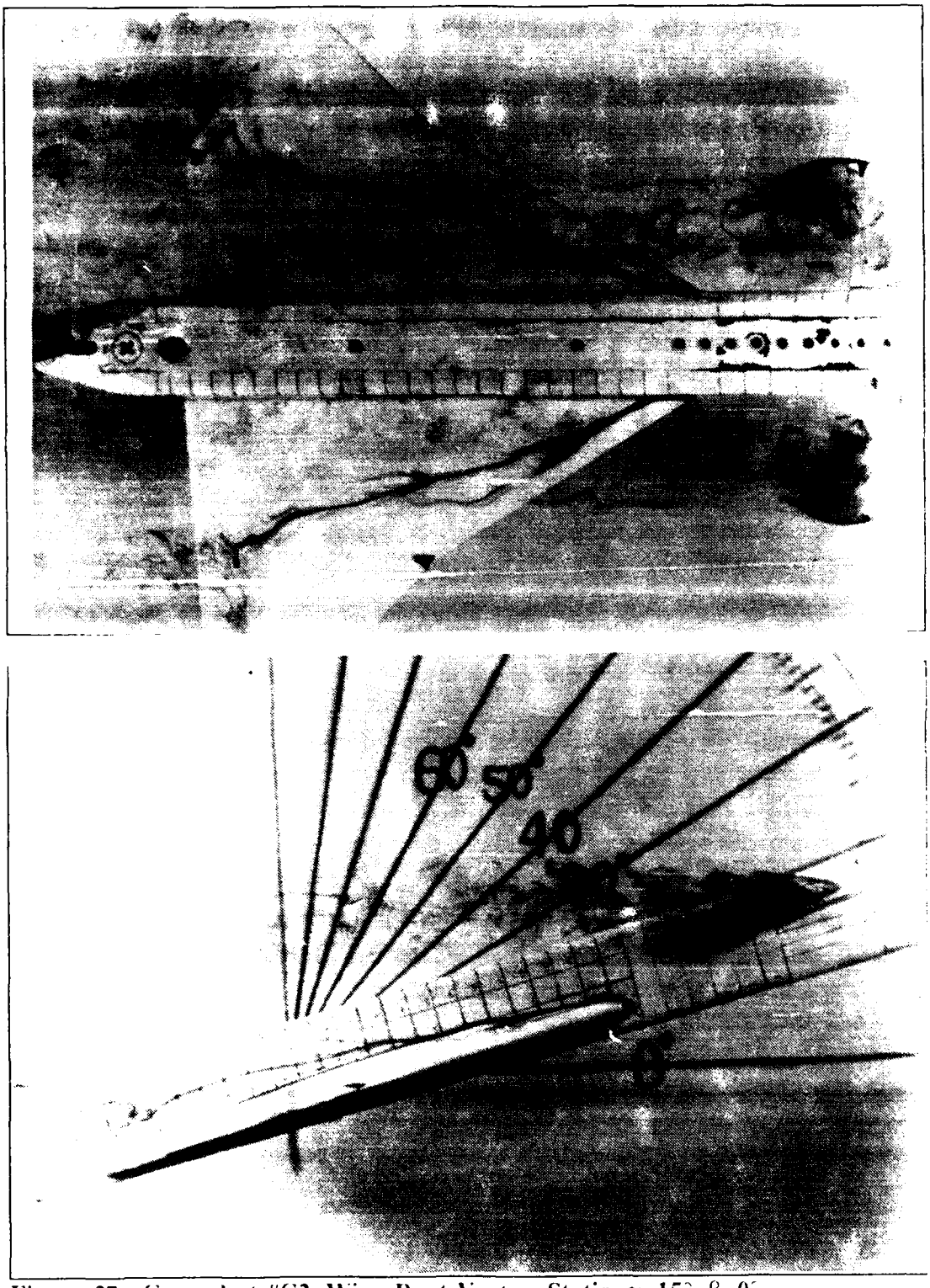

Figure 37. Canard at #C2, Wing Root Vortex, Static, α=15°, β=0°

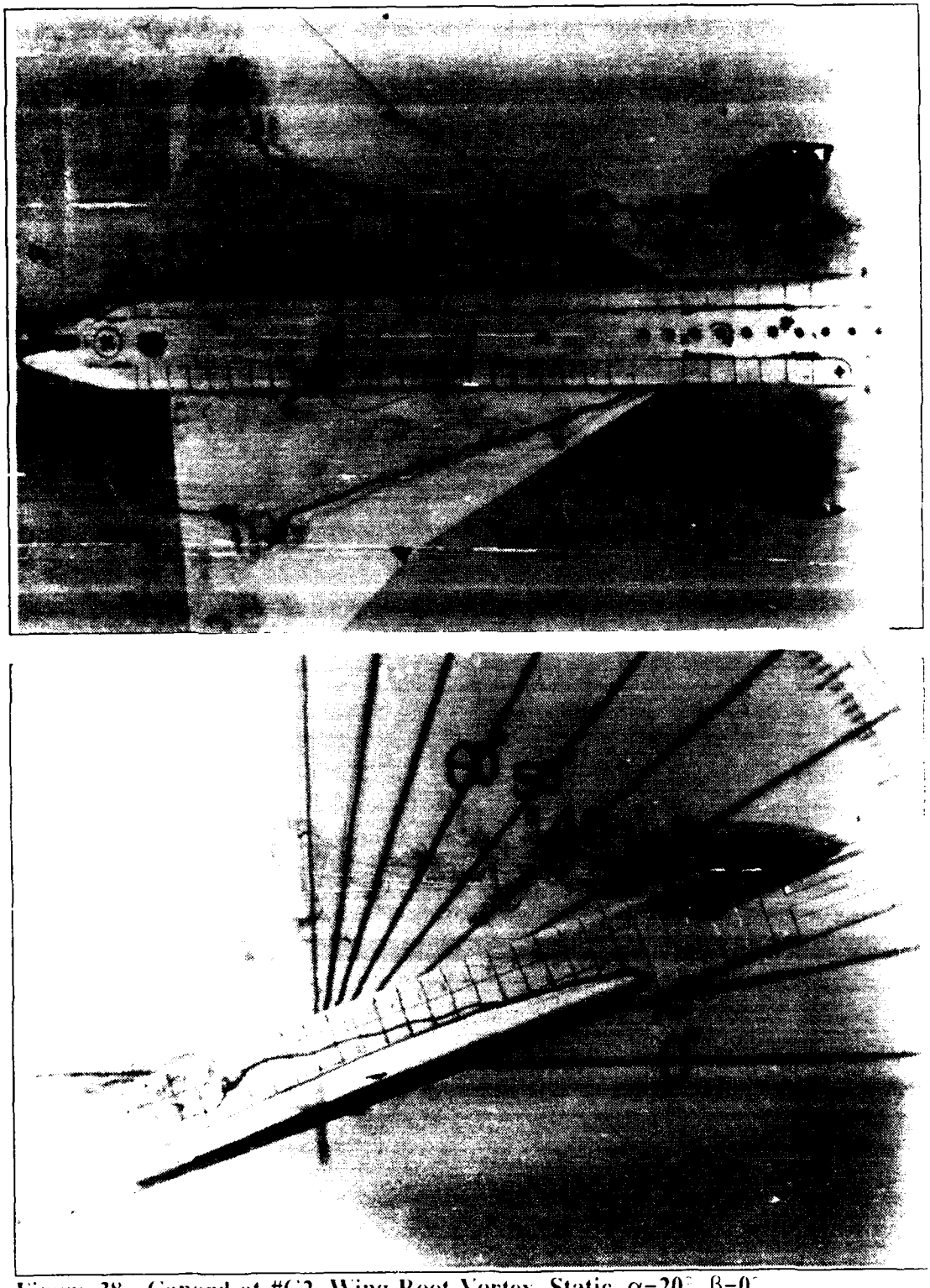

Figure 38. Canard at #C2, Wing Root Vortex, Static, $\alpha=20^{\circ}$, $\beta=0^{\circ}$

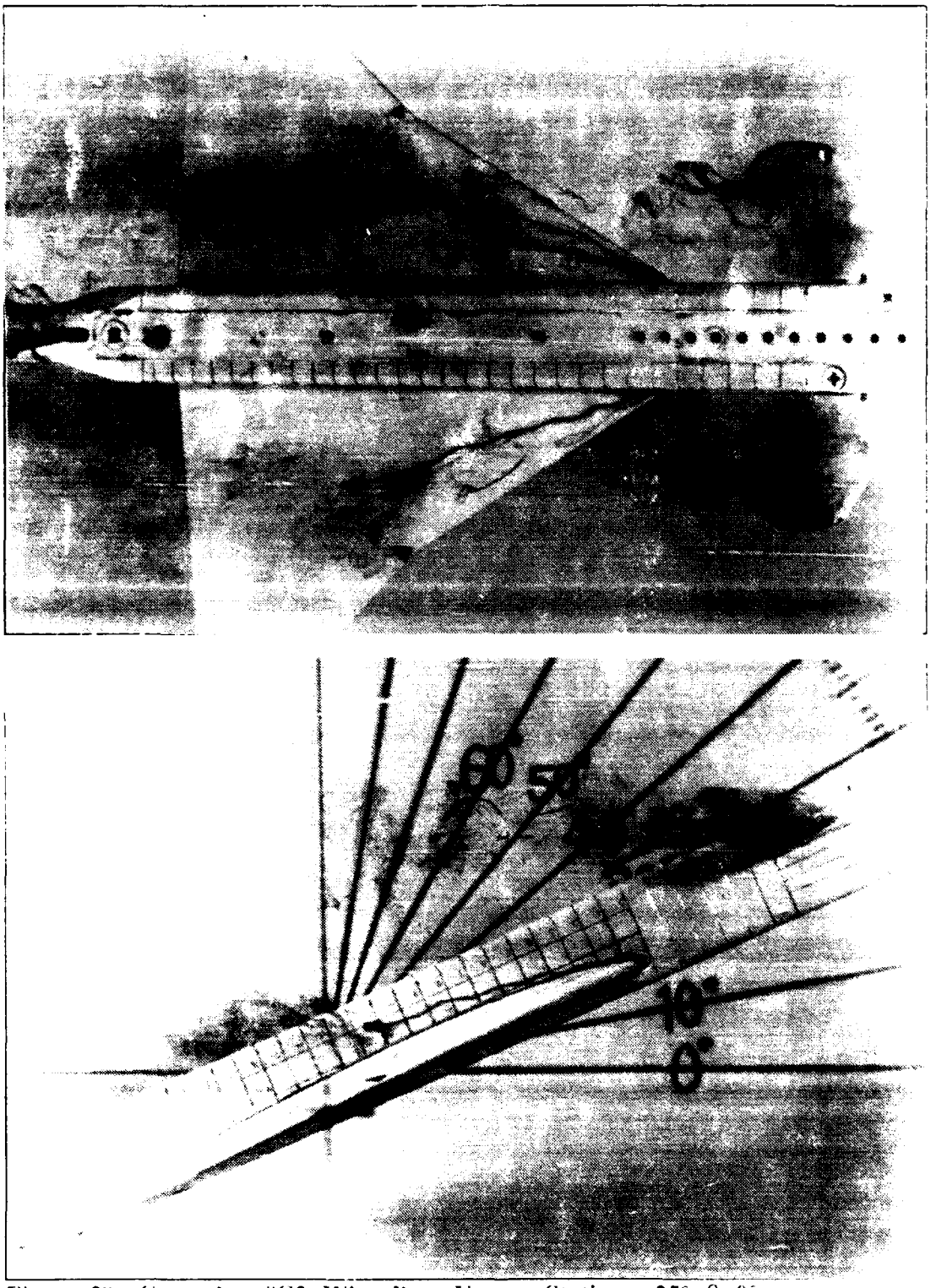

Figure 39. Canard at #C2, Wing Root Vortex, Static, $\alpha=25^{\circ}$, $\beta=0^{\circ}$

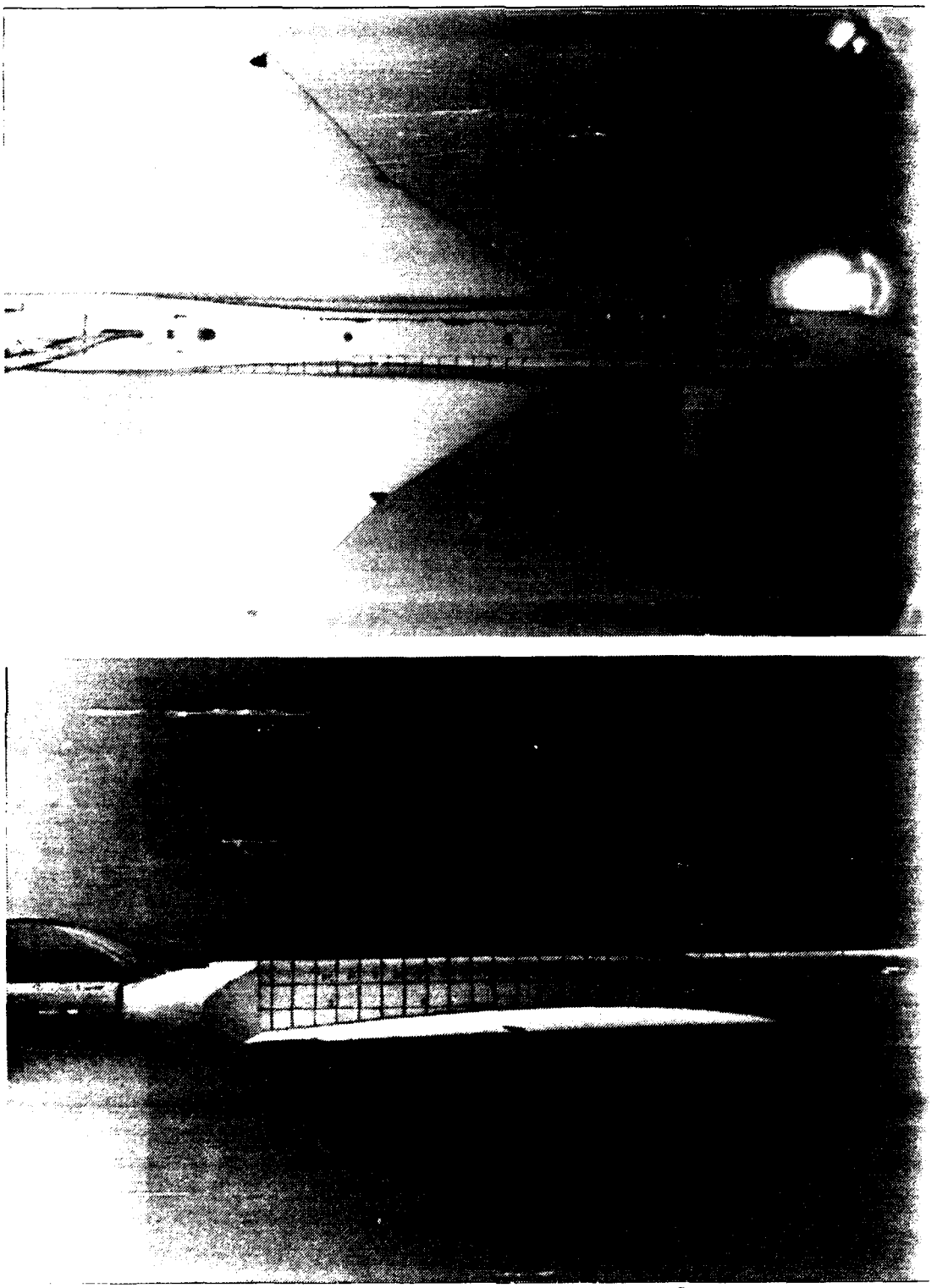

Figure 40. Canard at #C4, Wing Root Flow, Static, $\alpha=0^{\circ}$, $\beta=0^{\circ}$

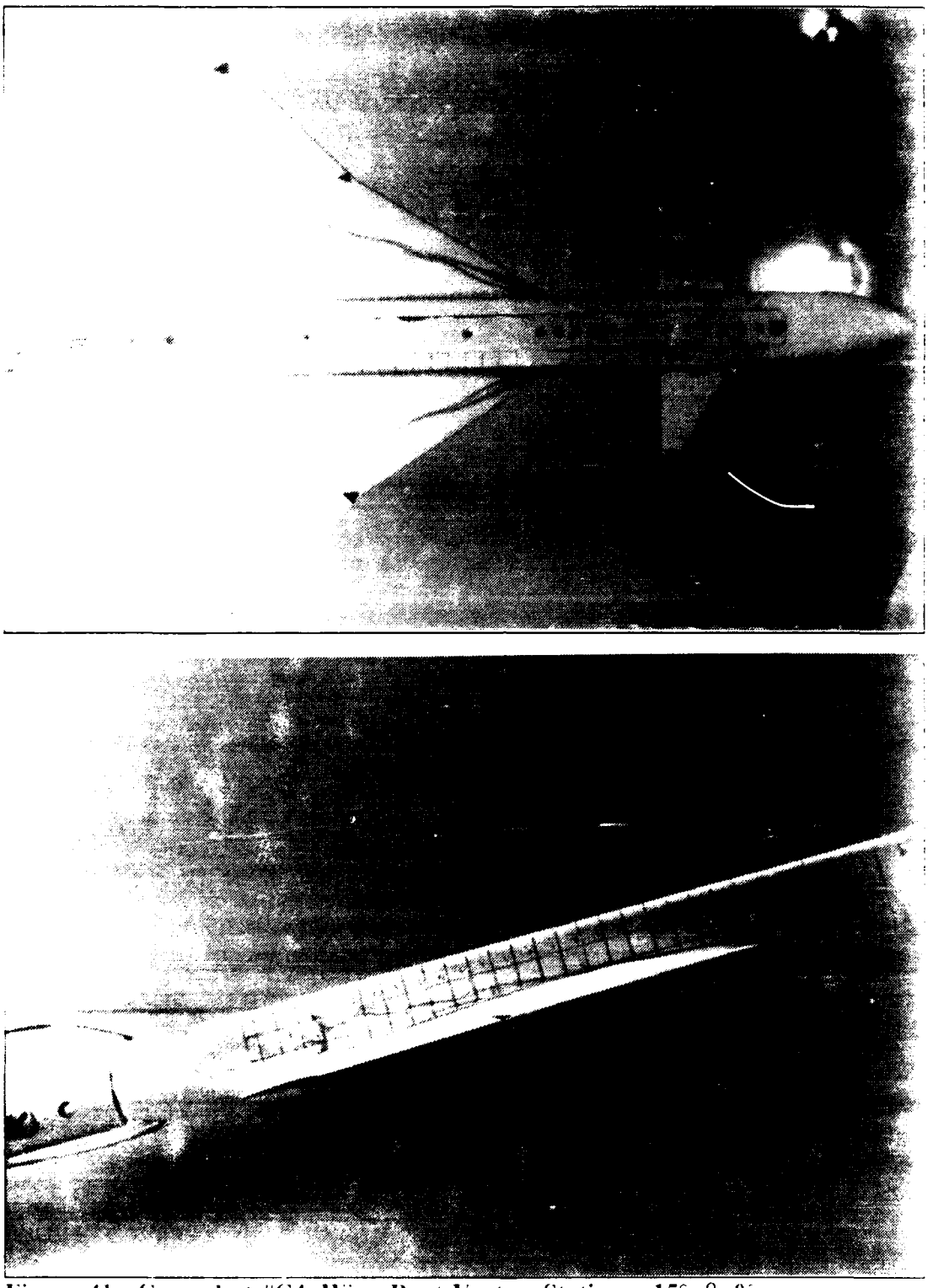

Figure 41. Canard at #C4, Wing Root Vortex, Static, $\alpha=15^{\circ}$, $\beta=0^{\circ}$

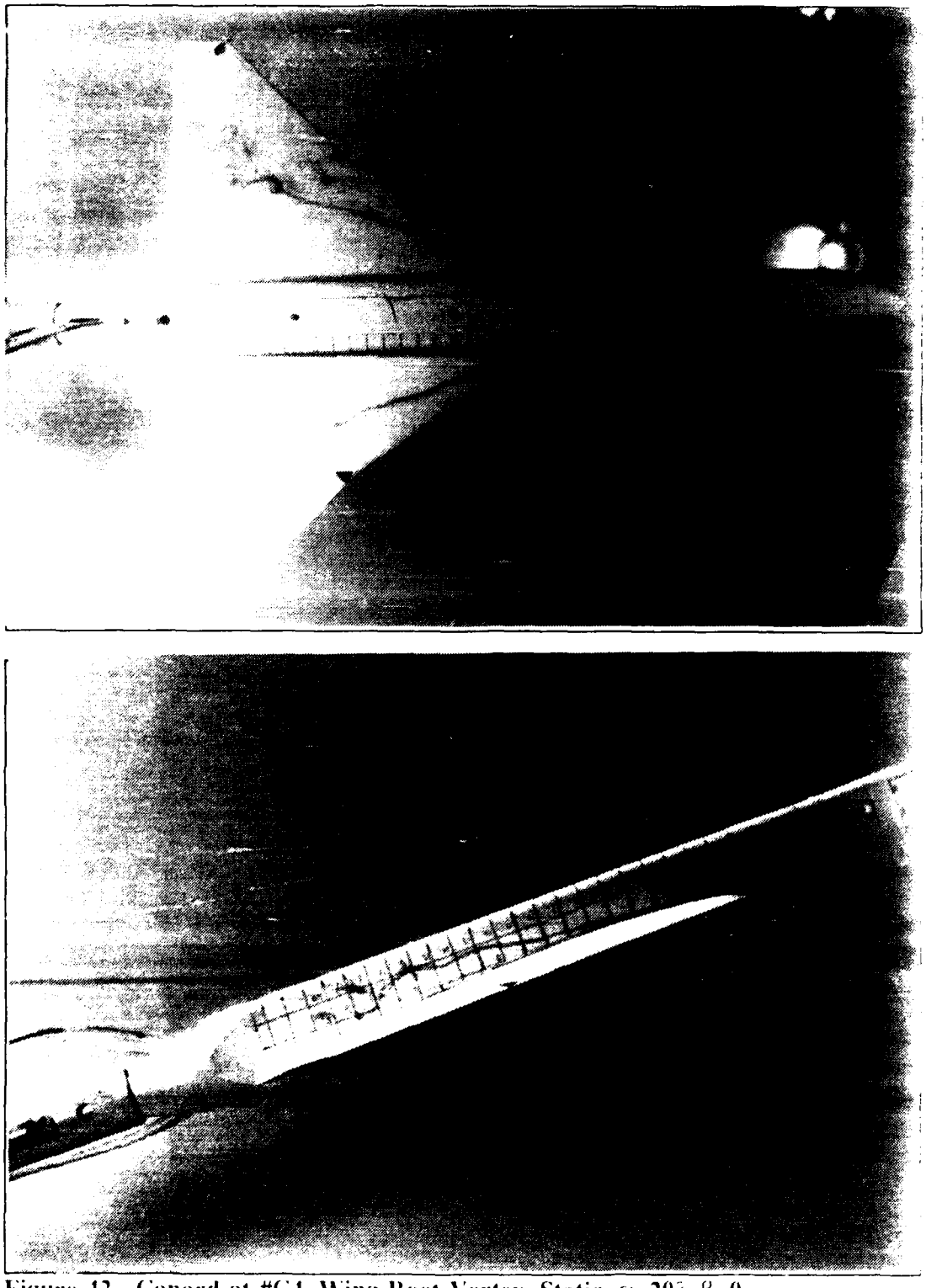

Figure 42. Canard at #C4, Wing Root Vortex, Static, $\alpha=20^{\circ}$, $\beta=0$

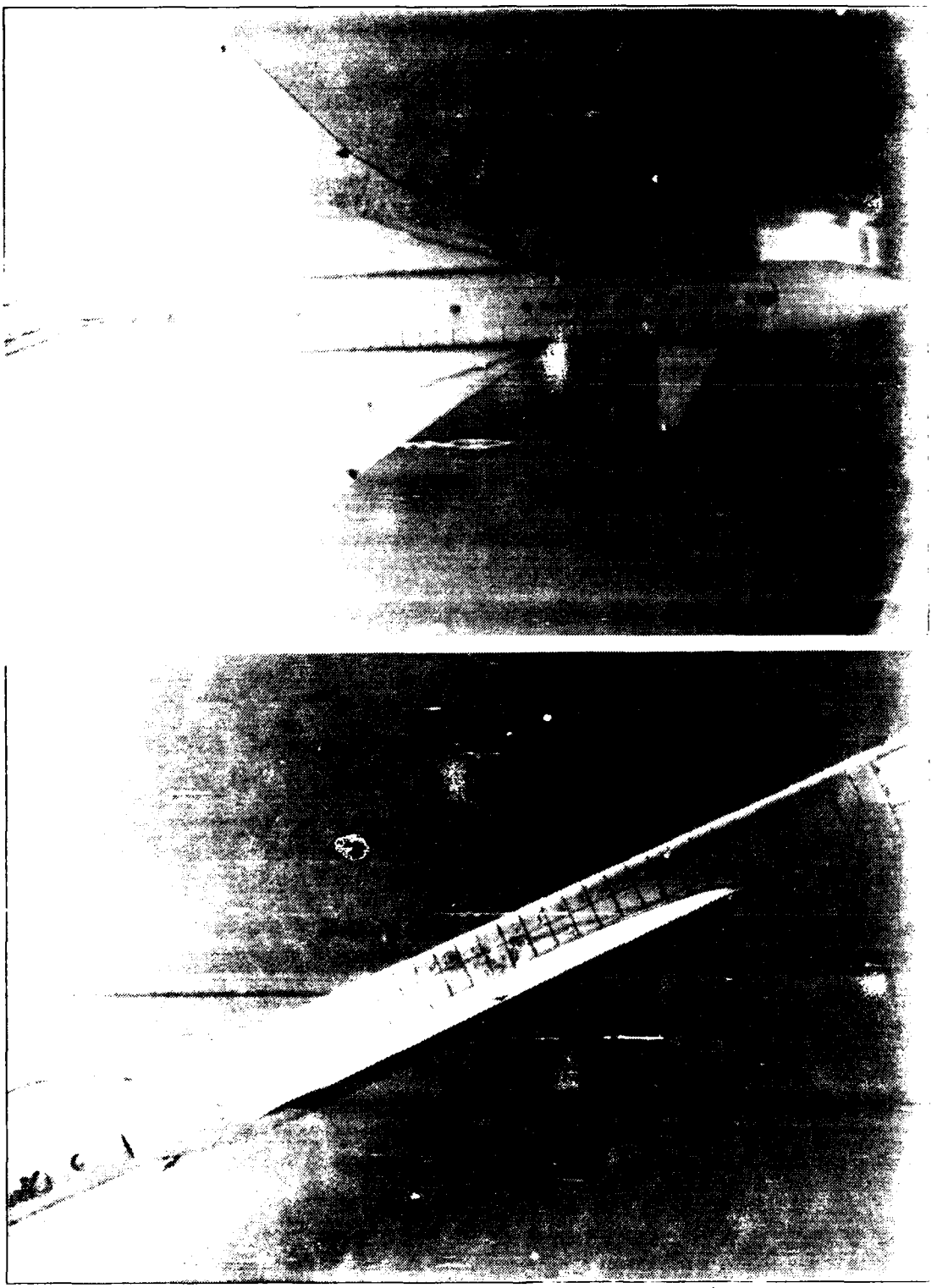

Figure 43. Canard at #C4, Wing Root Vortex, Static, α=25°, β=0

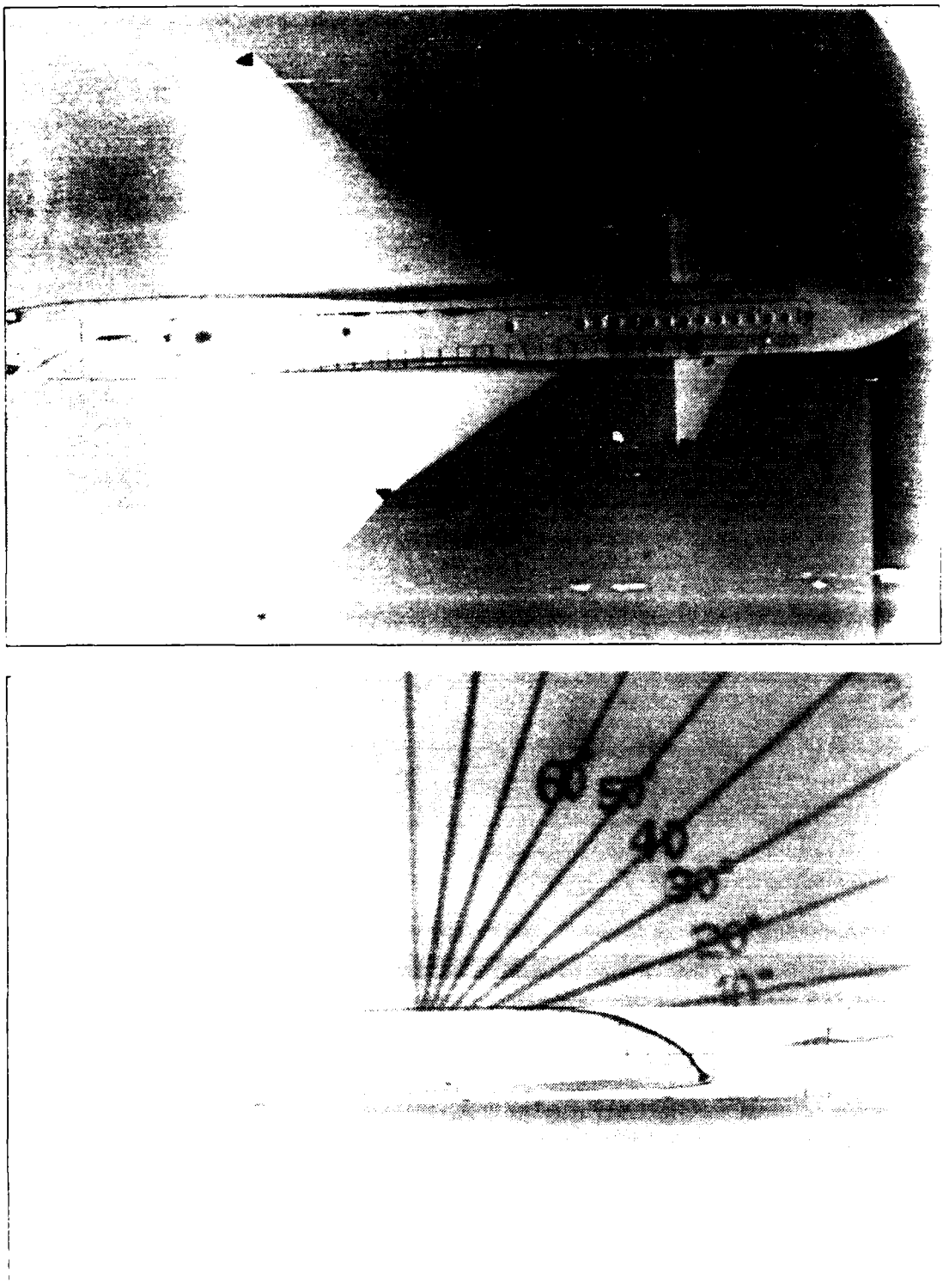

Figure 44. Canard at #D2, Wing Root Flow, Static, α=0°, β=0

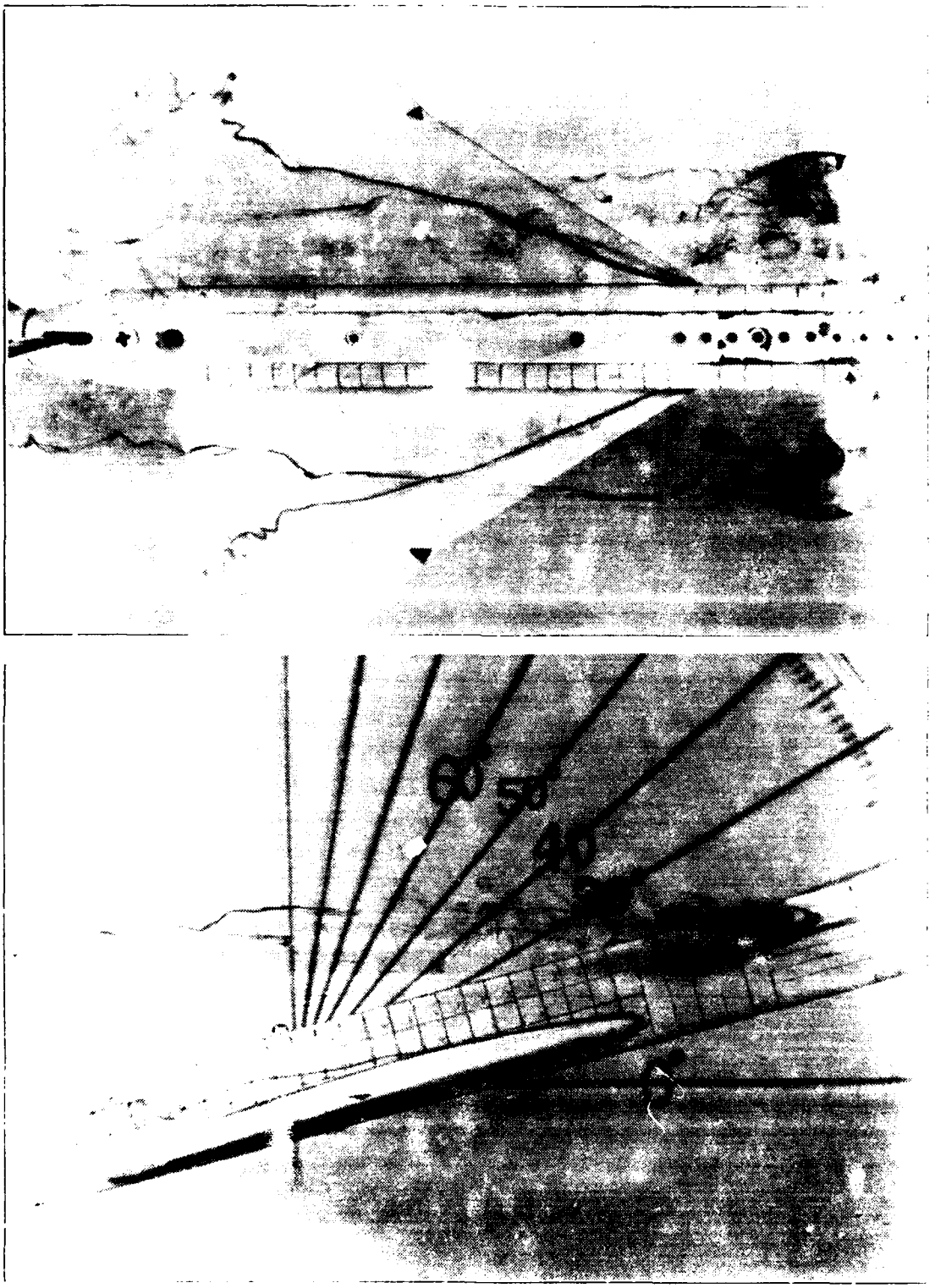

Figure 45. Canard at #D2, Wing Root Vortex, Static, α=15 , β=0

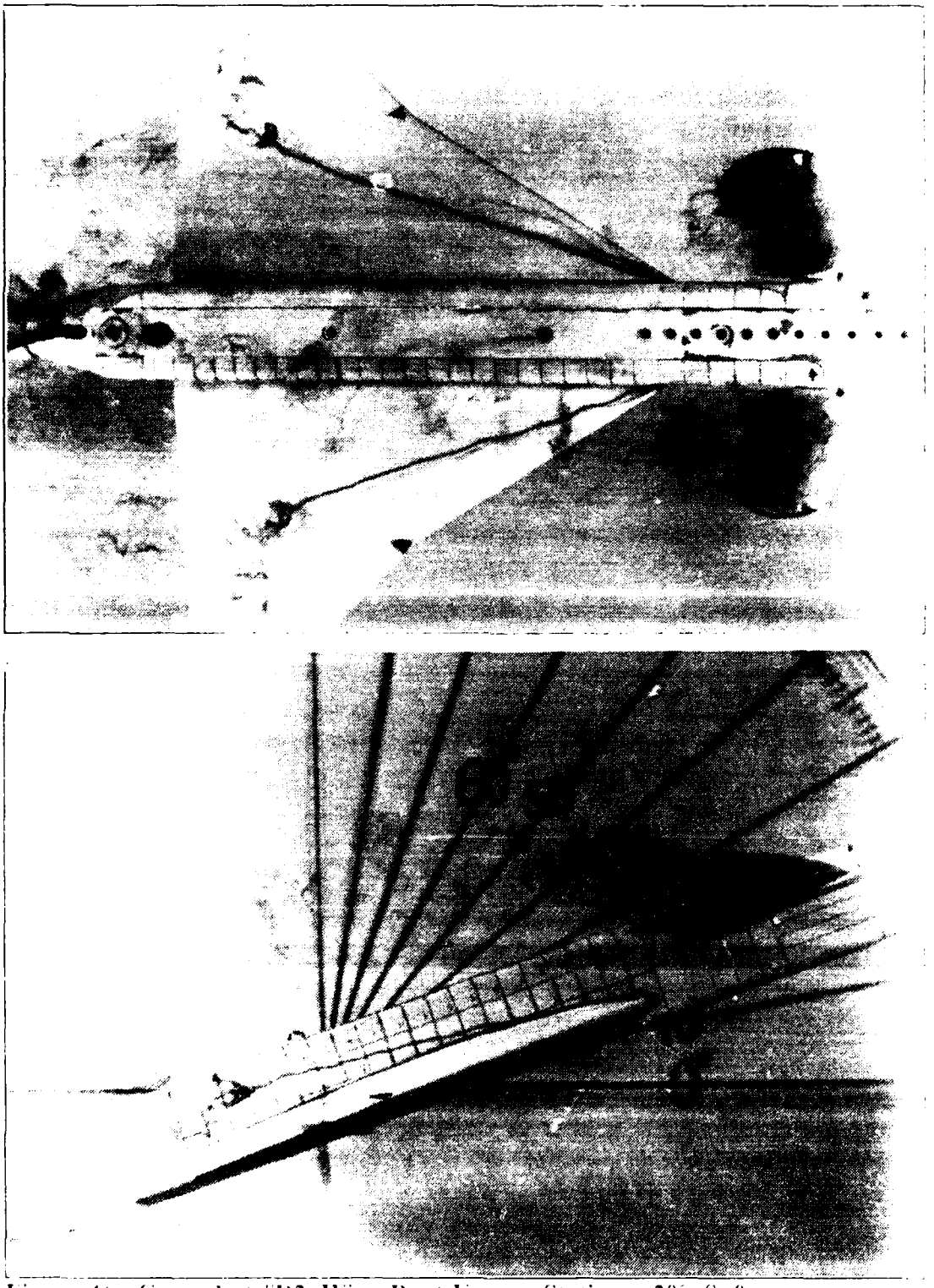

Figure 46. Canard at #D2, Wing Root Vortex, Static, α=20°, β=0

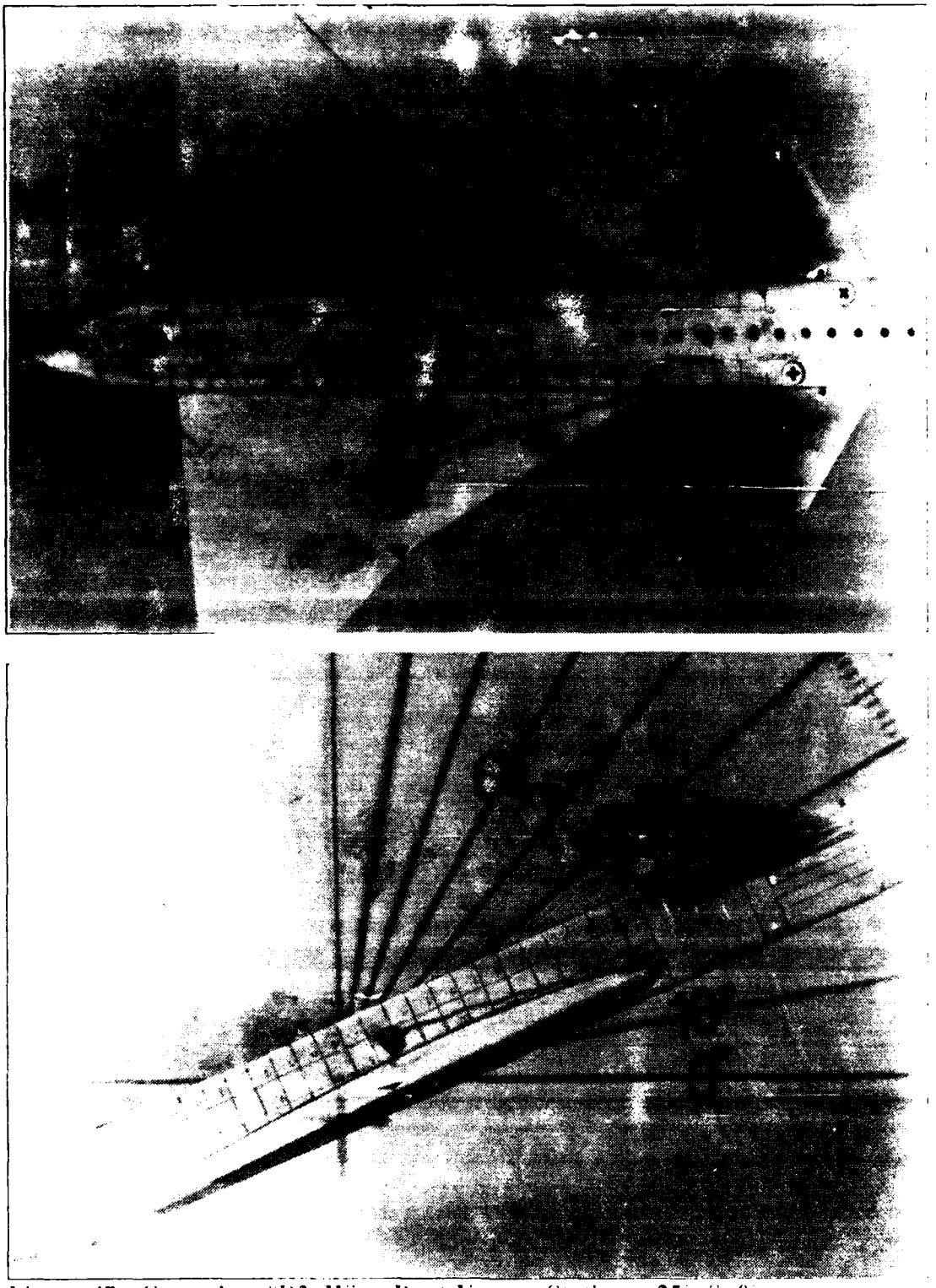

Figure 47. Canard at #D2, Wing Root Vortex, Static, α=25°, β=0

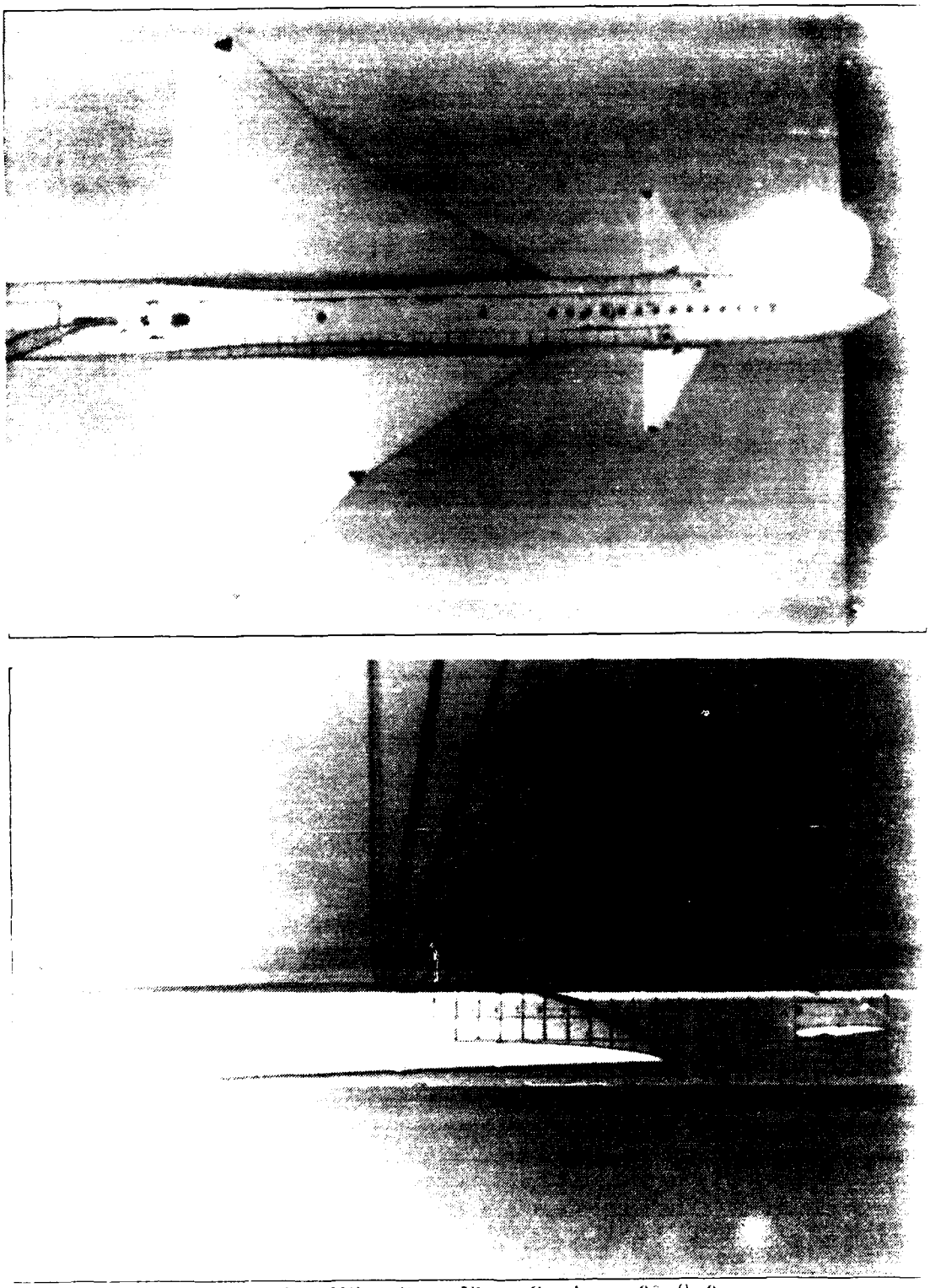

Figure 48. Canard at #D3, Wing Root Flow, Static, α=0°, β=0

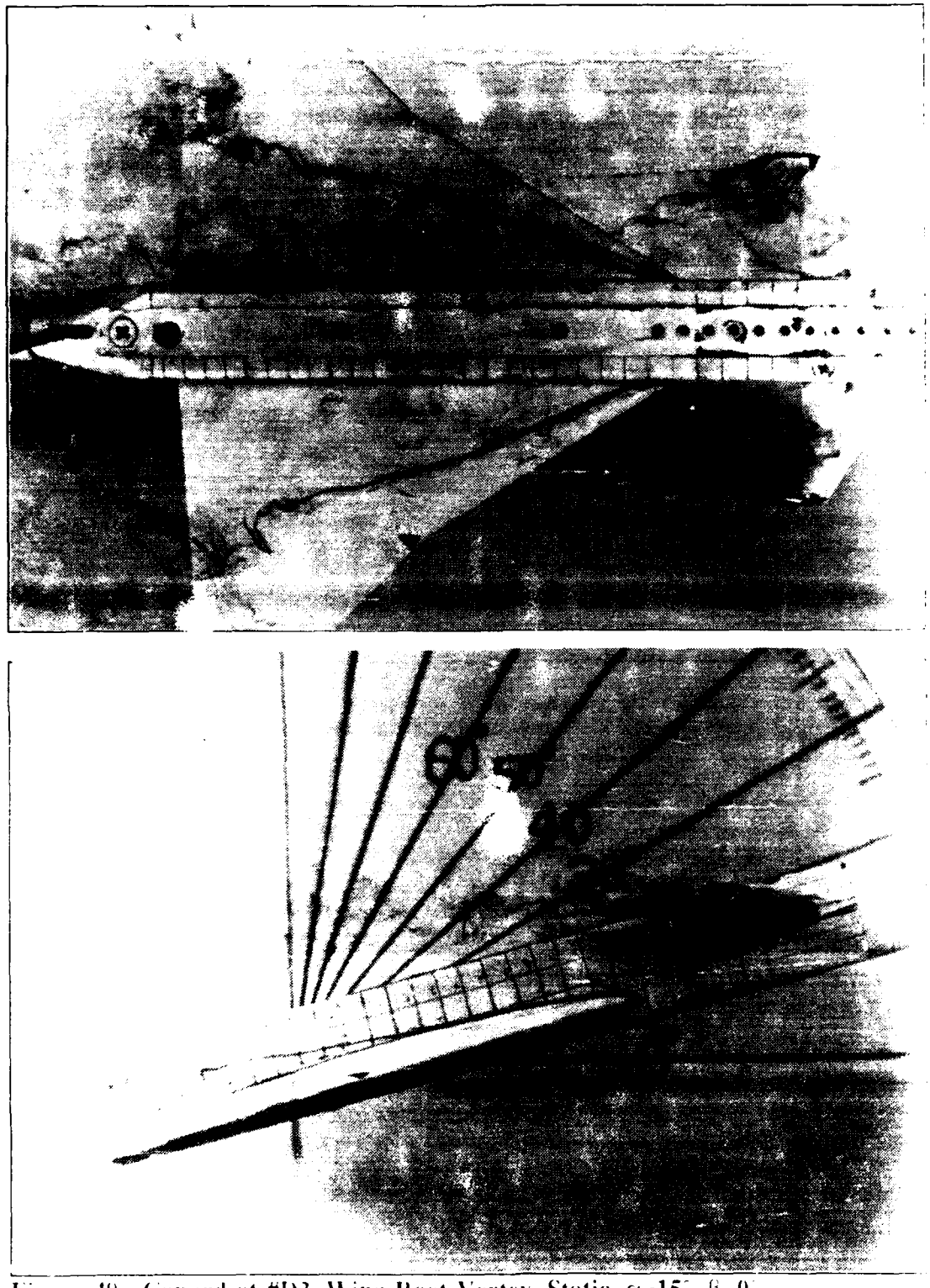

Figure 49. Canard at #D3, Wing Root Vortex, Static, α=15°, β=0°

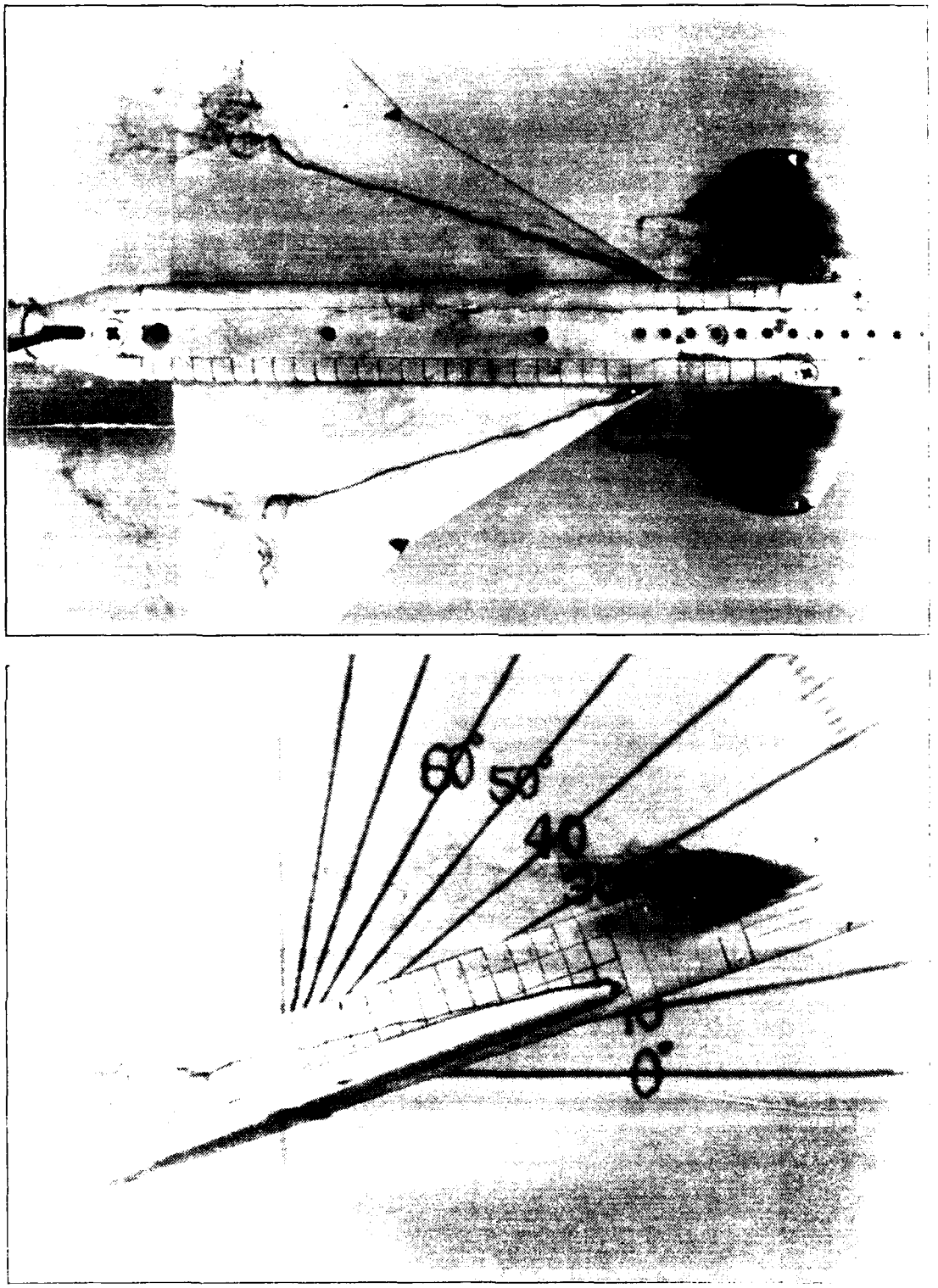

Figure 50. Canard at #D3. Wing Root Vortex, Static, α=20°, β=0

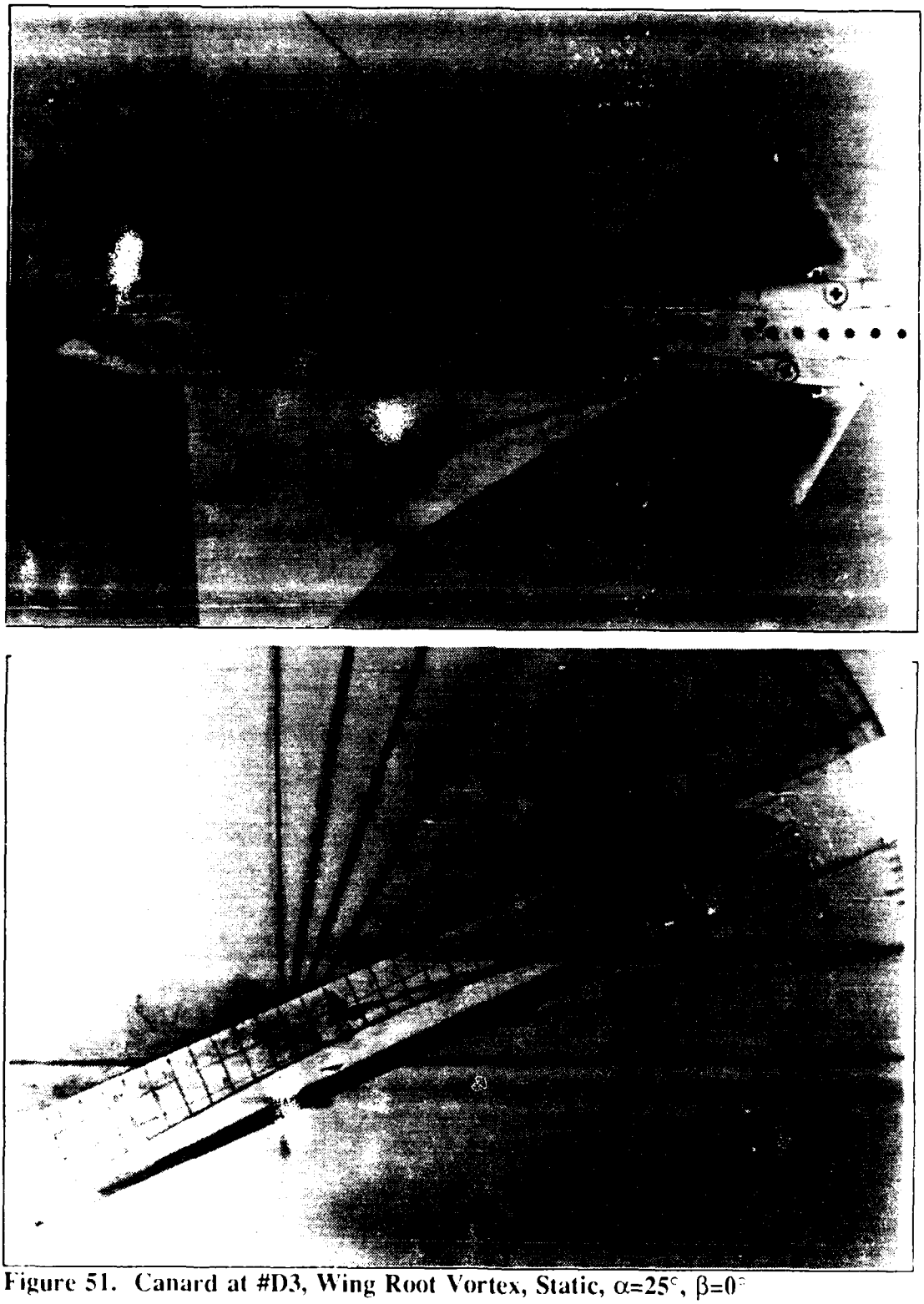

Figure 51. Canard at #D3, Wing Root Vortex, Static, α=25°, β=0°

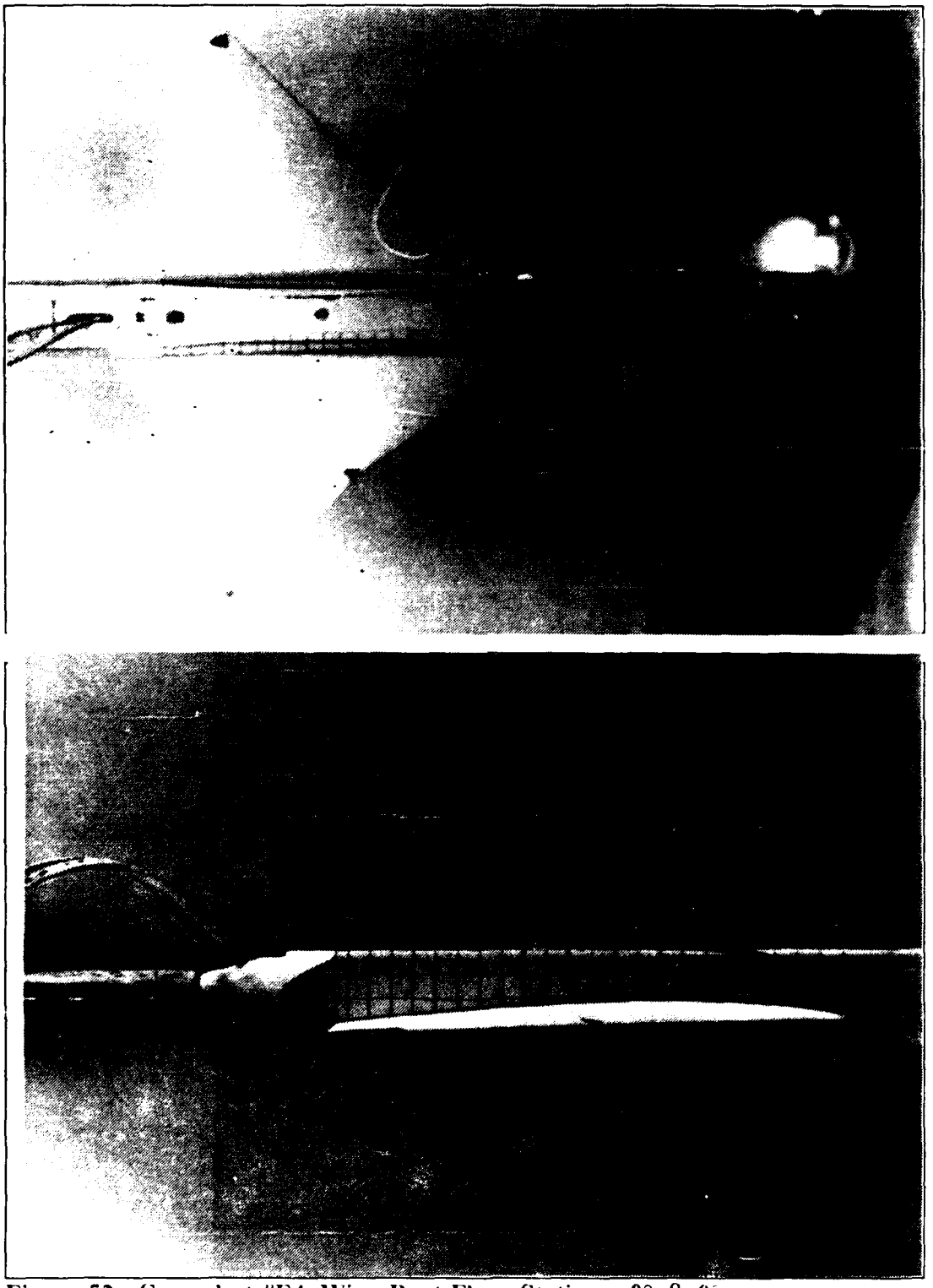

Figure 52. Canard at #E4, Wing Root Flow, Static, $\alpha=0°$, $\beta=0°$

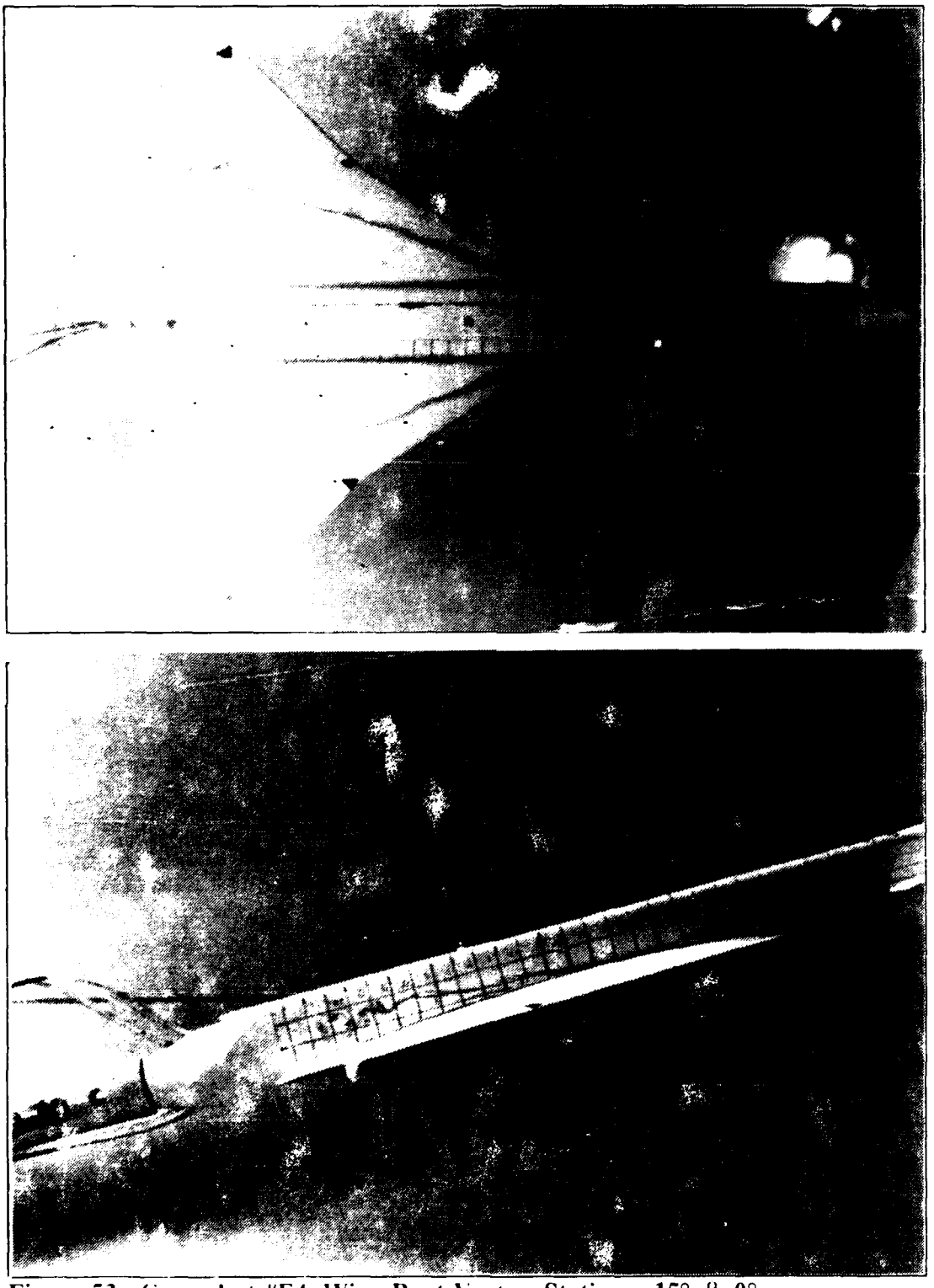

Figure 53. Canard at #E4, Wing Root Vortex, Static, α=15°, β=0°

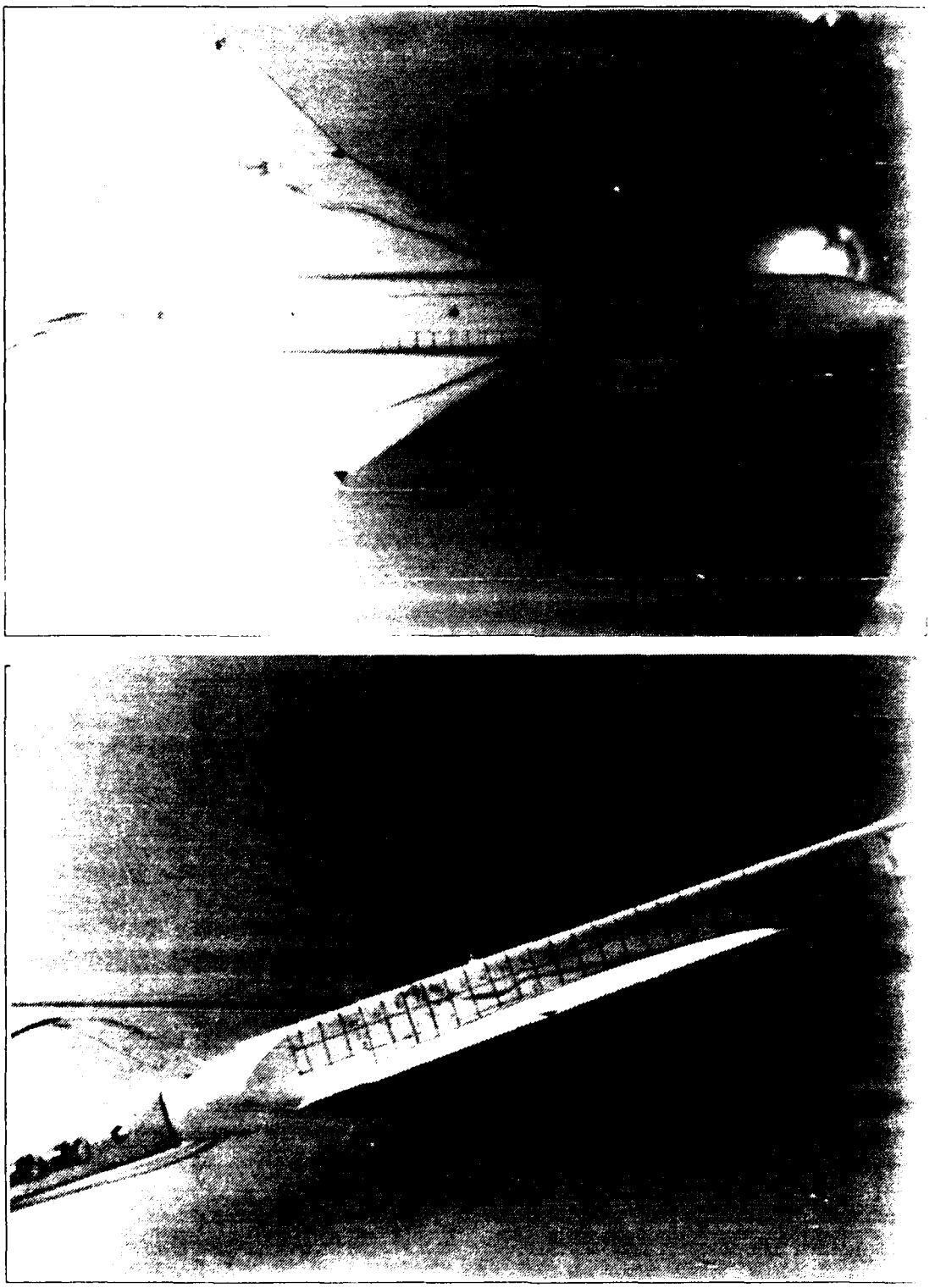

Figure 54. Canard at #E4, Wing Root Vortex, Static, α=20 , β=0

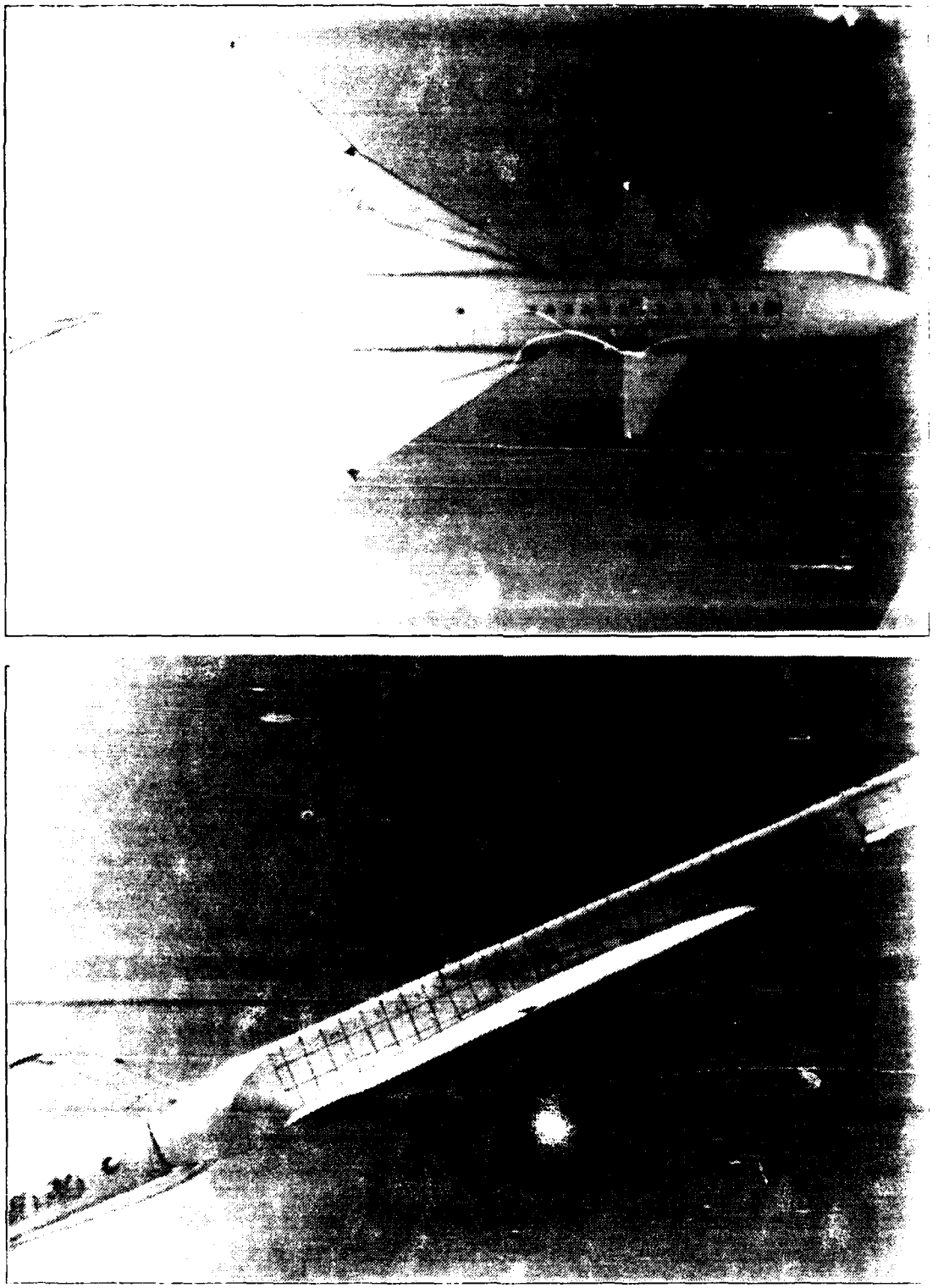

Figure 55. Canard at #E4, Wing Root Vortex, Static, α=25°, β=0

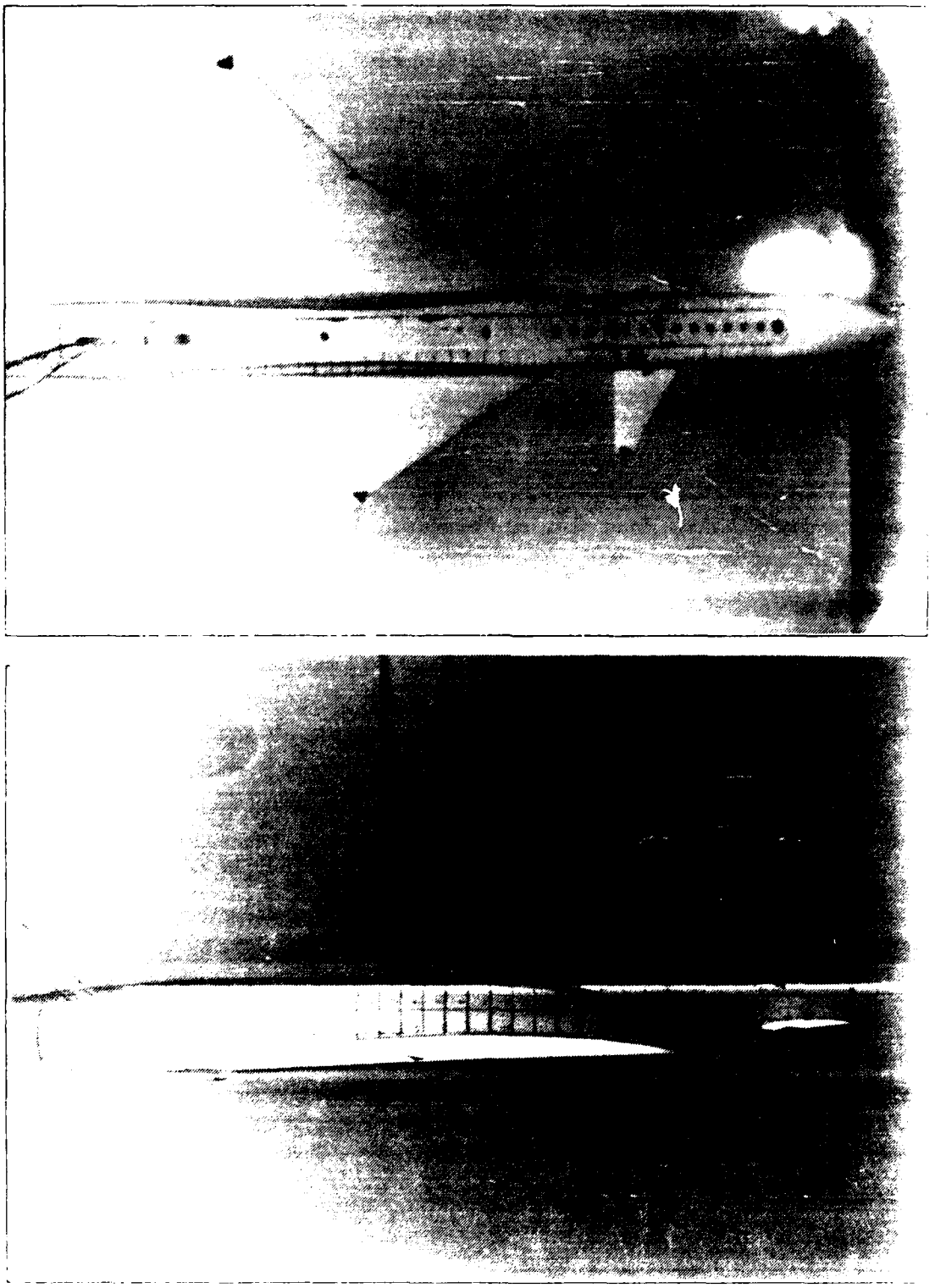

Figure 56. Canard at #13, Wing Root Flow, Static, α=0 , β=0

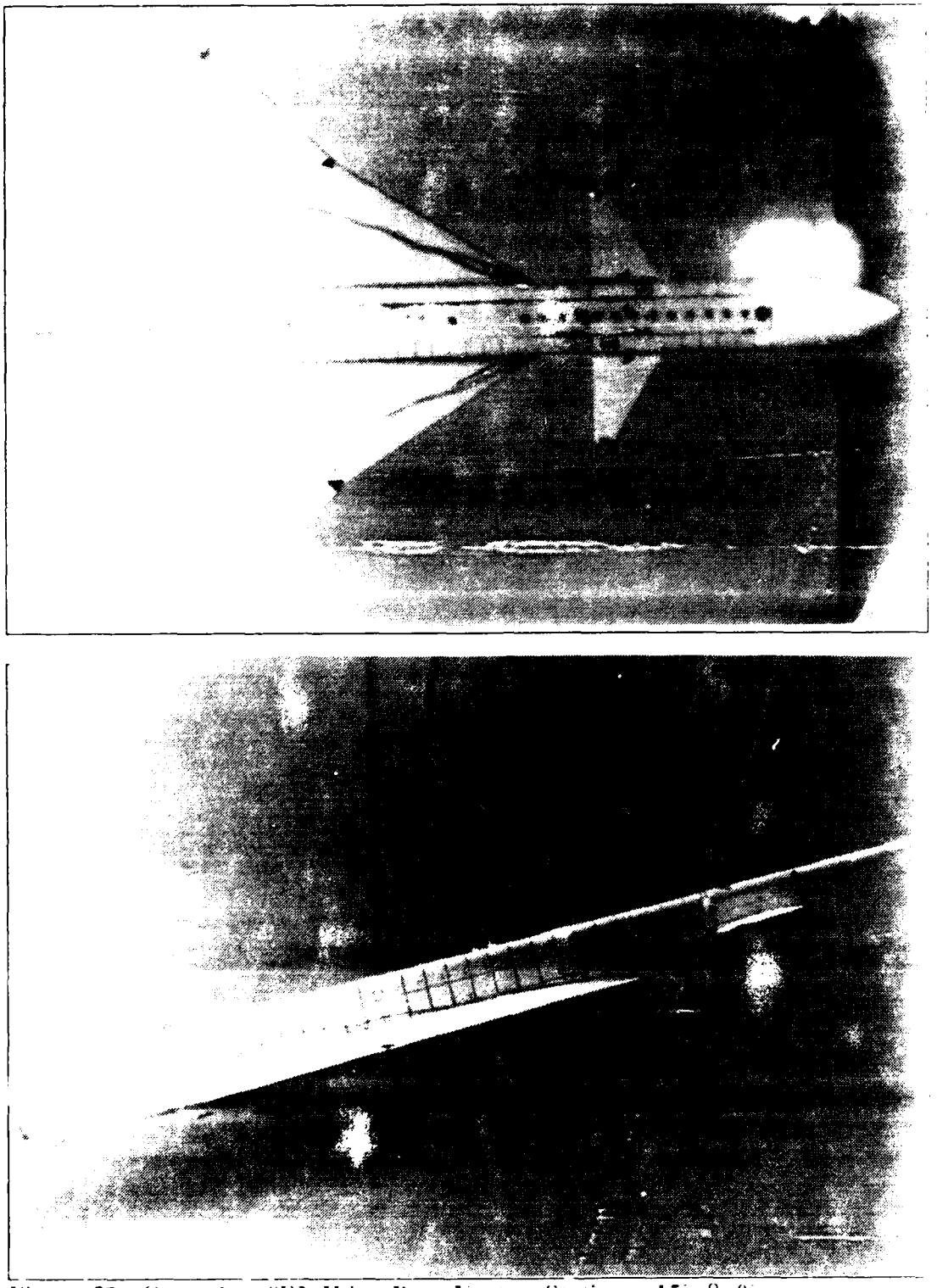

Figure 57. Canard at #F3, Wing Root Vortex, Static, α=15°, β=0

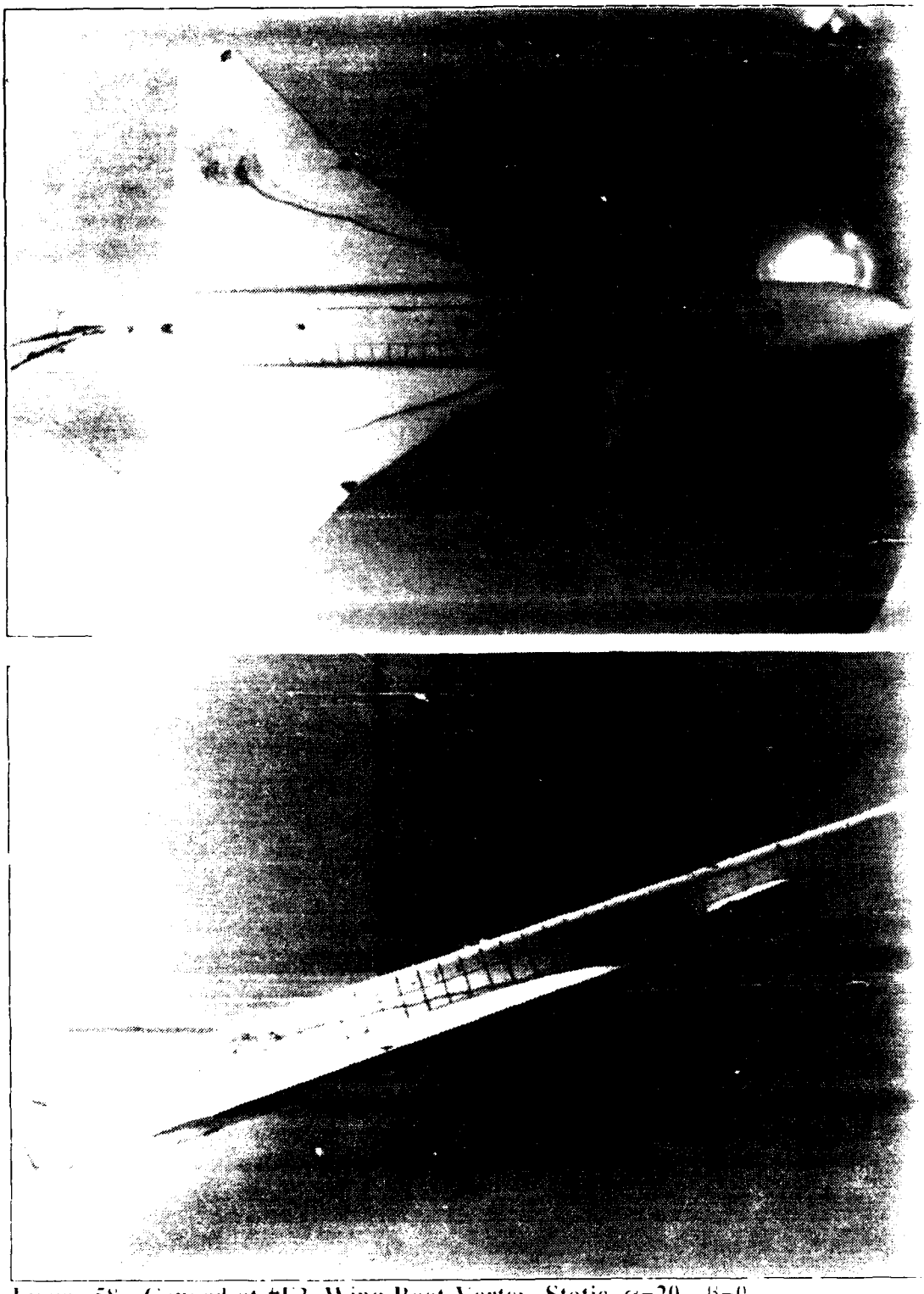

Figure 58. Canard at #F3, Wing Root Vortex, Static, α=20 , β=0

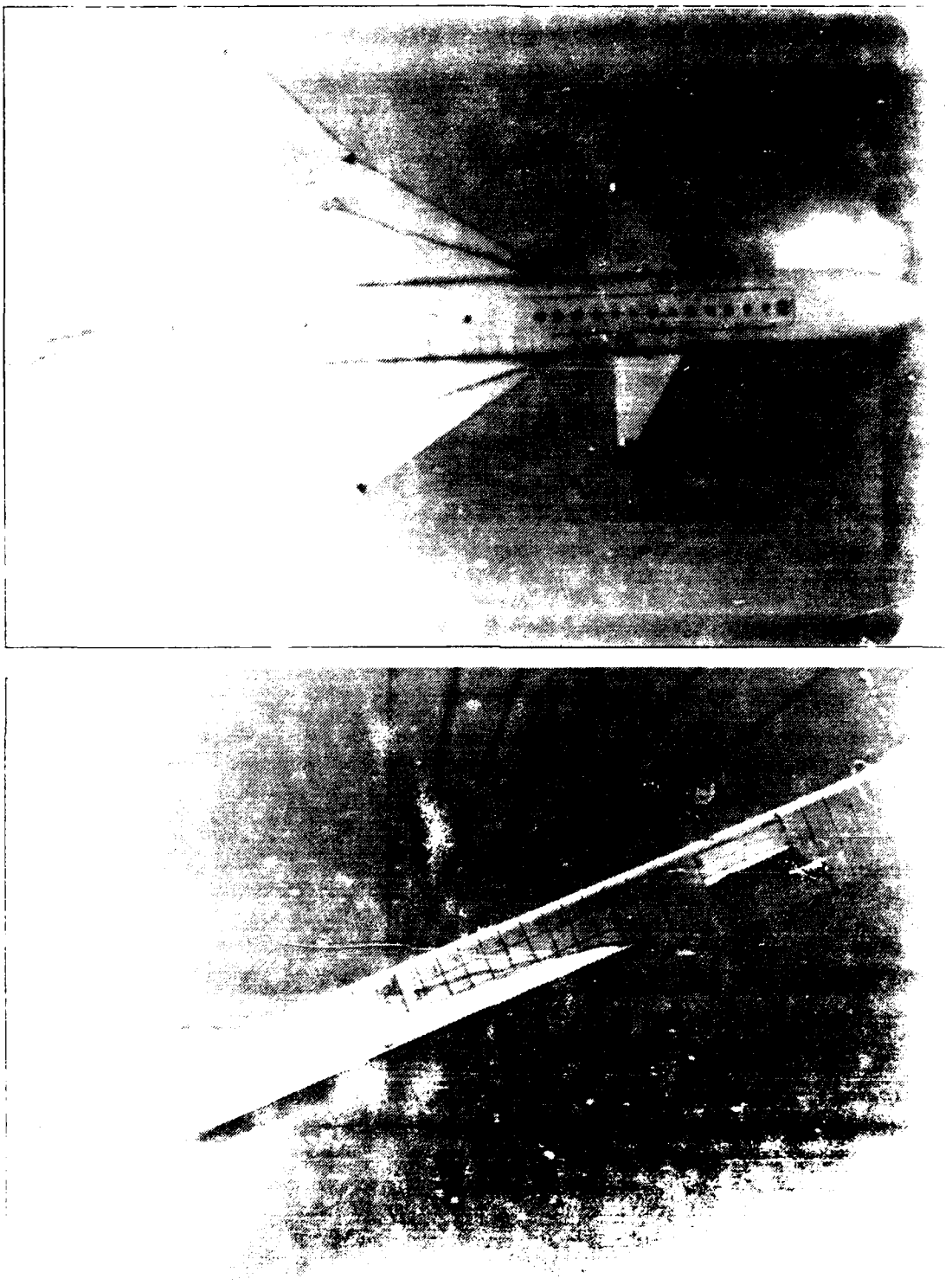

Figure 5. Canard at #13, Wing Root Vortex, Static, $\alpha = 25°$, $\beta = 0°$

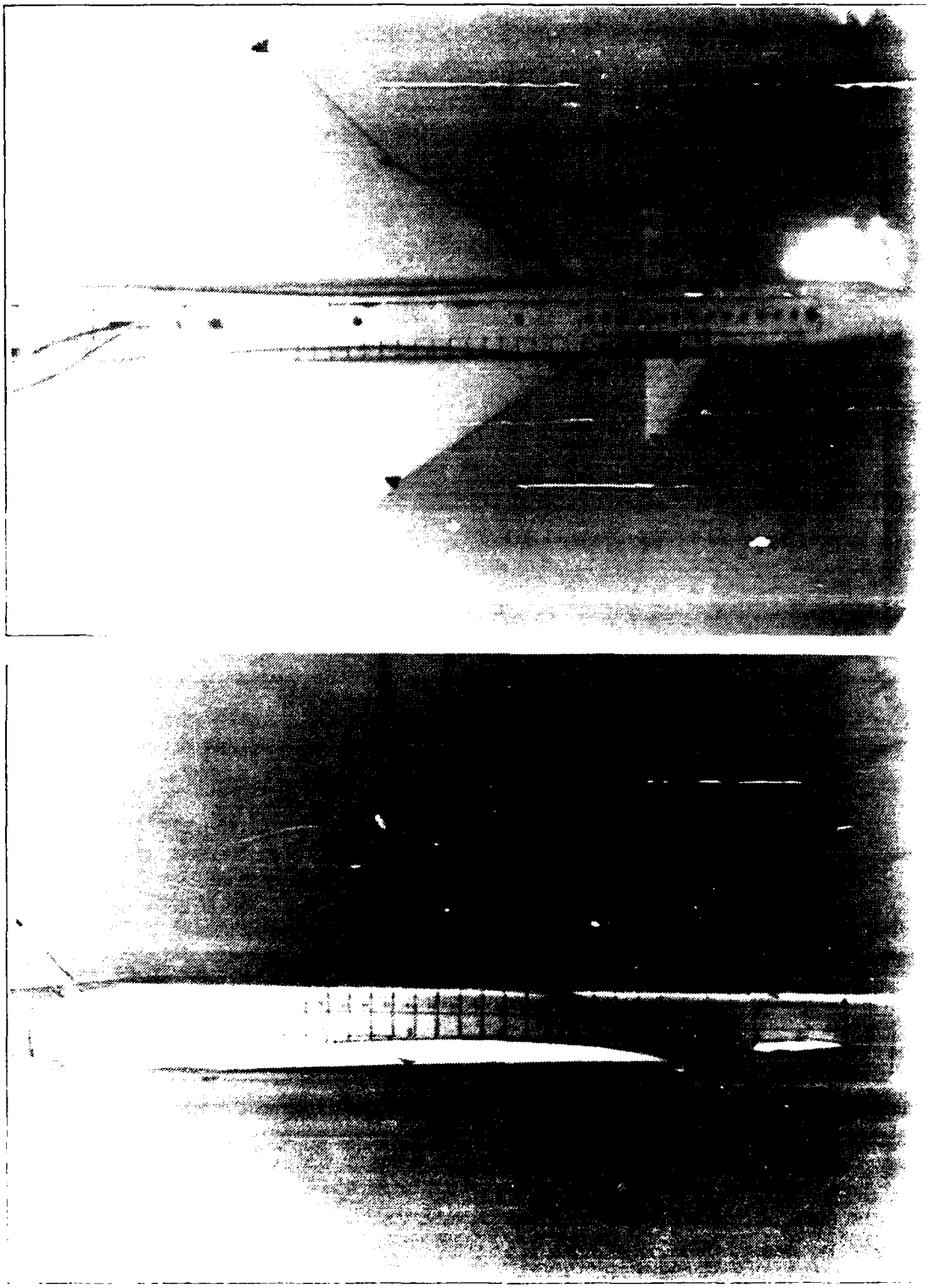

Figure 60. Canard at #14, Wing Root Flow, Static, α=0 , β=0

Figure 61. Canard at #14, Wing Root Vortex, Static, α=15 , β=0

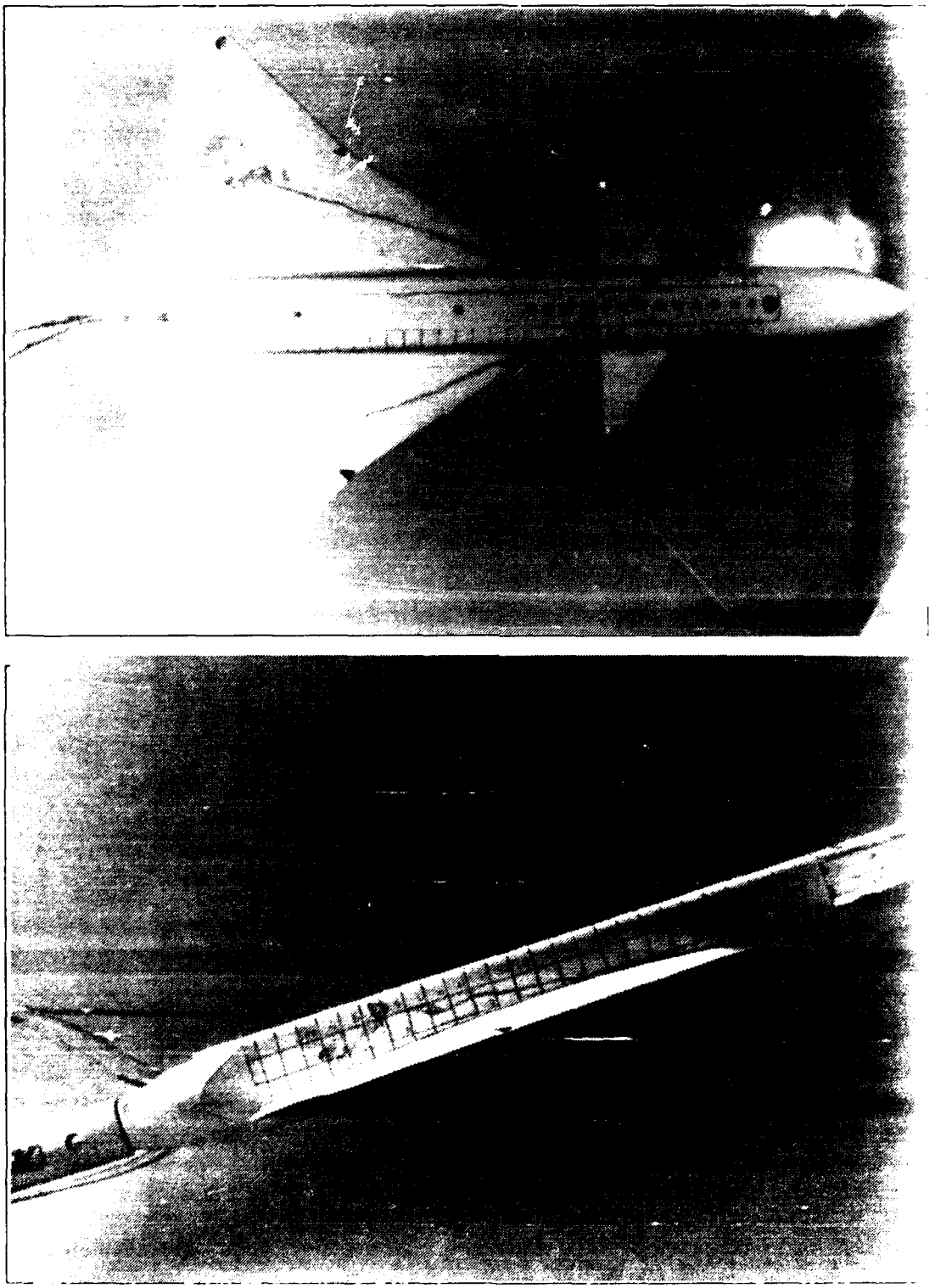

Figure 62. Canard at #F4, Wing Root Vortex, Static, α=20 , β=0

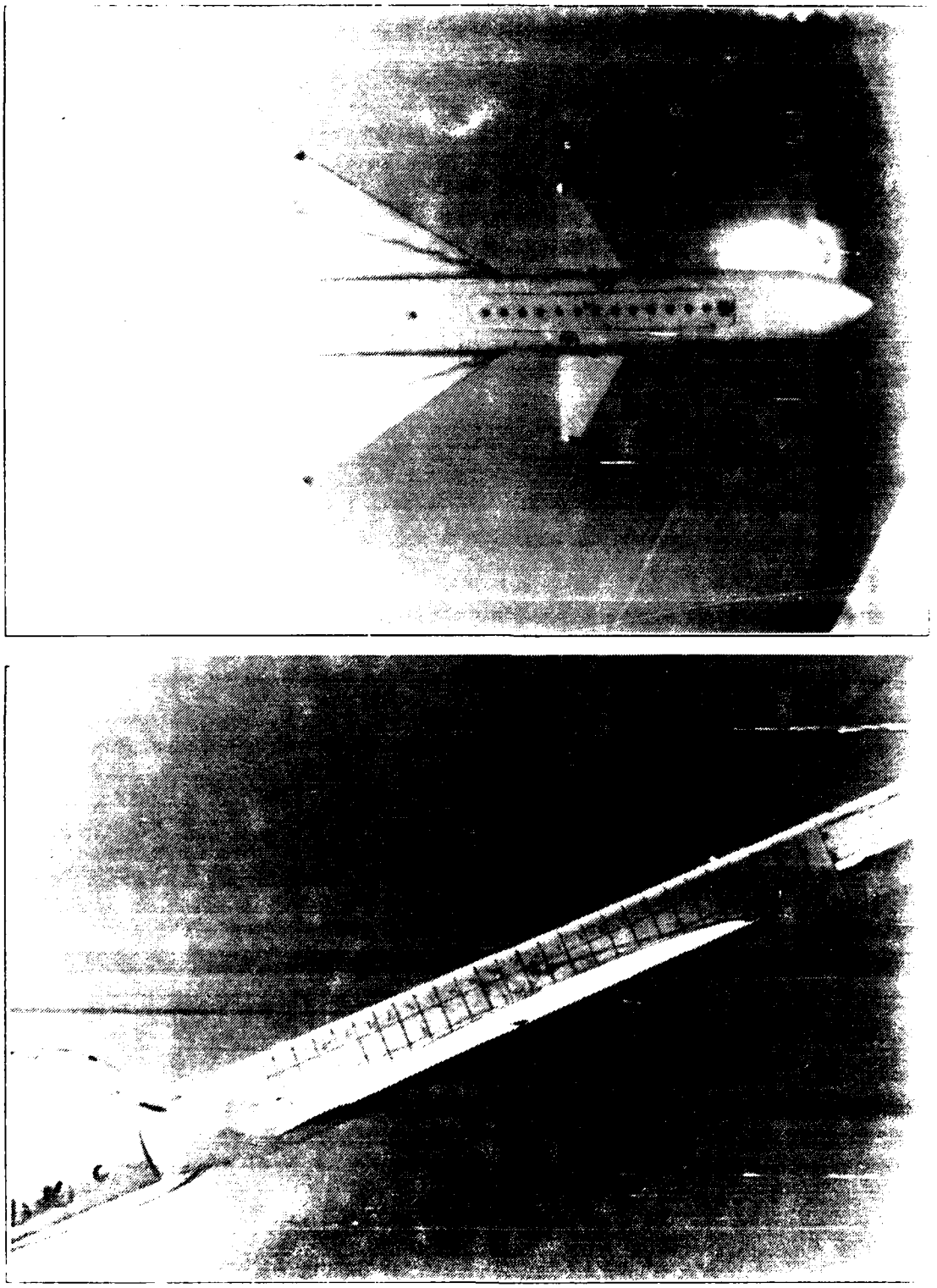

Figure 63. Canard at #F4, Wing Root Vortex, Static, α=25°, β=0

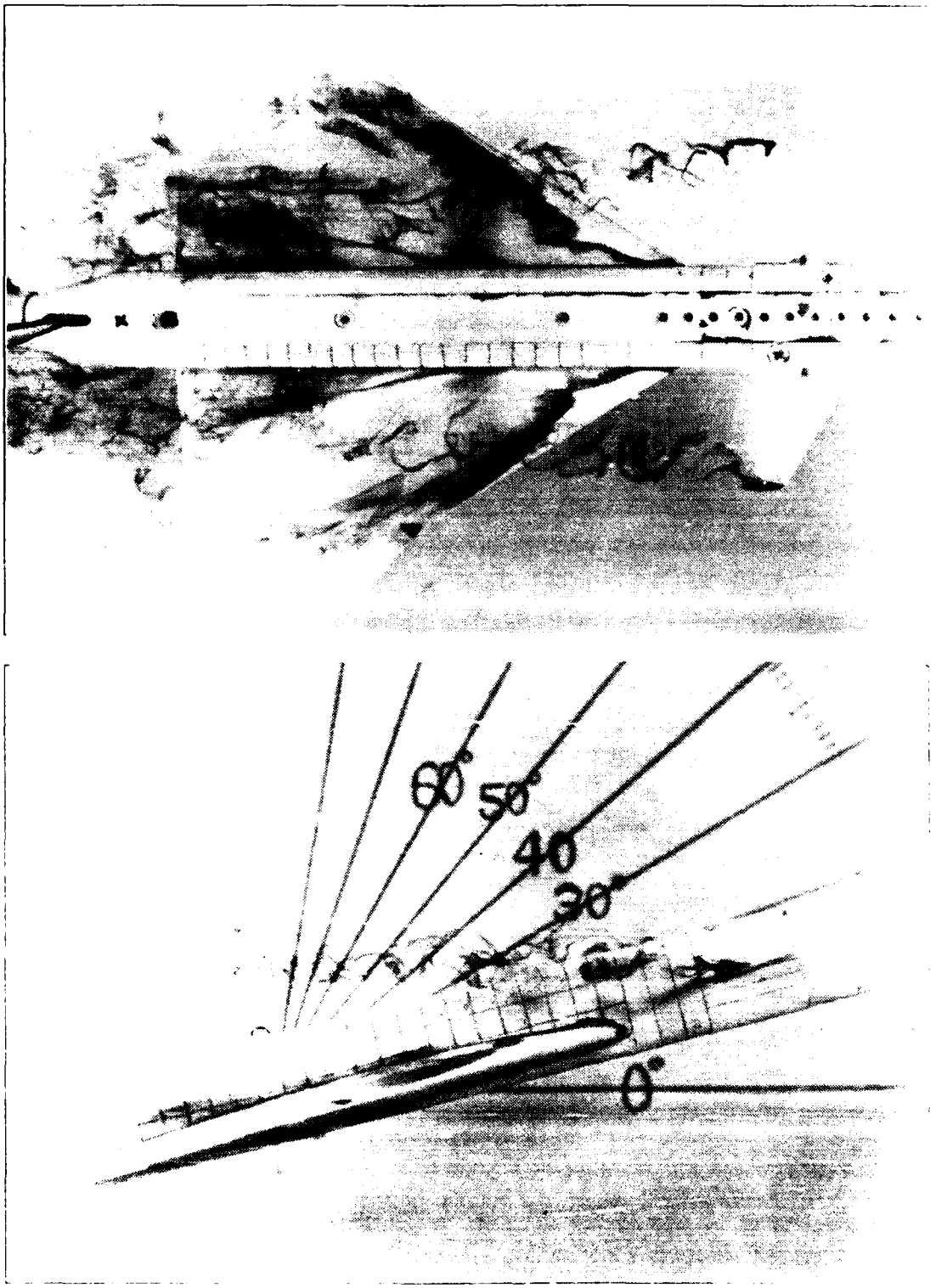

Figure 64. Wing Root Vortex, Low pitch rate UP, α=15 , β=0

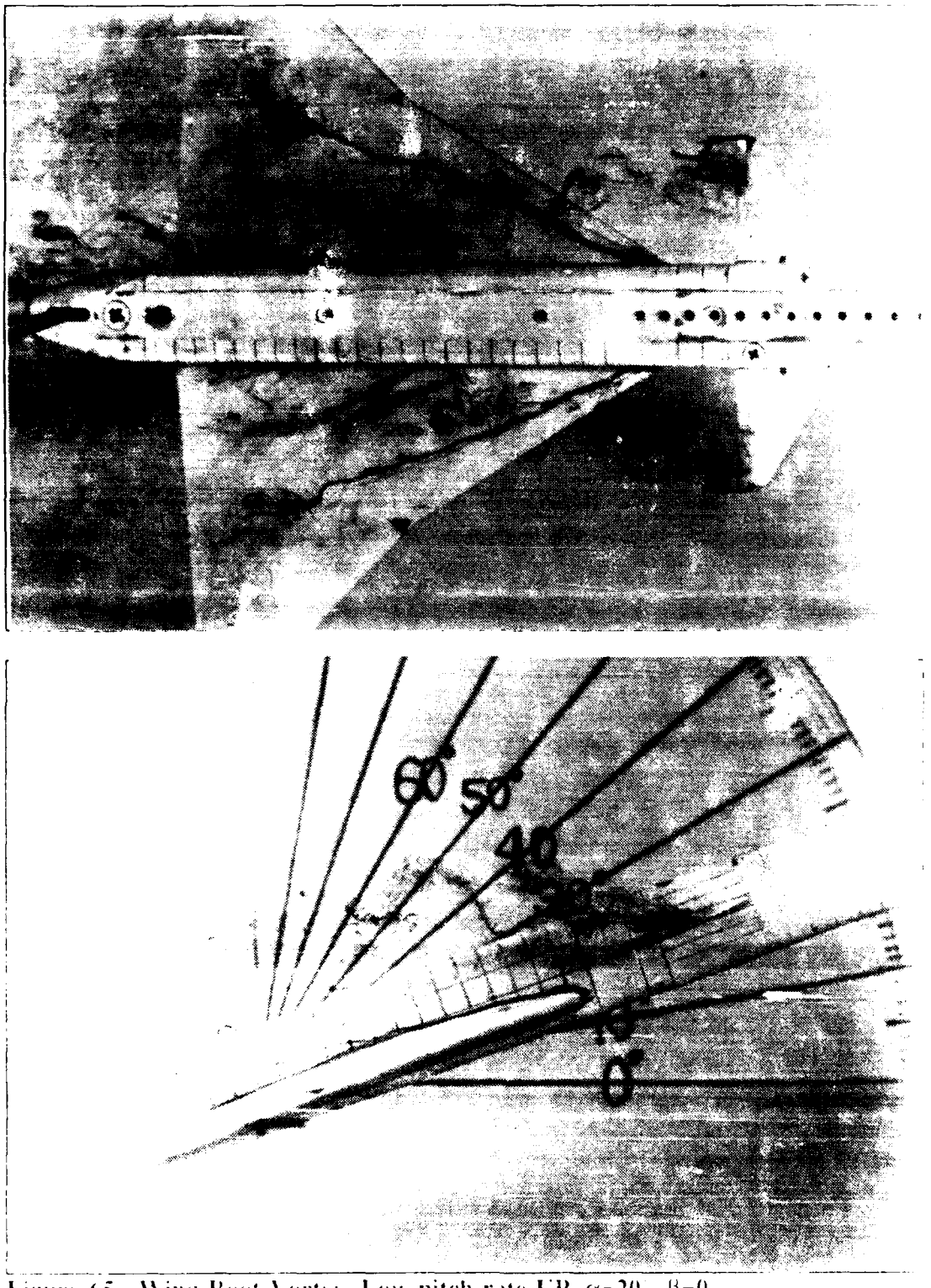

Figure 65. Wing Root Vortex, Low pitch rate UP, α=20 , β=0

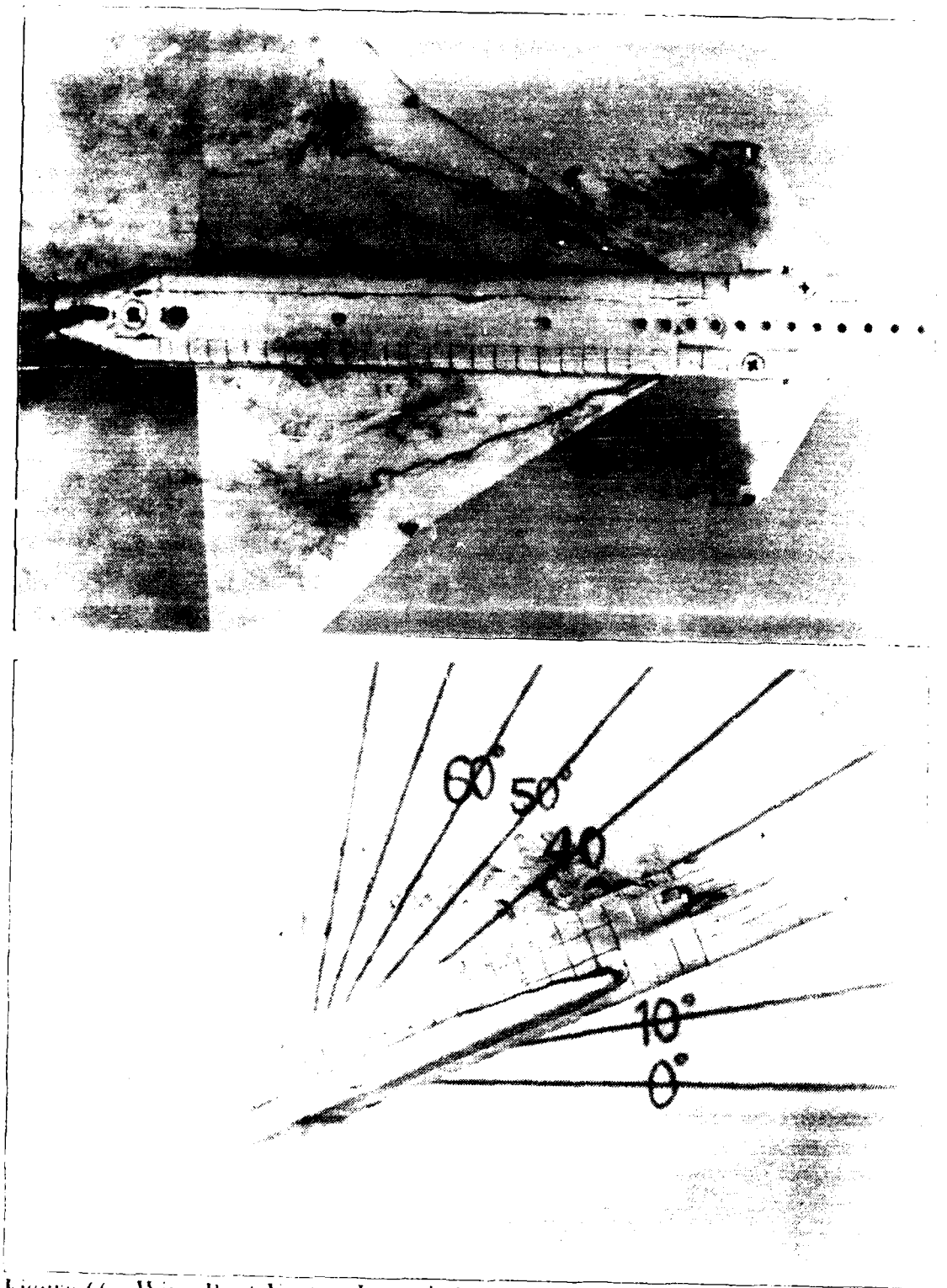

Figure 66. Wing Root Vortex, Low pitch rate UP, α=25 , β=0

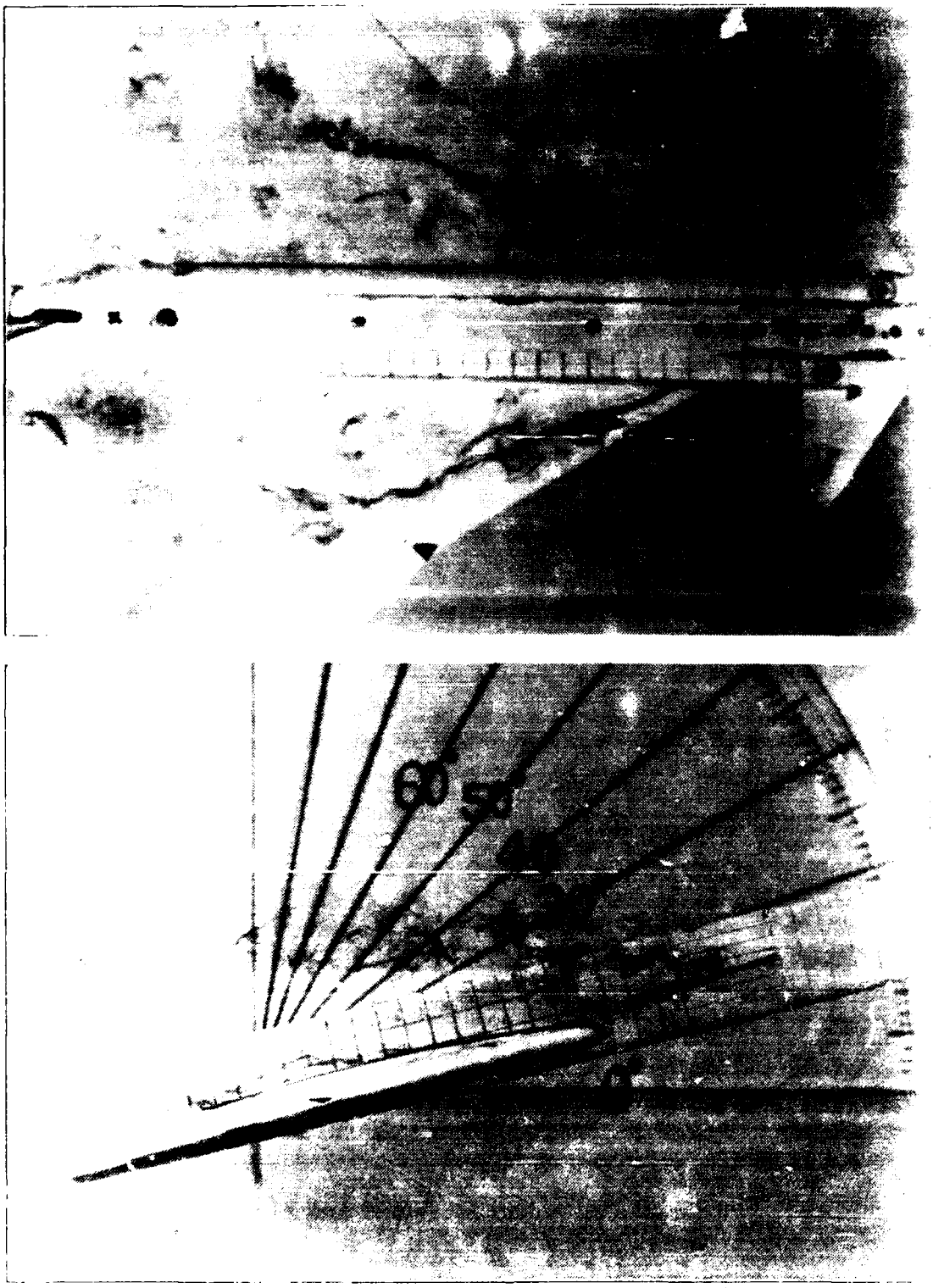

Figure 67. Wing Root Vortex, Low pitch rate DOWN, α=15°, β=0°

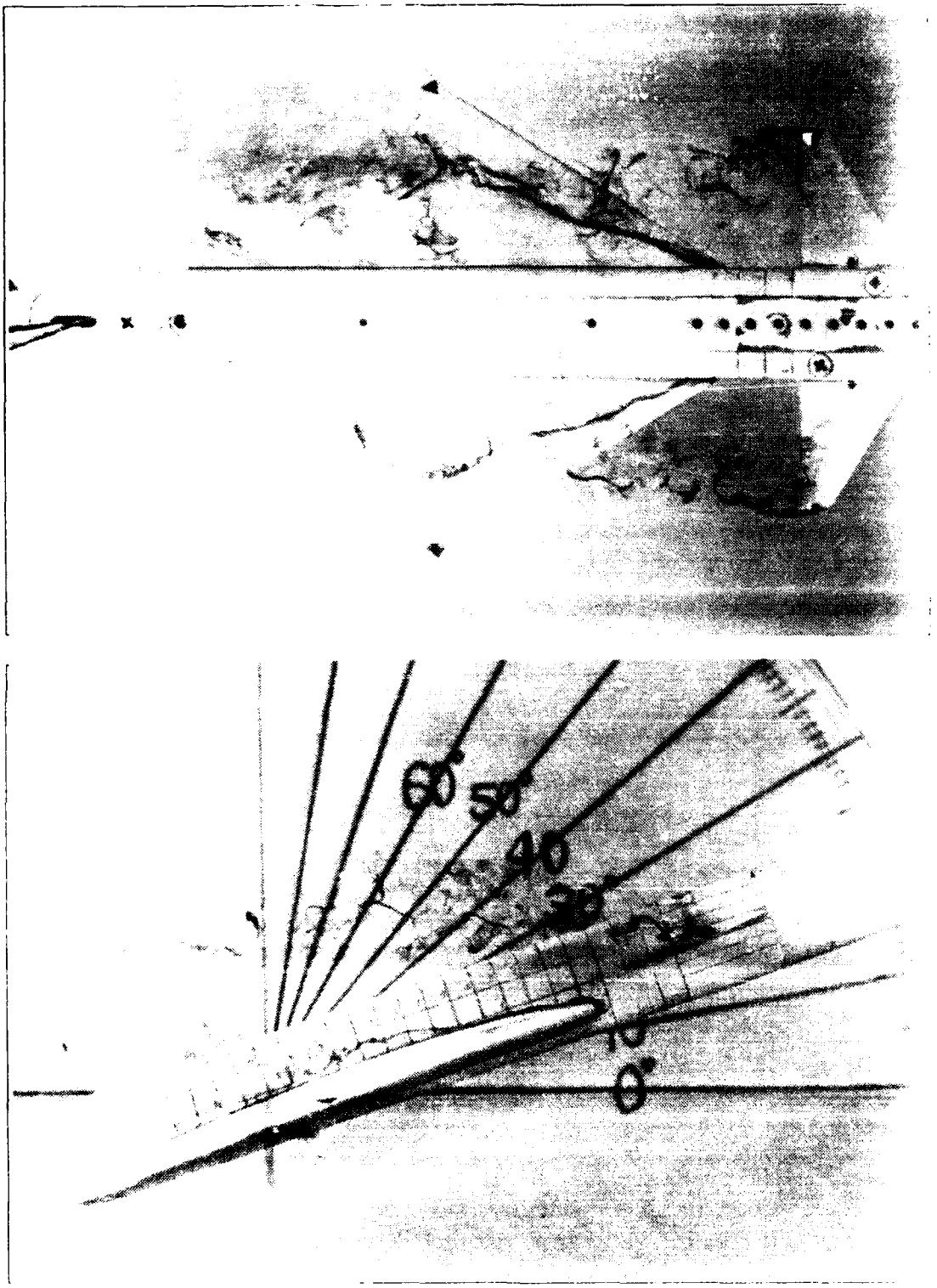

Figure 68. Wing Root Vortex, Low pitch rate DOWN, α=20 , β=0

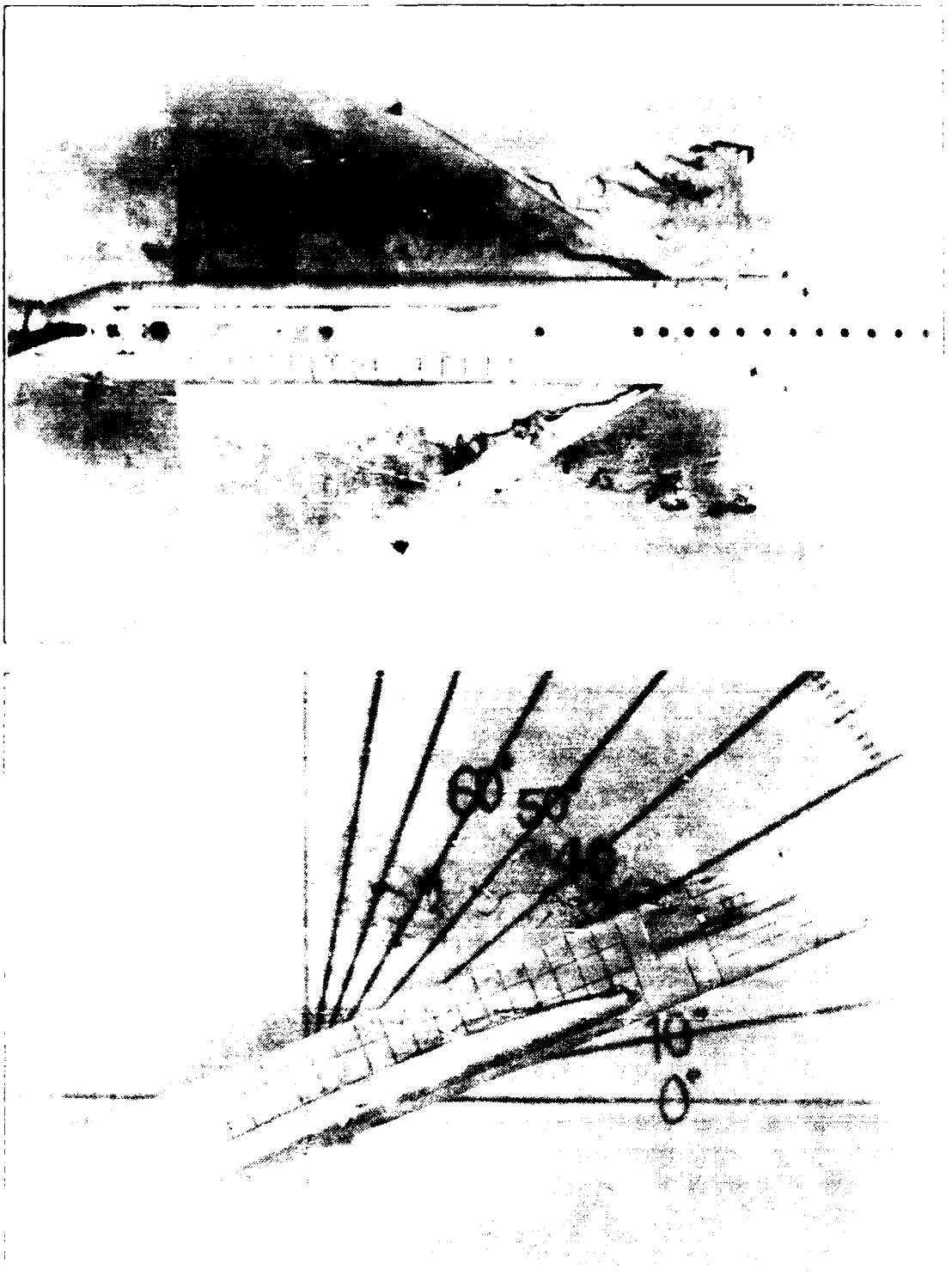

Figure 6a. Wing Root Vortex. Low pitch rate DOWN, $\alpha = 25^\circ$, $q = 0$

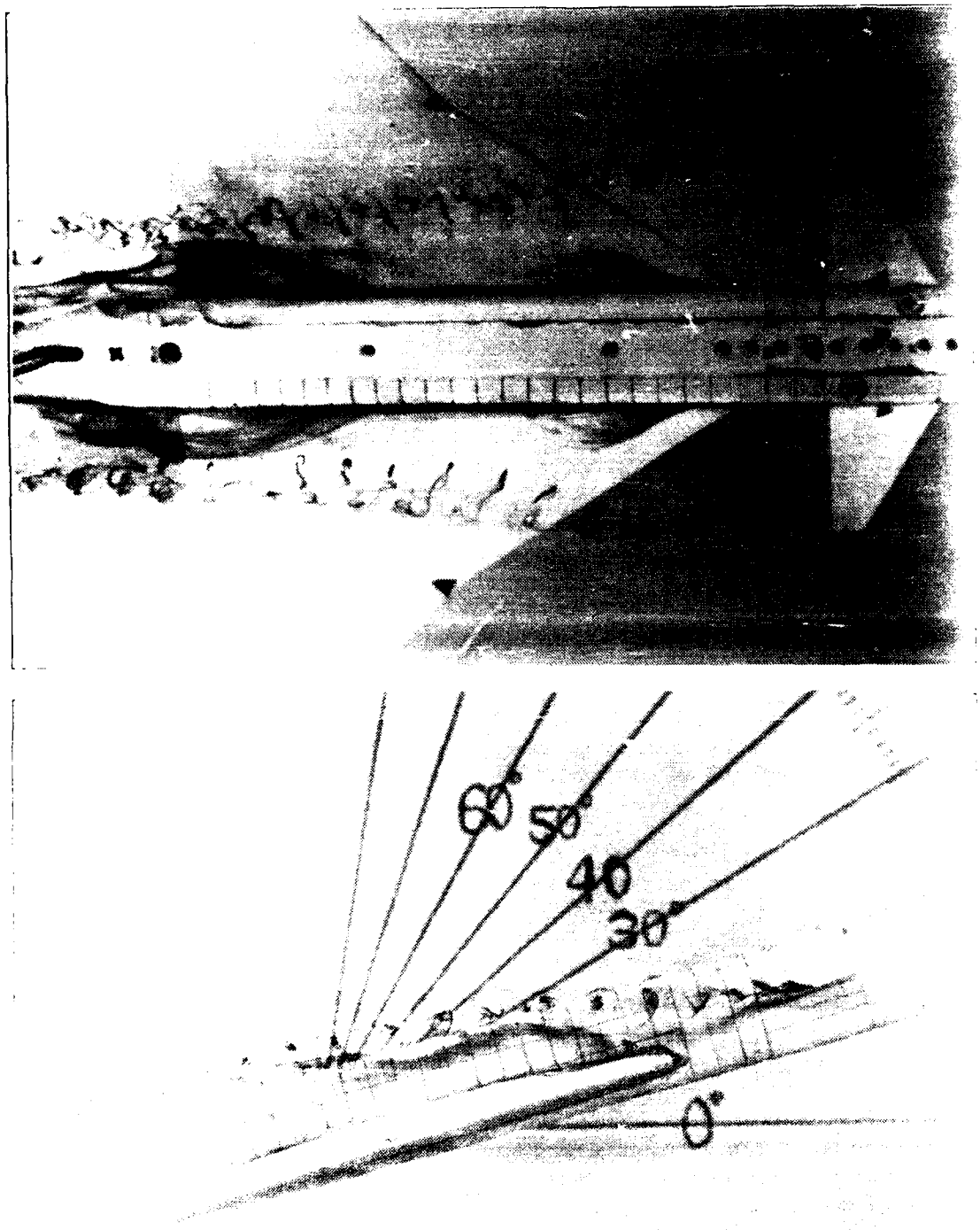

Figure [illegible] Wing Root Vortex. High pitch rate (P, α=15°, p=0

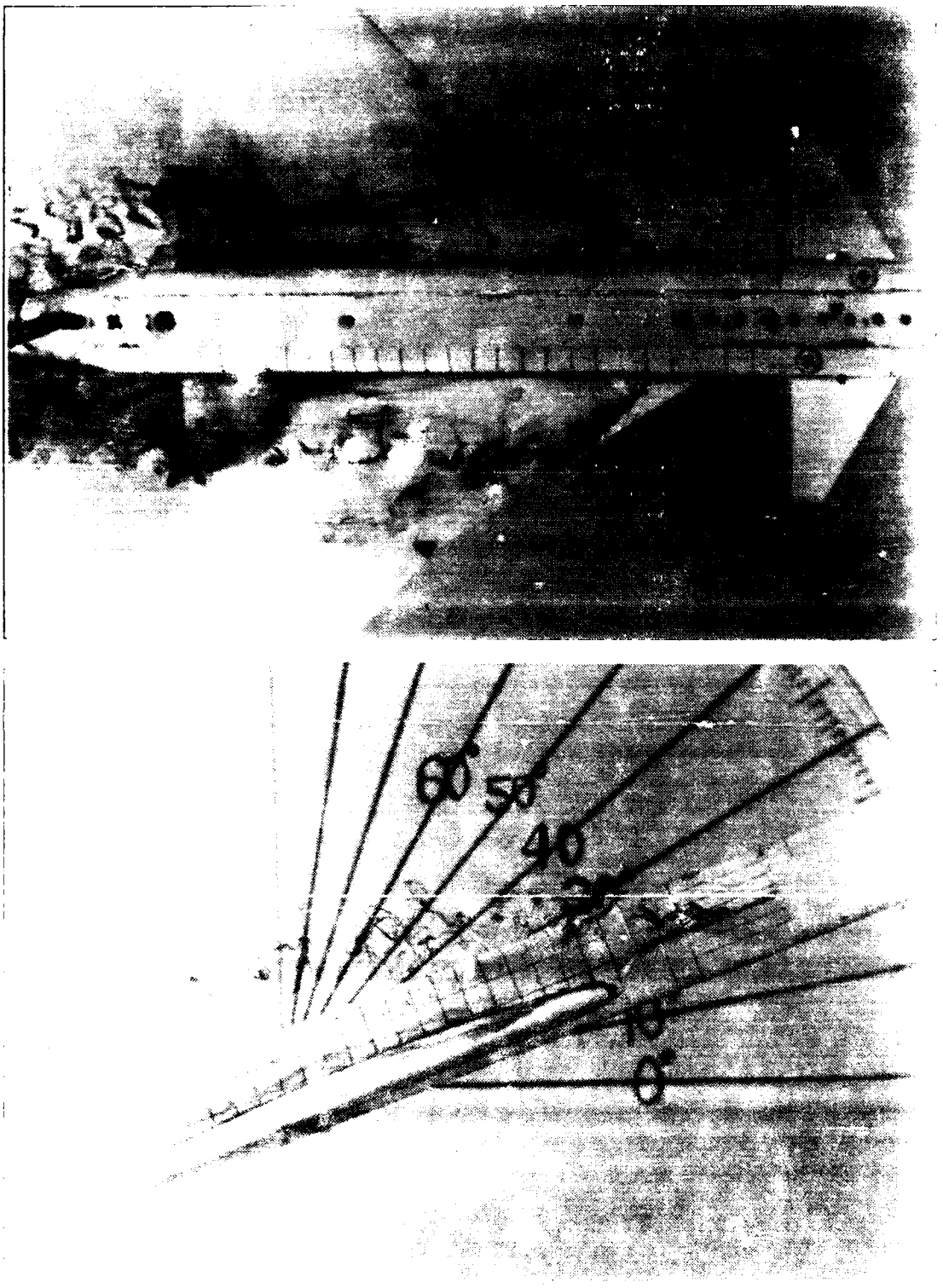

Fig. [illegible]. Wing Root Vortex, High pitch rate UP, $\alpha = 20°$, $p = 0$

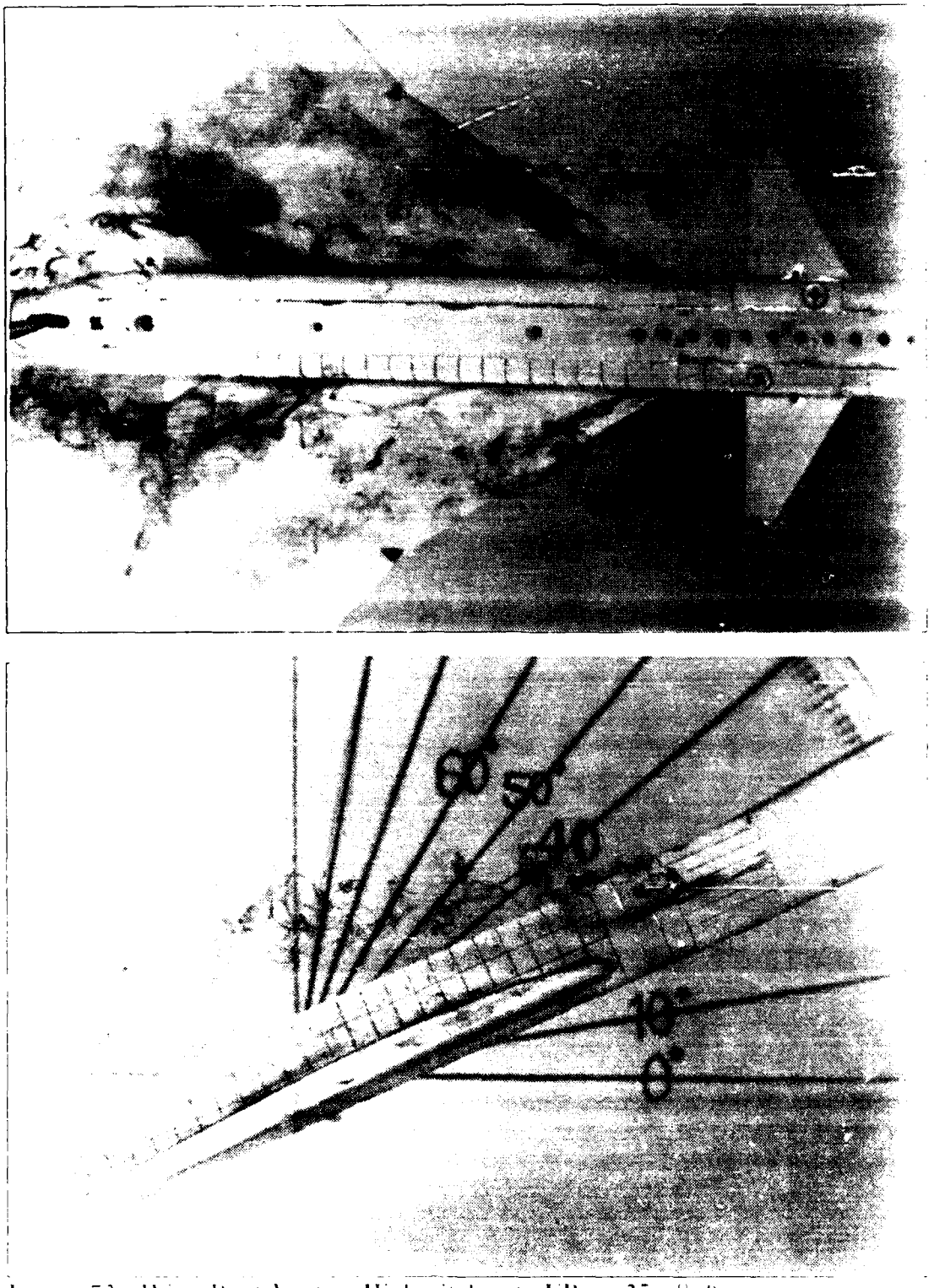

Figure 72. Wing Root Vortex, High pitch rate UP, α=25 , β=0

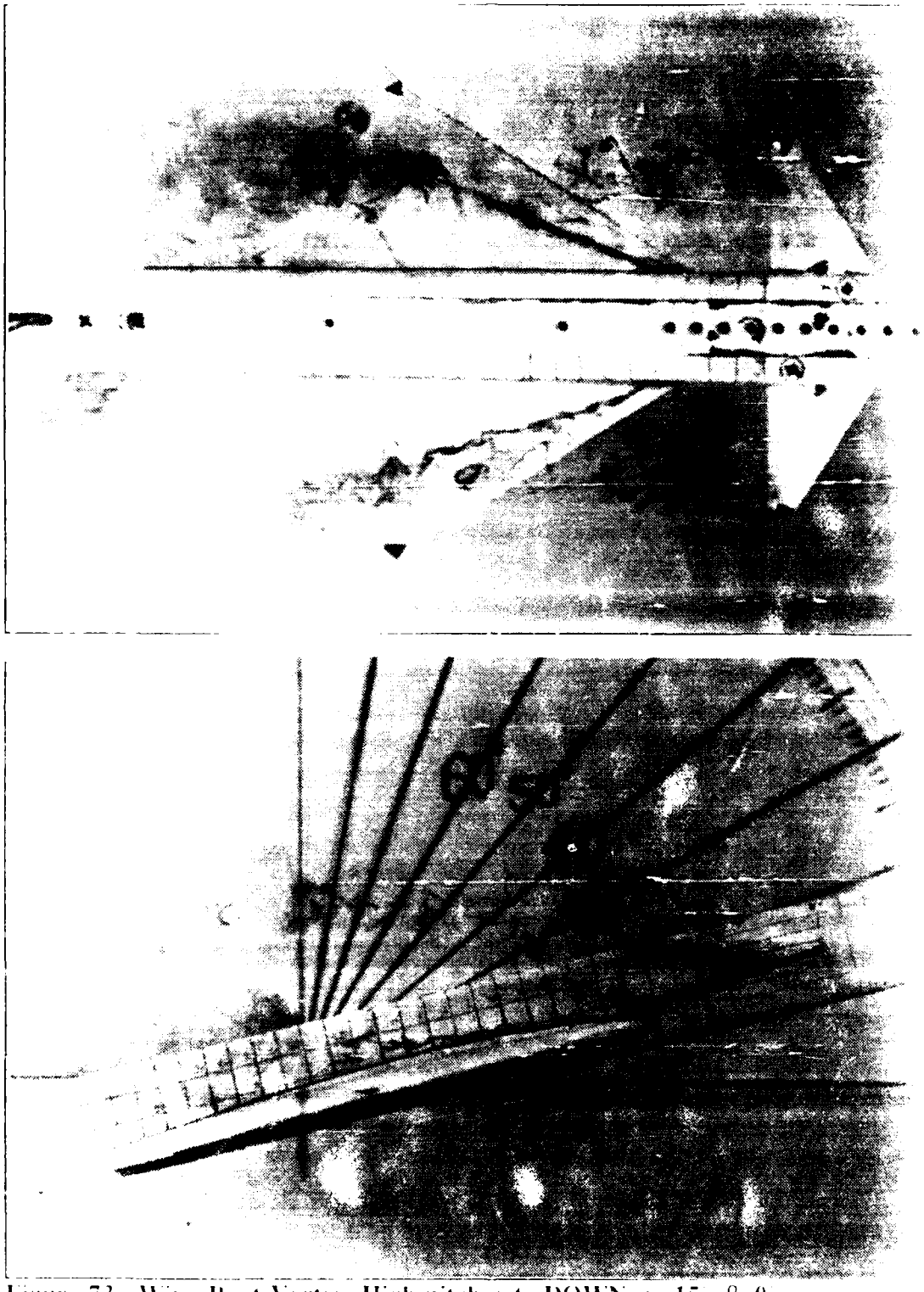

Figure 73. Wing Root Vortex, High pitch rate DOWN, α=15 , β=0

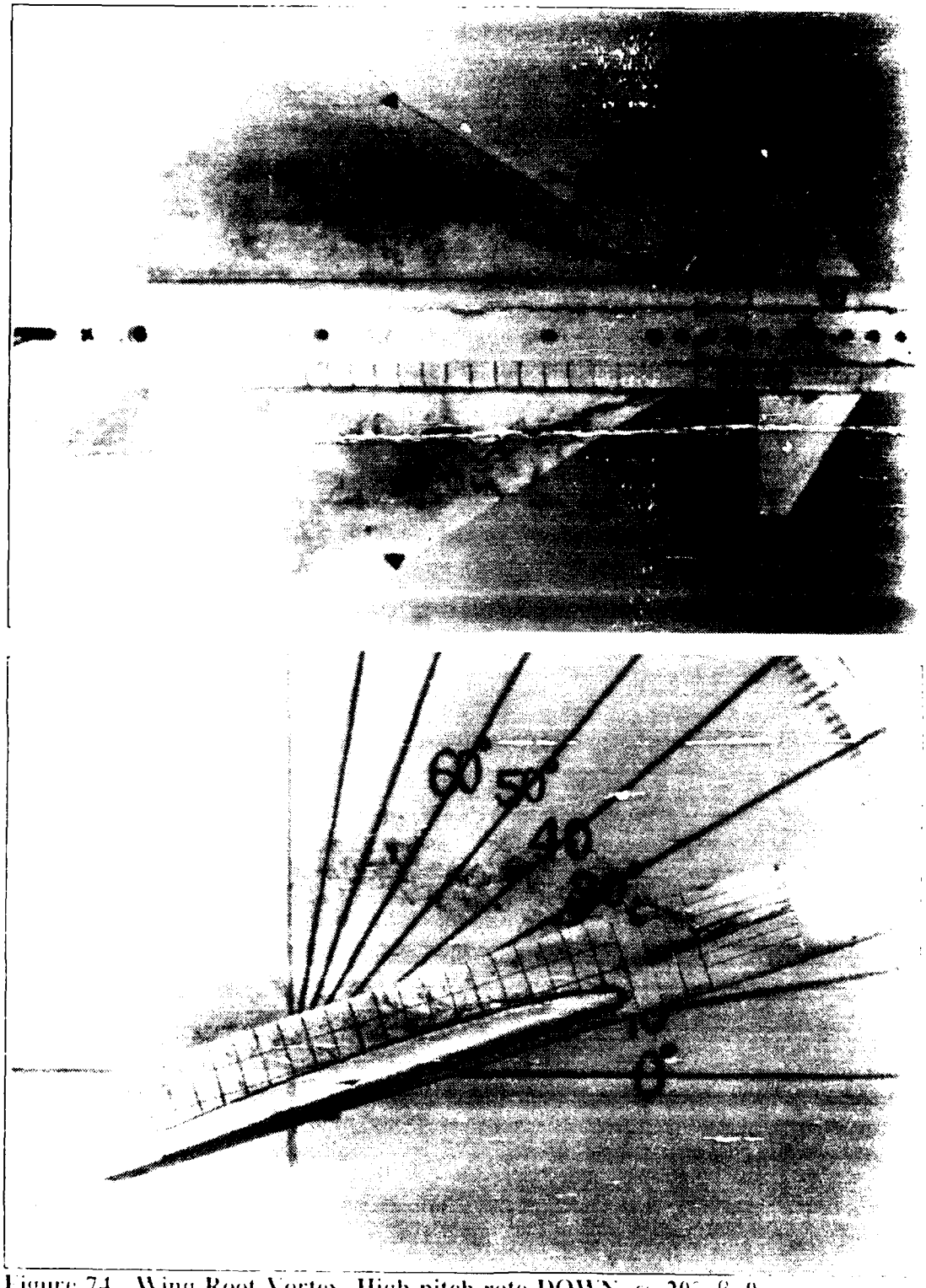

Figure 74. Wing Root Vortex, High pitch rate DOWN, α=20°, β=0

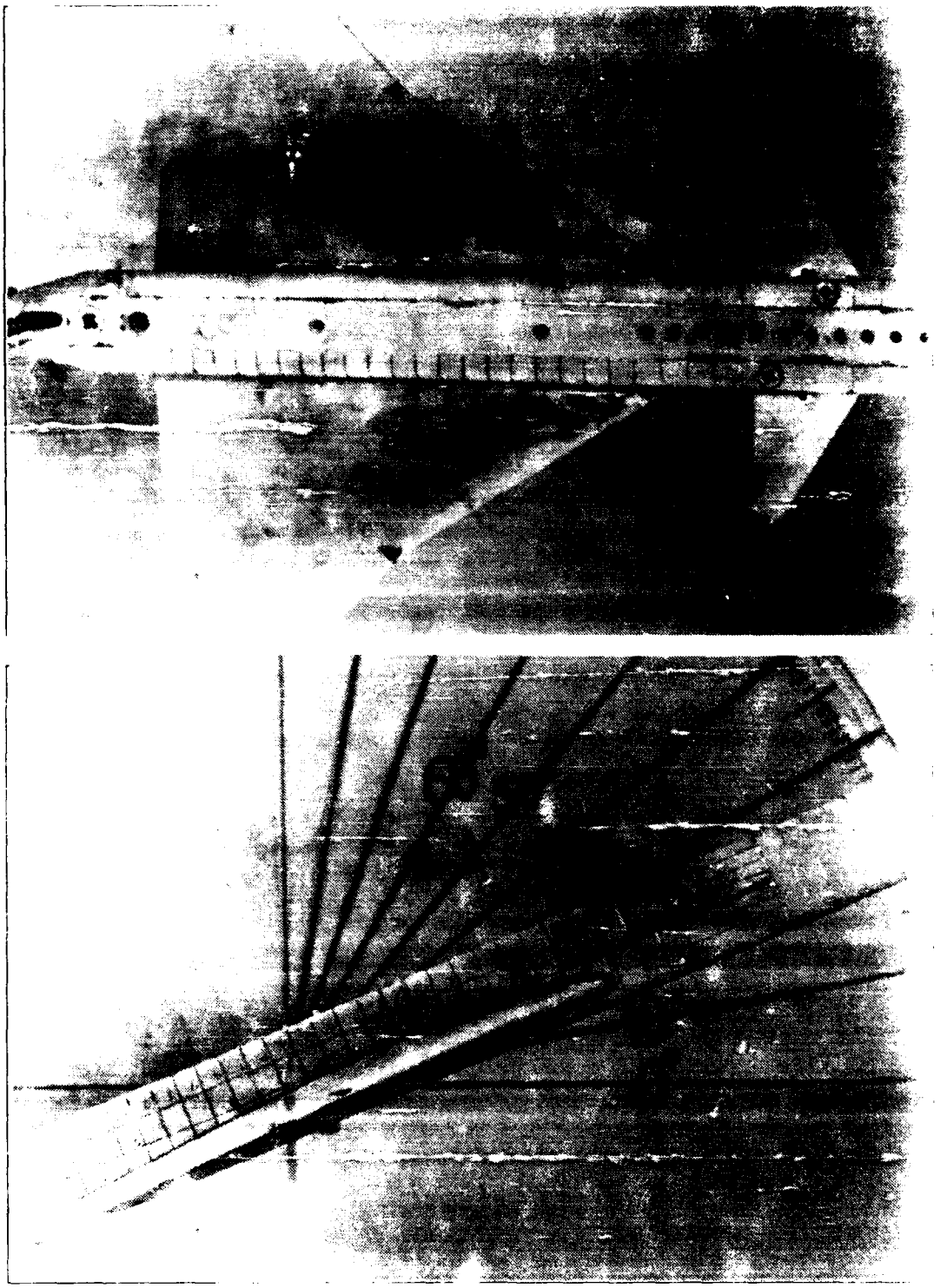

Figure 75. Wing Root Vortex, High pitch rate DOWN, α=25 , β=0

APPENDIX B. EXPERIMENTAL RESULTS (GRAPHS)
FIGURES 76 THROUGH 92

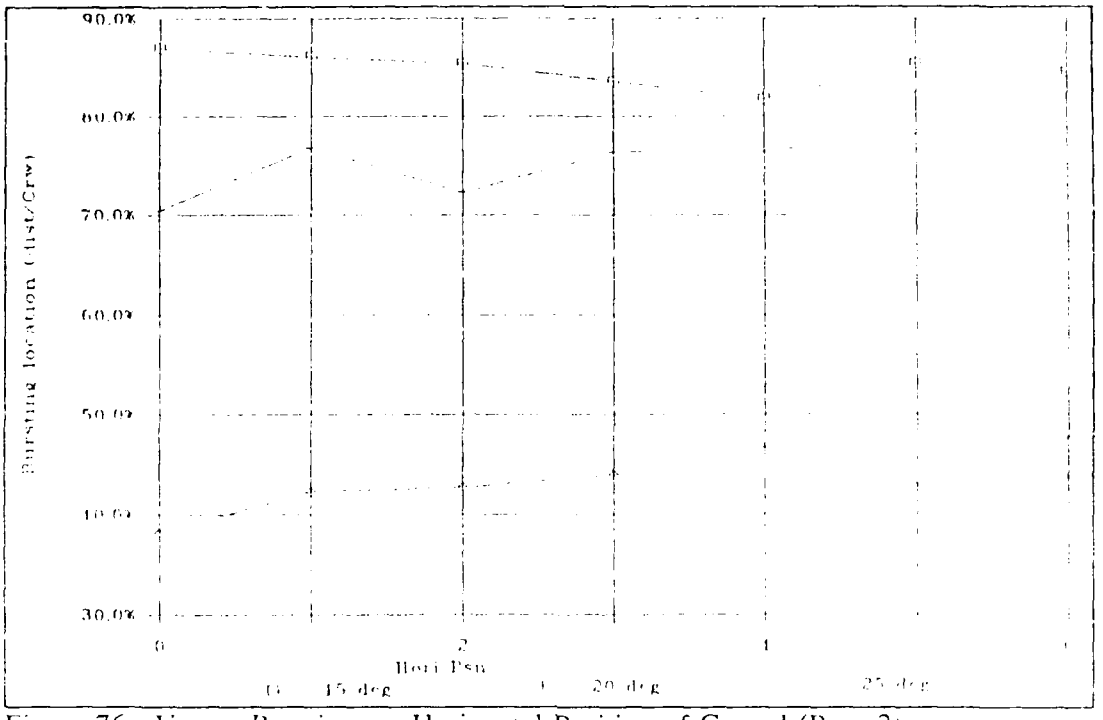

Figure 76. Vortex Bursting vs. Horizontal Position of Canard (Row 2)

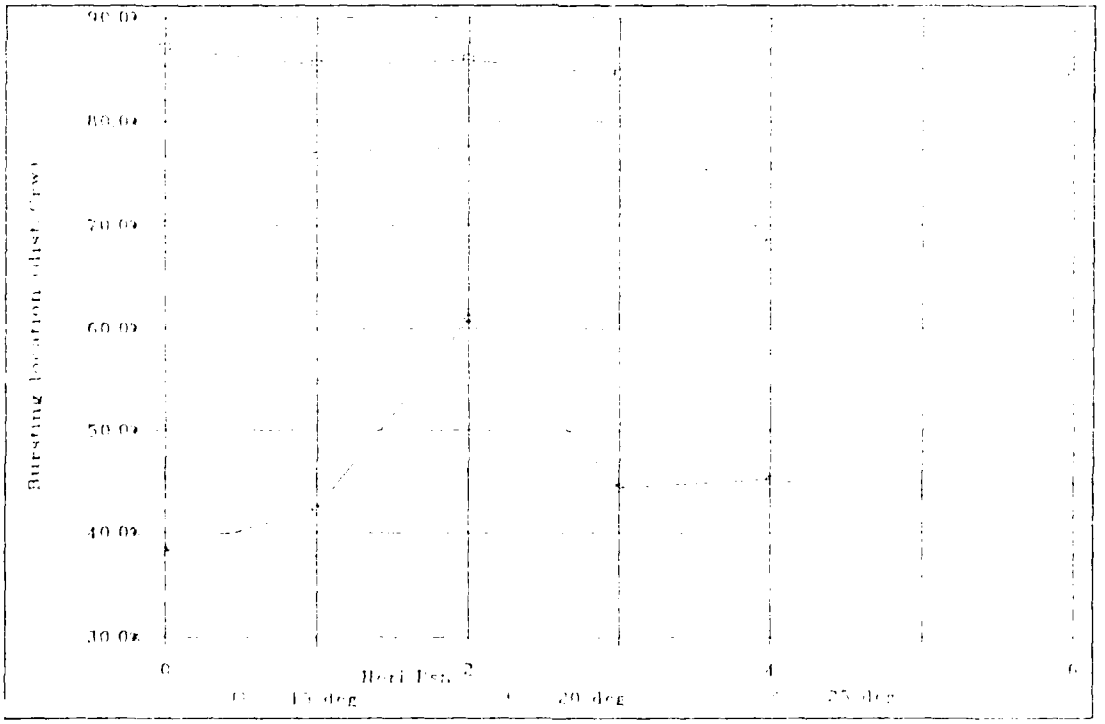

Figure 77. Vortex Bursting vs. Horizontal Position of Canard (Row 3)

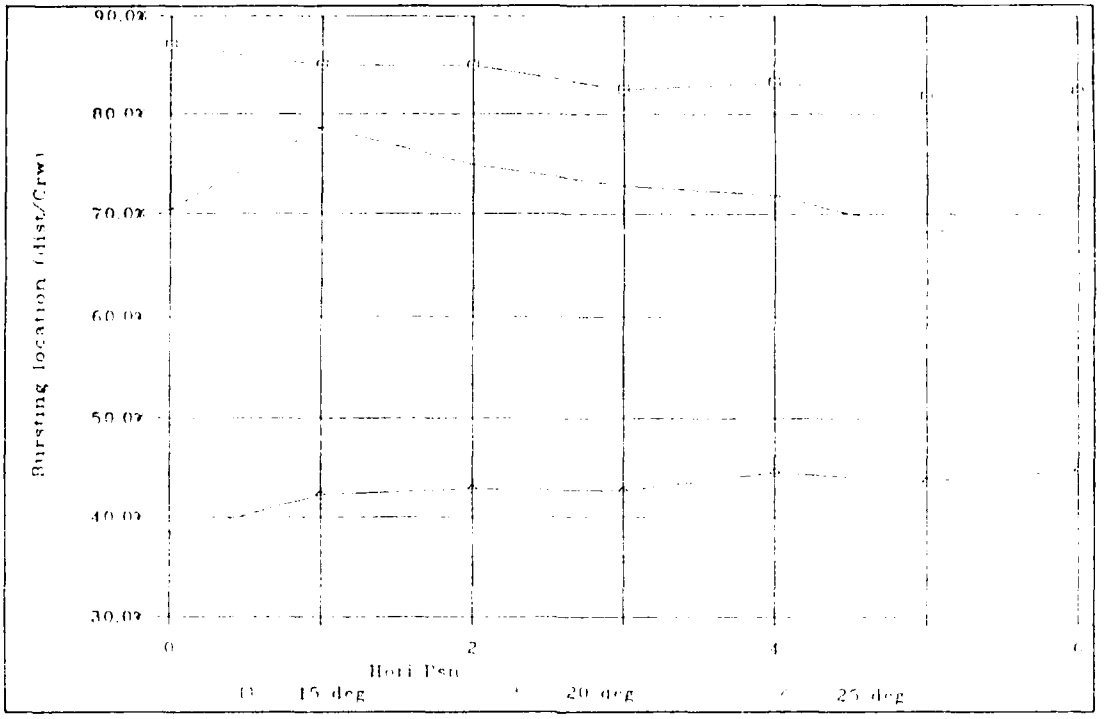

Figure 78. Vortex Bursting vs. Horizontal Position of Canard (Row 4)

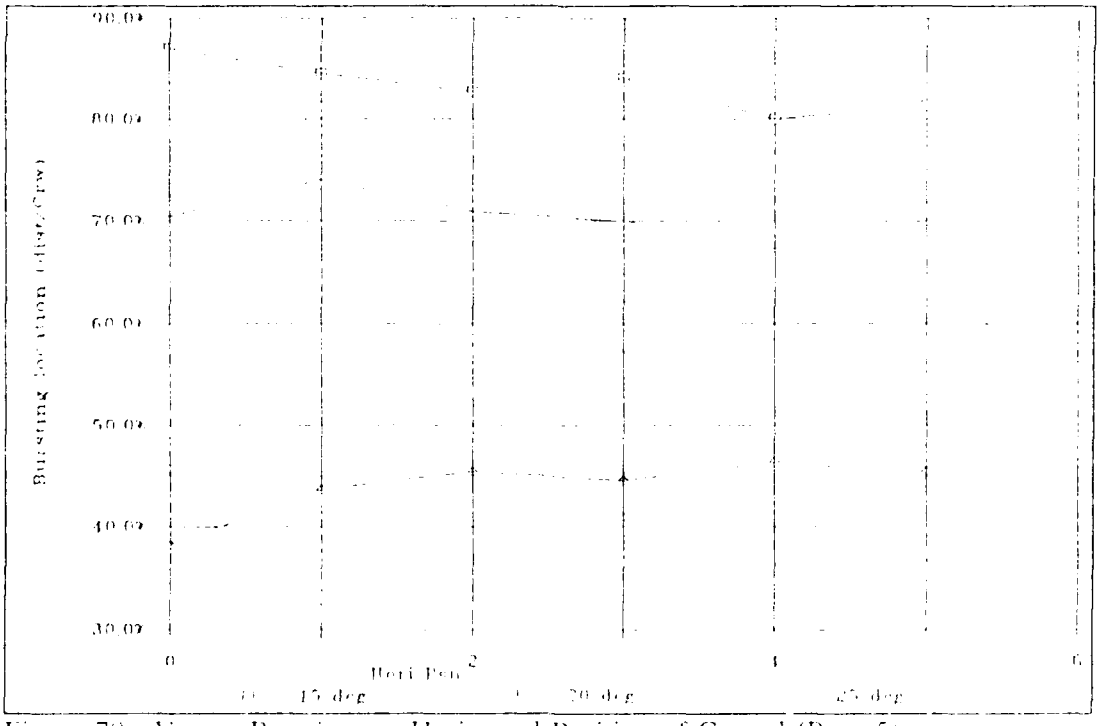

Figure 79. Vortex Bursting vs. Horizontal Position of Canard (Row 5)

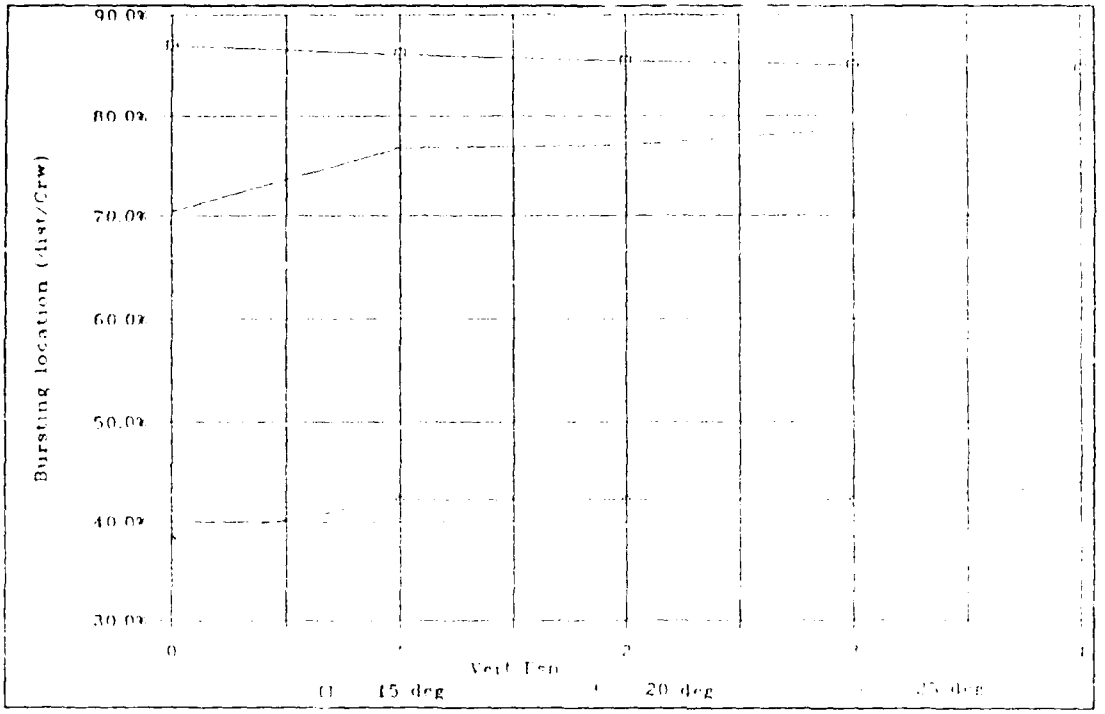

Figure 80. Vortex Bursting vs. Vertical Position of Canard (Location A)

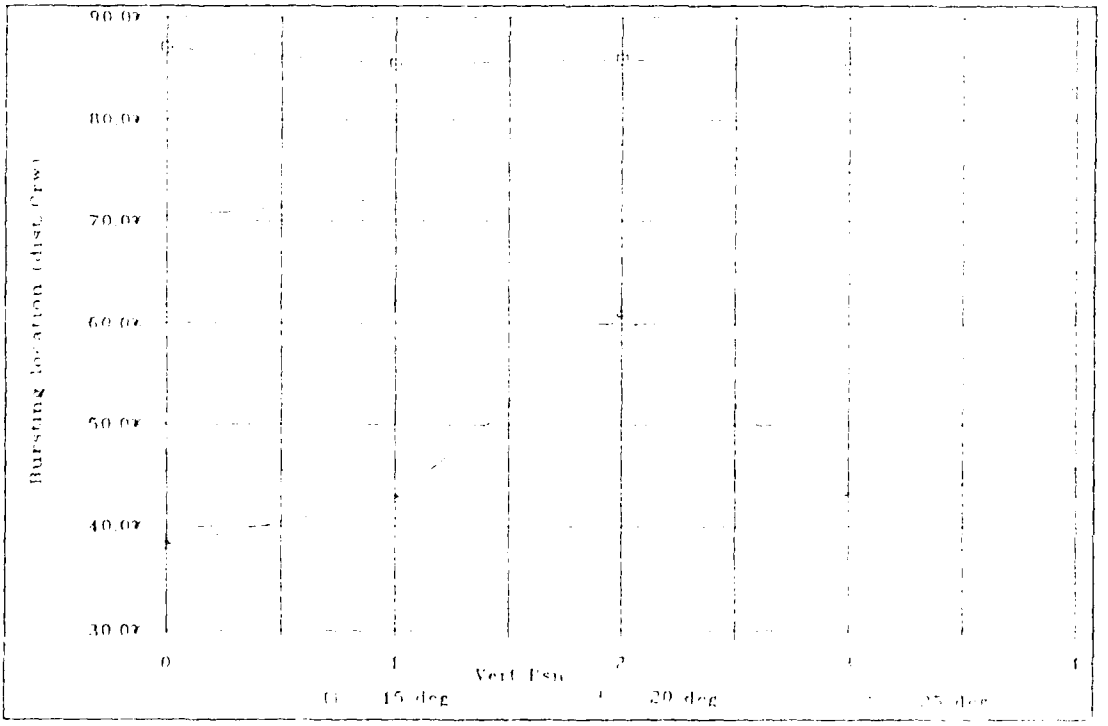

Figure 81. Vortex Bursting vs. Vertical Position of Canard (Location B)

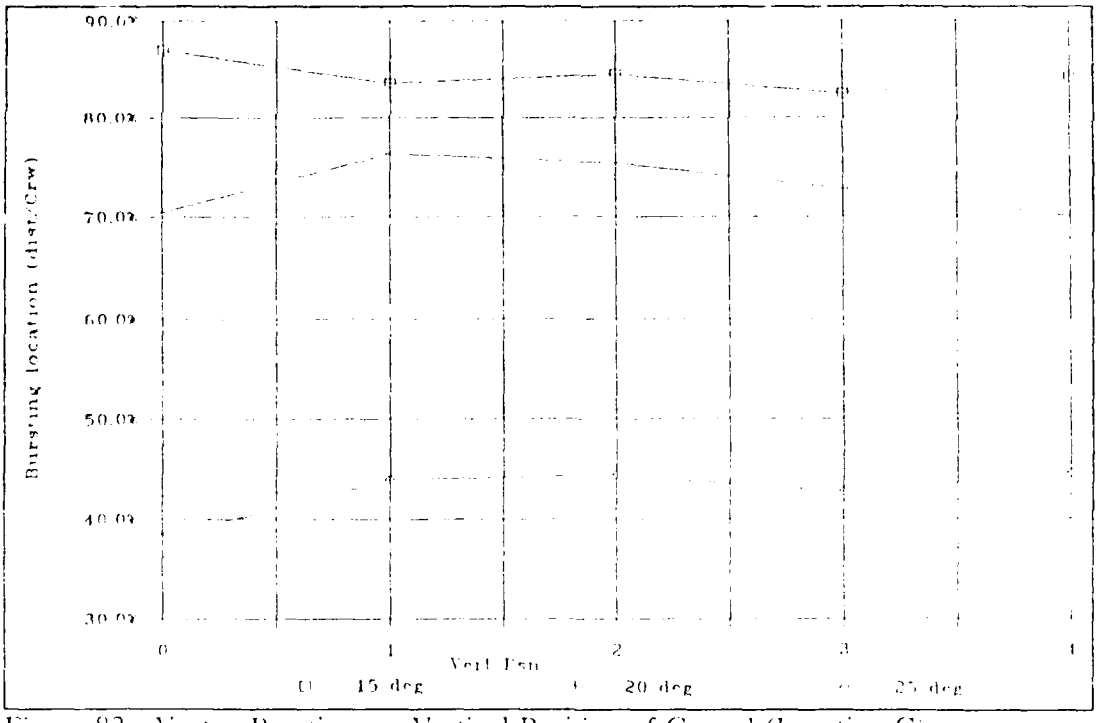

Figure 82. Vortex Bursting vs. Vertical Position of Canard (Location C)

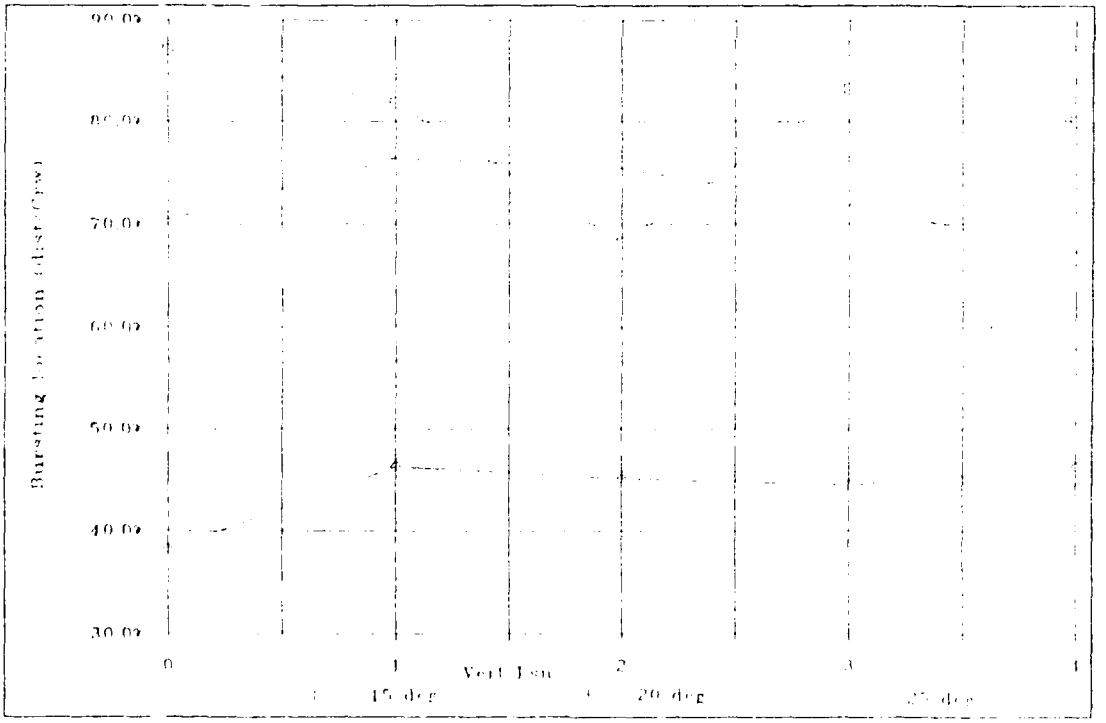

Figure 83. Vortex Bursting vs. Vertical Position of Canard (Location D)

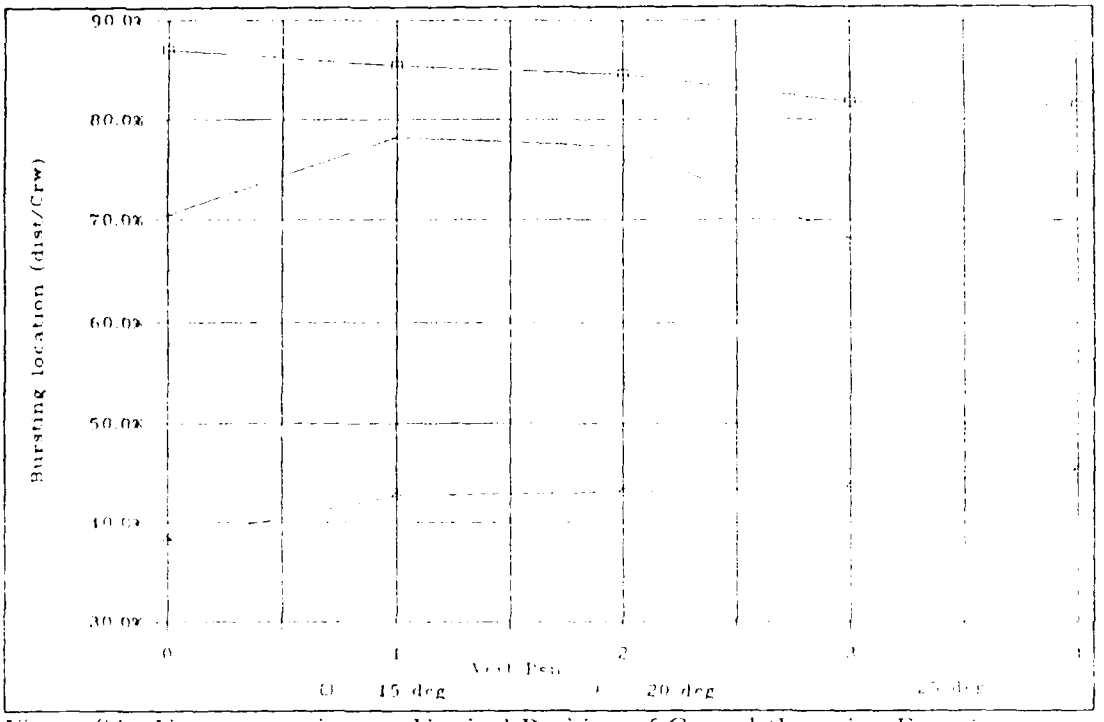

Figure 84. Vortex Bursting vs. Vertical Position of Canard (Location F)

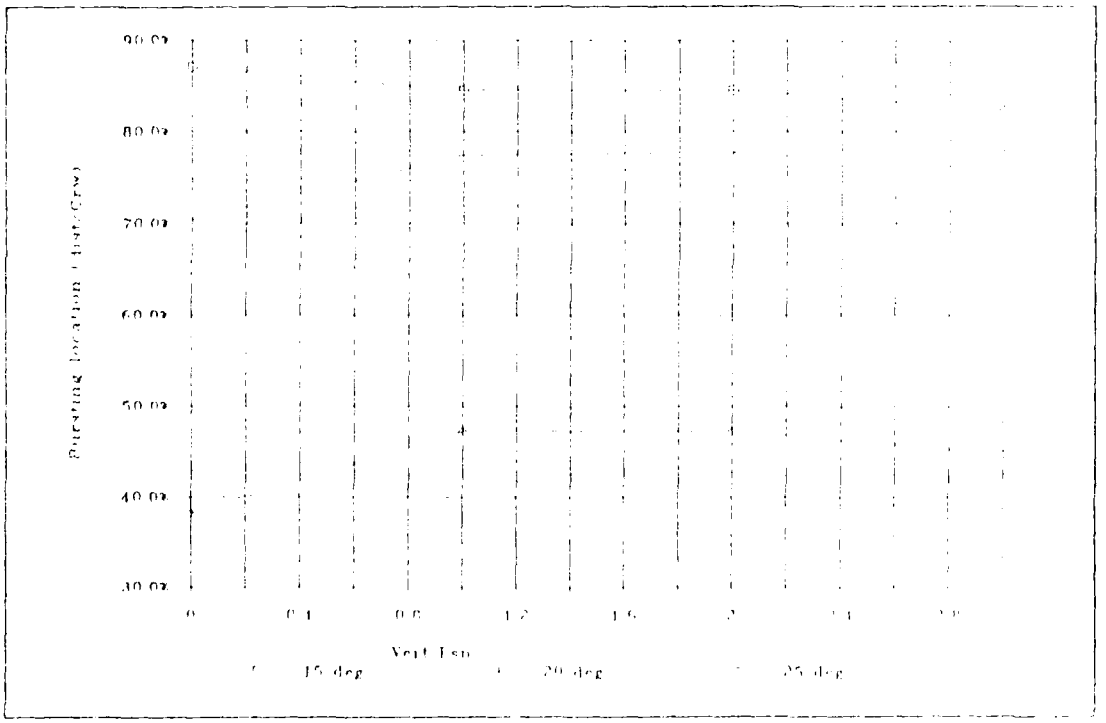

Figure 85. Vortex Bursting vs. Vertical Position of Canard (Location F)

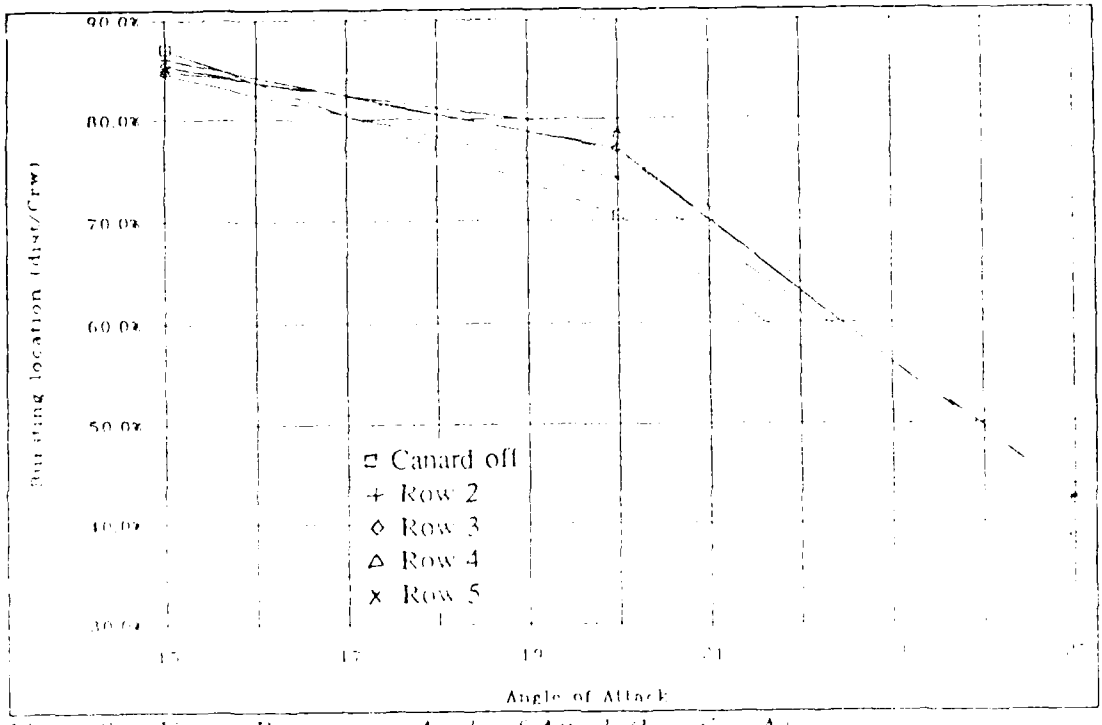

Figure 86. Vortex Bursting vs. Angle of Attack (Location A)

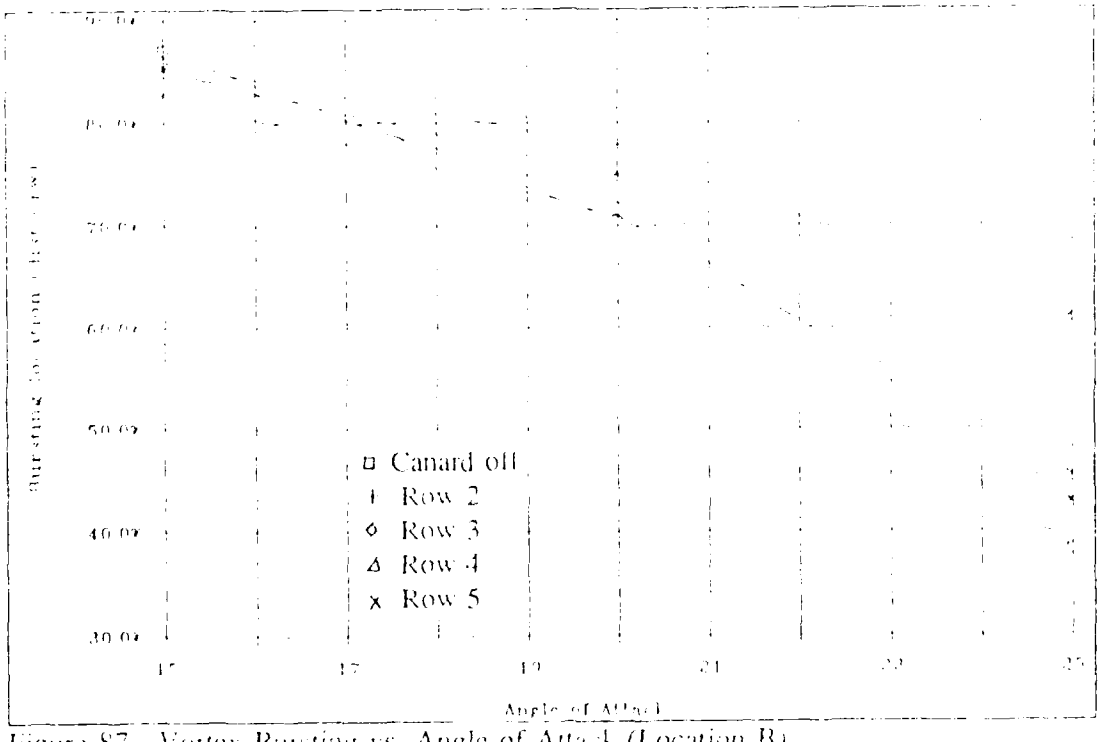

Figure 87. Vortex Bursting vs. Angle of Attack (Location B)

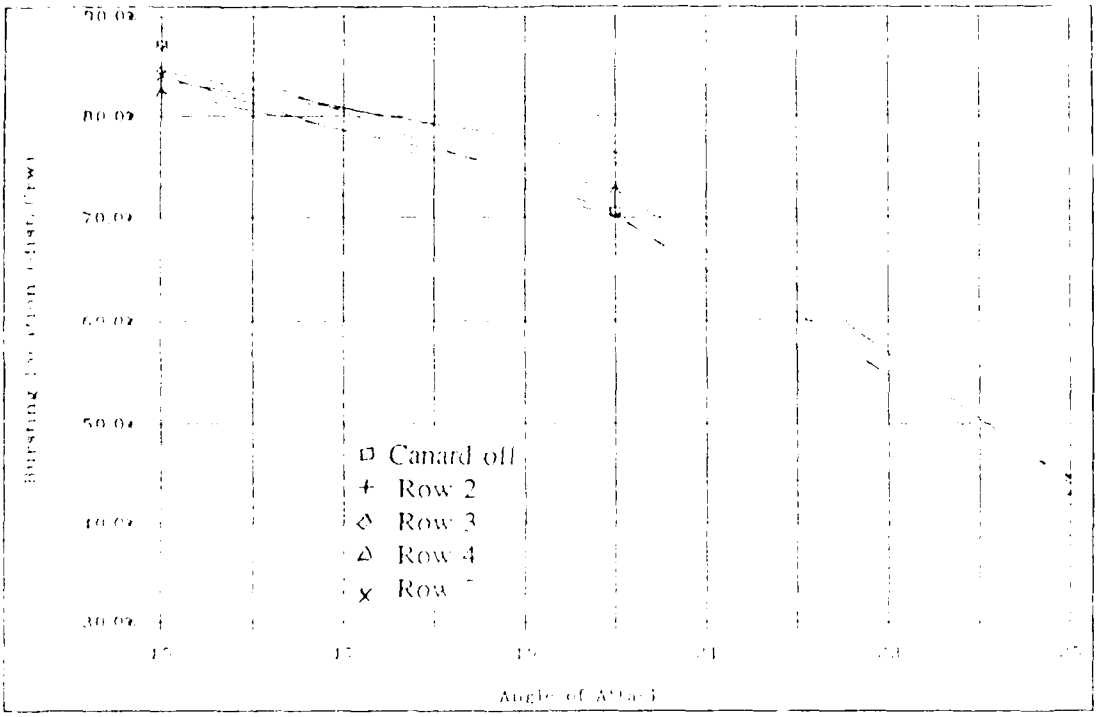

Figure 88. Vortex Bursting vs. Angle of Attack (Location C)

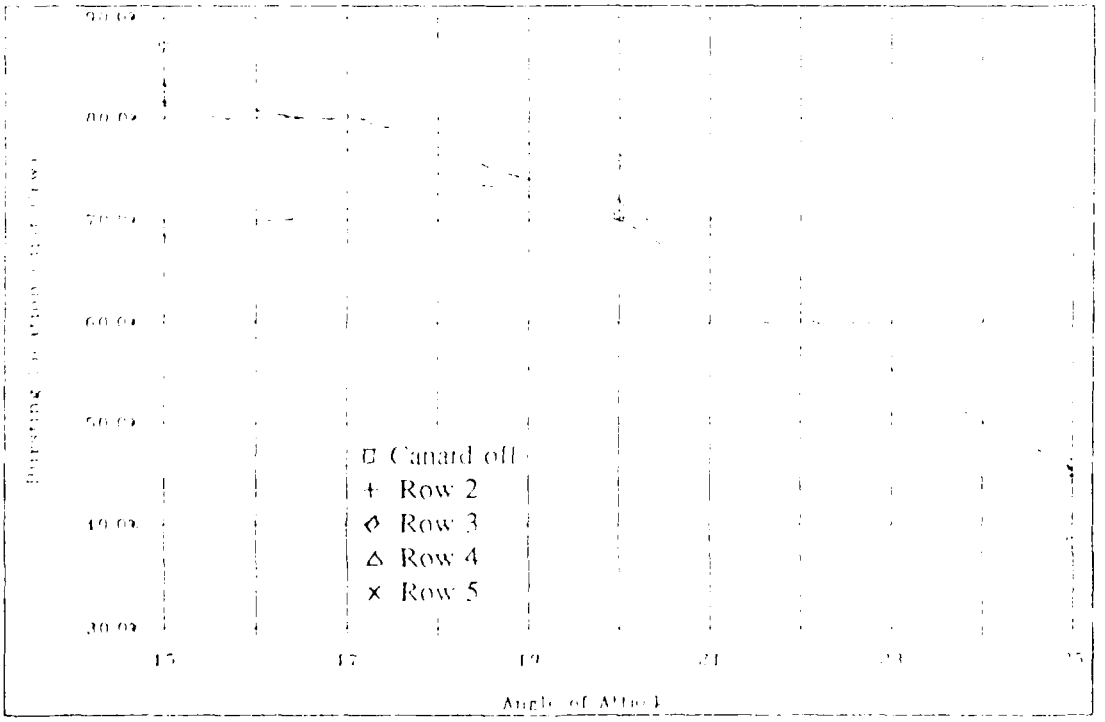

Figure 89. Vortex Bursting vs. Angle of Attack (Location D)

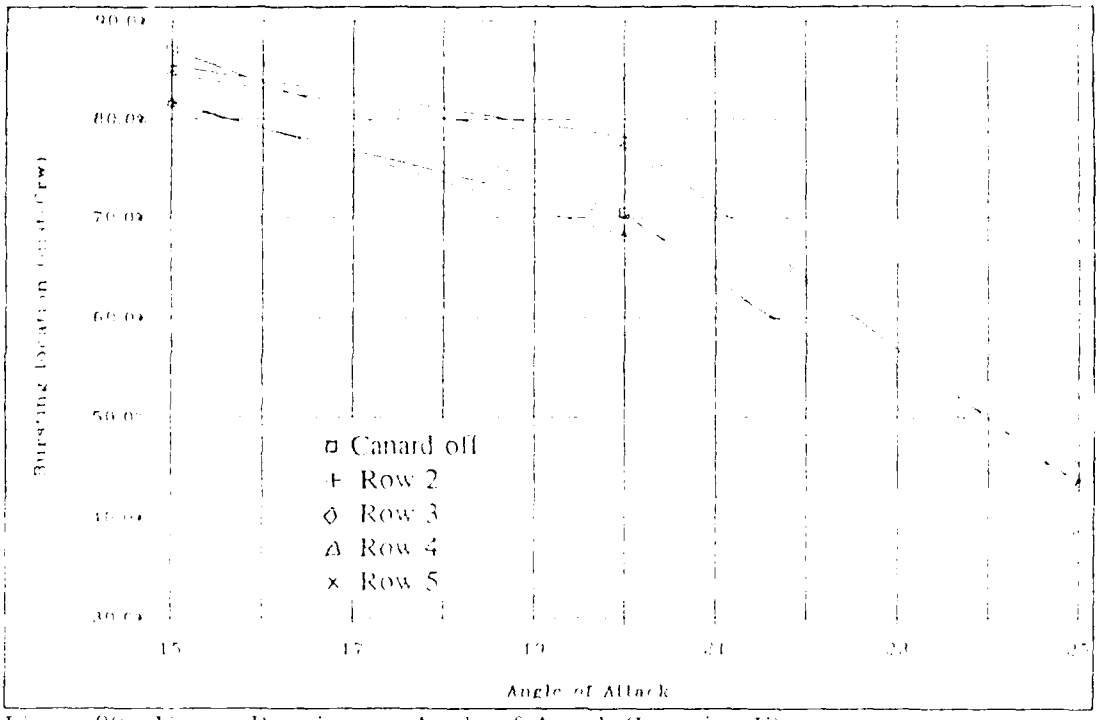

Figure 90. Vortex Bursting vs. Angle of Attack (Location E)

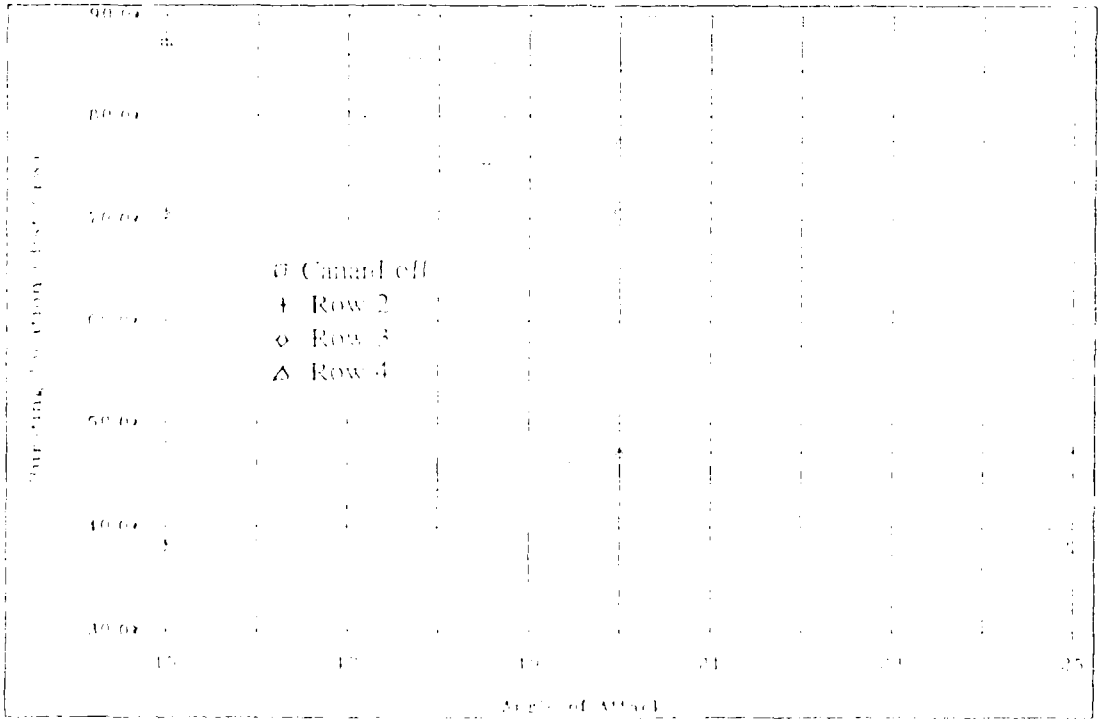

Figure 91. Vortex Bursting vs. Angle of Attack (Location F)

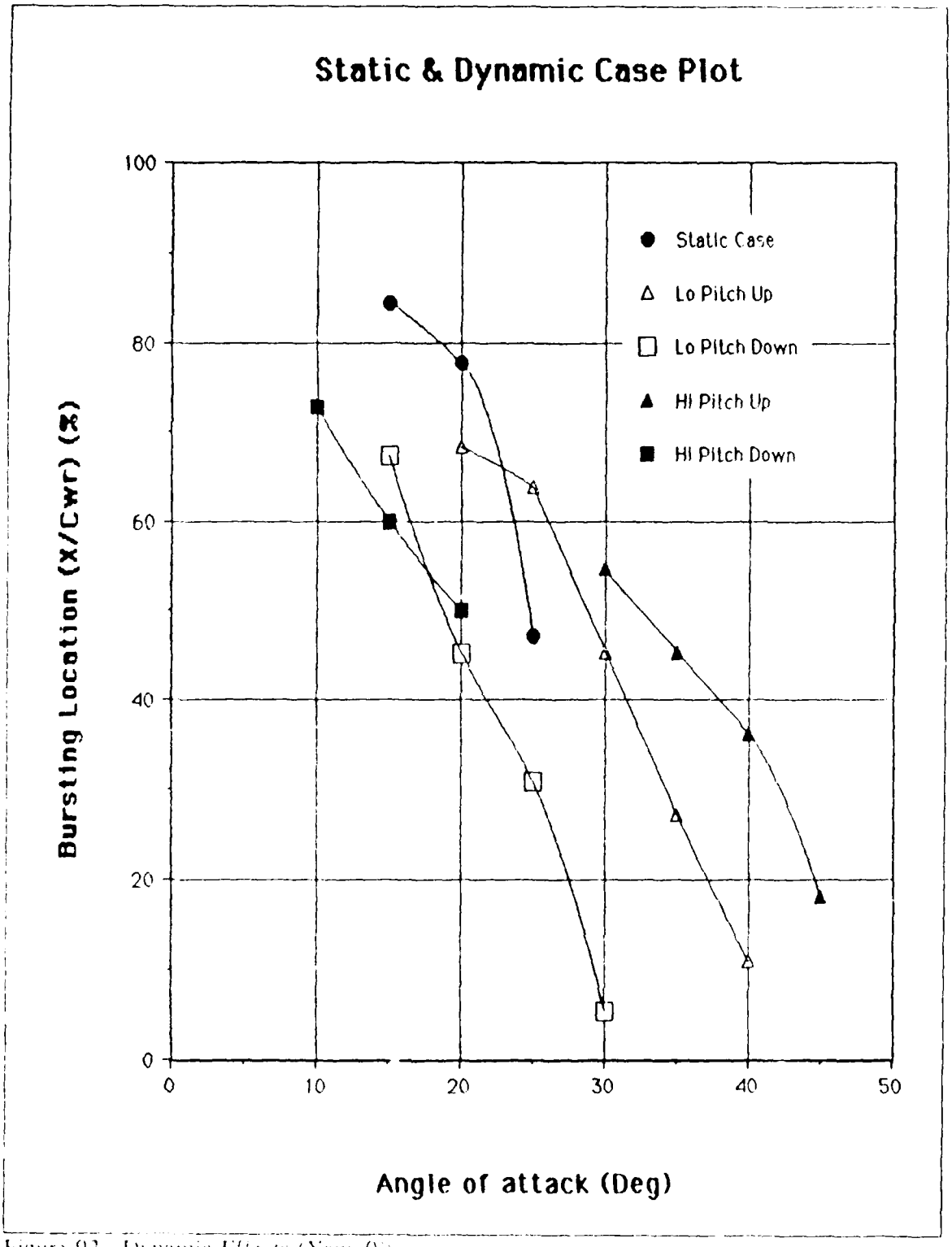

Figure 92 Dynamic Effects (Yaw=0°)

Intentional Blank

APPENDIX C. MISCELLANEOUS DATA

Table I. GEOMETRIC COORDINATES OF THE CANARD

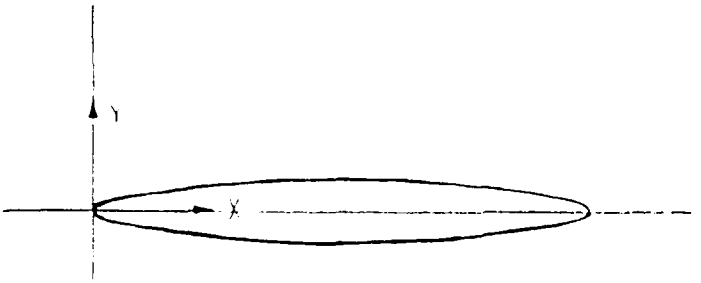

ROOT SECTION		TIP SECTION	
X	Y	X	Y
0.000	± 0.000	0.000	± 0.000
0.012	± 0.015	0.003	± 0.004
0.100	± 0.030	0.025	± 0.008
0.200	± 0.048	0.050	± 0.012
0.300	± 0.056	0.075	± 0.014
0.400	± 0.061	0.100	± 0.015
0.500	± 0.063	0.125	± 0.016
0.600	± 0.061	0.150	± 0.015
0.700	± 0.056	0.175	± 0.014
0.800	± 0.048	0.200	± 0.012
0.900	± 0.030	0.225	± 0.008
0.988	± 0.015	0.247	± 0.004
1.000	± 0.000	0.250	± 0.000

NOTE:
LEADING EDGE RADIUS AND TRAILING EDGE RADIUS ARE 0.0156 × CHORD.

Table I(continued). PLANFORM DRAWING OF THE WING

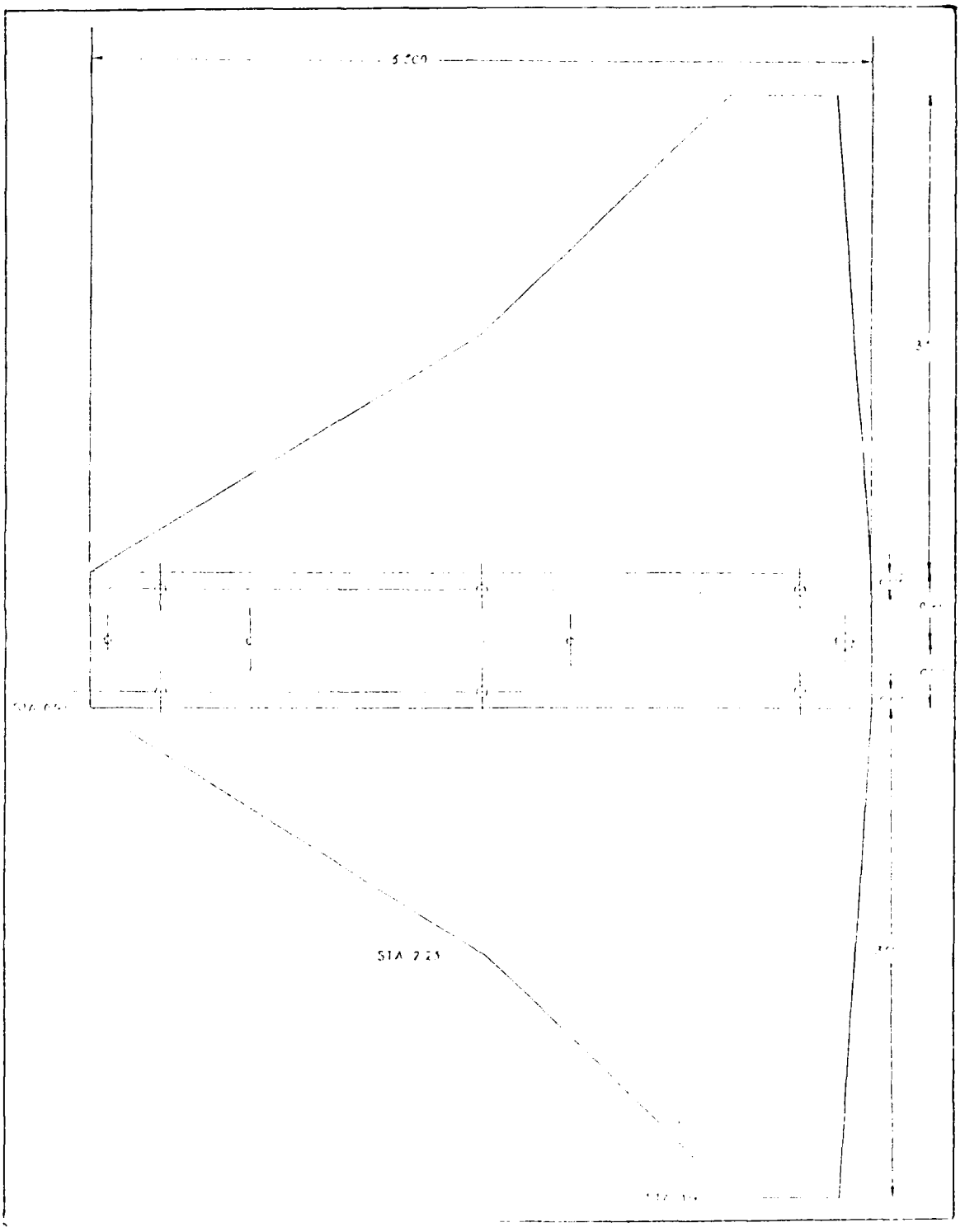

Table I(continued). GEOMETRIC COORDINATES OF THE WING

AIRFOIL COORDINATES

STATION 0.50				STATION 2.25				STATION 4.00			
X_{UPPER}	Y_{UPPER}	X_{LOWER}	Y_{LOWER}	X_{UPPER}	Y_{UPPER}	X_{LOWER}	Y_{LOWER}	X_{UPPER}	Y_{UPPER}	X_{LOWER}	Y_{LOWER}
0.0	0.0	0.0	0.0	0.0	0.0	0.0	0.0	0.0	0.0	0.0	0.0
0.025	0.028	0.050	-0.022	0.021	0.013	0.014	-0.011	0.003	0.004	0.004	-0.003
0.053	0.034	0.044	-0.027	0.019	0.016	0.021	-0.013	0.005	0.005	0.006	-0.004
0.066	0.044	0.071	-0.032	0.031	0.021	0.038	-0.015	0.009	0.006	0.010	-0.004
0.135	0.061	0.140	-0.040	0.064	0.029	0.067	-0.019	0.018	0.008	0.019	-0.005
0.272	0.086	0.278	-0.052	0.130	0.041	0.133	-0.025	0.037	0.012	0.038	-0.007
0.409	0.107	0.416	-0.060	0.195	0.051	0.198	-0.029	0.056	0.015	0.057	-0.008
0.547	0.125	0.553	-0.068	0.261	0.060	0.264	-0.032	0.075	0.017	0.075	-0.009
0.821	0.154	0.828	-0.079	0.392	0.073	0.595	-0.038	0.112	0.021	0.113	-0.011
1.097	0.176	1.103	-0.088	0.524	0.084	0.526	-0.042	0.150	0.024	0.150	-0.012
1.372	0.193	1.378	-0.095	0.655	0.092	0.657	-0.045	0.187	0.026	0.188	-0.013
1.648	0.206	1.652	-0.099	0.787	0.099	0.788	-0.048	0.225	0.028	0.225	-0.014
1.923	0.216	1.927	-0.103	0.918	0.103	0.920	-0.049	0.262	0.029	0.263	-0.014
2.199	0.222	2.201	-0.105	1.050	0.106	1.051	-0.050	0.300	0.030	0.300	-0.014
2.474	0.225	2.476	-0.105	1.181	0.107	1.182	-0.050	0.337	0.031	0.338	-0.014
2.750	0.225	2.750	-0.104	1.313	0.107	1.313	-0.049	0.375	0.031	0.375	-0.014
3.025	0.221	3.025	-0.101	1.444	0.106	1.444	-0.048	0.413	0.030	0.412	-0.014
3.301	0.214	3.299	-0.096	1.575	0.102	1.575	-0.046	0.450	0.029	0.450	-0.013
3.576	0.202	3.574	-0.089	1.707	0.096	1.706	-0.042	0.488	0.027	0.487	-0.012
3.852	0.181	3.848	-0.074	1.838	0.086	1.837	-0.035	0.525	0.025	0.525	-0.010
4.127	0.157	4.123	-0.058	1.970	0.075	1.968	-0.028	0.563	0.021	0.562	-0.008
4.402	0.129	4.398	-0.041	2.101	0.061	2.099	-0.020	0.600	0.018	0.600	-0.006
4.677	0.098	4.673	-0.024	2.232	0.047	2.230	-0.011	0.638	0.013	0.637	-0.003
4.953	0.065	4.949	-0.008	2.363	0.031	2.362	-0.004	0.675	0.009	0.675	-0.001
5.228	0.032	5.224	0.002	2.494	0.015	2.493	0.001	0.713	0.004	0.712	0.0

Table II. RAW DATA FROM EXPERIMENTS (LOCATION A THROUGH C)

Investigation of vortex bursting location (Cwr = 5.5 in.)

AOA ==>>	Bursting Location 15			20			25		
Canard Psn	Min	Ave	Max	Min	Ave	Max	Min	Ave	Max
W/O Cnd	4.7	4.75	4.8	3.7	3.9	4.1	2.2	2.35	2.5
	4.75	4.825	4.9	3.7	3.85	4	1.9	1.85	1.8
	4.725	4.7875	4.85	3.7	3.875	4.05	2.05	2.1	2.15
A2	4.65	4.775	4.9	4.15	4.225	4.3	2	2.25	2.5
	4.5	4.7	4.9	4.15	4.225	4.3	2.3	2.4	2.5
Ave	4.575	4.7375	4.9	4.15	4.225	4.3	2.15	2.325	2.5
A3	4.6	4.7	4.8	4.15	4.25	4.35	2.35	2.475	2.6
				4.1	4.225	4.35	2.1	2.3	2.5
							2	2.2	2.4
Ave	4.6	4.7	4.8	4.125	4.2375	4.35	2.15	2.325	2.5
A4	4.6	4.7	4.8	4.2	4.3	4.4	2.1	2.25	2.4
	4.5	4.65	4.8	4.25	4.35	4.45	2.3	2.4	2.5
Ave	4.55	4.675	4.8	4.225	4.325	4.425	2.2	2.325	2.45
A5				3.9	4.1	4.3	2.3	2.4	2.5
				3.9	4.05	4.2			
Ave	-----	-----	-----	3.9	4.075	4.25	2.3	2.4	2.5
B2	4.5	4.7	4.9	3.8	3.975	4.15	2.25	2.35	2.45
B3	4.5	4.625	4.75	4	4.15	4.3	2.25	2.375	2.5
	4.5	4.65	4.8	4.2	4.3	4.4	2.5	2.625	2.75
							2.5	2.6	2.7
	4.8	4.9	5	4.2	4.35	4.5	2.35	2.45	2.55
Ave	4.6	4.725	4.85	4.1333	4.2666	4.4	2.4	3.35	2.625
B4	4.5	4.65	4.8	4.1	4.175	4.25	2.2	2.35	2.5
	4.5	4.65	4.8	3.9	4.05	4.2	2.2	2.35	2.5
	4.6	4.725	4.85	4	4.125	4.25	2.25	2.375	2.5
Ave	4.5333	4.675	4.8166	4	4.1166	4.2333	2.2166	2.3583	2.5
B5	4.4	4.55	4.7	3.7	3.9	4.1	2.3	2.5	2.7
C2	4.3	4.5	4.7	4.1	4.2	4.3	2.25	2.375	2.5
	4.6	4.65	4.7	4.1	4.2	4.3	2.26	2.38	2.5
	4.5	4.65	4.8	4.1	4.2	4.3	2.3	2.5	2.7
Ave	4.4666	4.6	4.7333	4.1	4.2	4.3	2.27	2.4183	2.5666
C3	4.5	4.65	4.8	4	4.15	4.3	2.2	2.35	2.5
	4.5	4.65	4.8	4	4.15	4.3	2.5	2.625	2.75
							2.2	2.35	2.5
Ave	4.5	4.65	4.8	4	4.15	4.3	2.3	2.4416	2.5833
C4	4.3	4.5	4.7	3.8	4	4.2	2.2	2.35	2.5
	4.4	4.575	4.75	3.8	4	4.2	2.25	2.35	2.45
Ave	4.35	4.5375	4.725	3.8	4	4.2	2.225	2.35	2.475
C5	4.5	4.625	4.75	3.7	3.85	4	2.3	2.45	2.6

Table II(cont.). RAW DATA FROM EXPERIMENTS (LOCATION D THROUGH F)

Investigation of vortex bursting location (Cwr = 5.5 in.)

AOA ==>>	Bursting Location 15			20			25		
Canard Psn	Min	Ave	Max	Min	Ave	Max	Min	Ave	Max
D2	4.3	4.5	4.7	4.1	4.2	4.3	2.4	2.55	2.7
D3	2.6	2.8	3	3.9	4.1	4.3	2.3	2.525	2.75
	4.5	4.7	4.9	4.1	4.2	4.3	2.3	2.45	2.6
Ave	3.55	3.75	3.95	4	4.15	4.3	2.3	2.4875	2.675
D4	4.4	4.575	4.75	3.7	3.95	4.2	2.3	2.45	2.6
D5	4.2	4.4	4.6	3.5	3.7	3.9	2.4	2.55	2.7
E2	4.6	4.7	4.8	4.2	4.3	4.4	2.2	2.35	2.5
E3	4.5	4.65	4.8	4.1	4.25	4.4	2.15	2.375	2.6
E4	4.35	4.525	4.7	3.6	3.75	3.9	2.2	2.35	2.5
	4.24	4.47	4.7	3.6	3.75	3.9	2.2	2.45	2.7
Ave	4.295	4.4975	4.7	3.6	3.75	3.9	2.2	2.4	2.6
E5	4.3	4.475	4.65	3.7	3.85	4	2.3	2.5	2.7
F2	4.2	4.4	4.6	3.8	4.025	4.25	2.3	2.5	2.7
	4.65	4.75	4.85						
	4.55	4.7	4.85	4.25	4.35	4.45	2.3	2.525	2.75
	4.6	4.75	4.9	4.2	4.4	4.6	2.55	2.775	3
Ave	4.5	4.65	4.8	4.0833	4.2583	4.4333	2.3833	2.6	2.8166
F3	4.6	4.7	4.8	4.2	4.275	4.35	2.45	2.6	2.75
	4.5	4.6	4.7	4.15	4.275	4.4	2.45	2.6	2.75
Ave	4.55	4.65	4.75	4.175	4.275	4.375	2.45	2.6	2.75
F4	4.3	4.5	4.7	3.6	3.8	4	2.4	2.575	2.75
	4.4	4.55	4.7	3.7	3.825	3.95	2.3	2.4	2.5
	4.35	4.525	4.7	3.75	3.875	4	2.3	2.5	2.7
							2.25	2.375	2.5
Ave	4.35	4.525	4.7	3.6833	3.8333	3.9833	2.3125	2.4625	2.6125
F5	--	--	--	--	--	--	--	--	--